FACILITATING MULTI-ELECTRON CHEMISTRY IN THE F-BLOCK USING IMINOQUINONE LIGANDS

by
Ezra J. Coughlin

A Dissertation

Submitted to the Faculty of Purdue University
In Partial Fulfillment of the Requirements for the degree of

Doctor of Philosophy

Department of Chemistry

West Lafayette, Indiana

May 2019

THE PURDUE UNIVERSITY GRADUATE SCHOOL
STATEMENT OF COMMITTEE APPROVAL

Dr. Suzanne C. Bart, Chair

Department of Chemistry

Dr. Corey M. Thompson

Department of Chemistry

Dr. Shelley A. Claridge

Department of Chemistry

Dr. Jianguo Mei

Department of Chemistry

Approved by:

Dr. Christine Hrycyna

Head of the Graduate Program

ACKNOWLEDGMENTS

I would like to start by thanking my advisor, Professor Suzanne Bart. She mentored me through new chemistry projects and empowered me to pursue research questions of my own. I was also very fortunate to work with many members (and honorary members–Matthias Zeller) of the Bart lab from 2015 to 2019. The discussions, collaborations and friendships have made my time at Purdue enjoyable. Additionally, I have enjoyed working with the faculty at Purdue (especially Dr. McMillin, regarding discussions about the electronic structure of transition metal complexes.) I am grateful for the funding from the U.S. Department of Energy (grant award numbers DE-SC0008479, DE-SC0016568) and Purdue (Emerson Kampen Fellowship). I would also like to thank the Amy Facility staff for providing such great analytical support.

Outside of Purdue, I would like to thank our collaborators including Prof. Eric Schelter, Prof. Mike Neidig, Prof. Scott Daly and all of the students who make research go. Finally, I would like to thank my family, friends and fiancé for supporting me up to and throughout my time in graduate school.

TABLE OF CONTENTS

LIST OF TABLES

LIST OF FIGURES

LIST OF ABBREVIATIONS

Abbreviation	Meaning
THF	Tetrahydrofuran
Et_2O	Diethyl ether
Tol	Toluene
Pent	Pentane
Pyr	Pyridine
ACN	Acetonitrile
18-C-6	18 Crown-6
dipp	2,6-diisopropylphenyl group
iq^0	Iminoquinone
isq^{1-}	Iminosemiquinone
ap^{2-}	Amidophenolate
pTol	*p*-tolyl group
pCF_3	*p*-(trifluoromethyl) group
^tBu	*tert*-butyl group
Ln	Lanthanide
An	Actinide
TM	Transition Metal
IR	Infrared
UV-Vis	Ultraviolet-Visible
NMR	Nuclear Magnetic Resonance
EPR	Electron Paramagnetic Resonance
SQUID	Superconducting Quantum Interference Device

ABSTRACT

Author: Coughlin, Ezra, J. PhD
Institution: Purdue University
Degree Received: May 2019
Title: Facilitating Multi-Electron Chemistry in the F-Block Using Iminoquinone Ligands.
Committee Chair: Suzanne C. Bart

The chemistry of the *f*-block is relatively unknown when compared to the rest of the periodic table. Transition metals and main group elements have enjoyed thorough study and development over the last 200 years, while many of the lanthanides and actinides weren't even discovered until the 1940's. This is troublesome, as knowledge of these elements is critical for environmental, industrial and technological advances. Understanding bonding motifs and reactivity pathways is fundamental to advancing the field of *f*-block chemistry. The use of redox-active ligands has aided in the construction of new bonding modes and discovery of new reaction pathways by providing electrons for these transformations. A particularly successful partnership is formed when redox-active ligands are combined with lanthanides, as these elements are usually considered redox-restricted. A series of lanthanide complexes featuring the iminoquinone ligand in three oxidation states will be discussed. The use of the ligands as a source of electrons for reactivity is also described, with new bonding motifs for lanthanides being realized. The iminoquinone ligand can also serve to break bonds. The uranyl (UO_2^{2+}) ion is notoriously difficult to handle due to its strong U-O multiple bonds. To overcome this, we developed a series of uranyl complexes and studied the ability of the iminoquinone ligand to serve as an electron source for reduction of uranium, with concomitant U-O bond cleavage.

CHAPTER 1. SYNTHESIS, CHARACTERIZATION AND REACTIVITY OF LANTHANIDE IMINOQUINONE COMPLEXES

1.1 Introduction

Nuclear energy operates without major greenhouse gas emission, which makes it an attractive option for clean energy. Harnessing heat from nuclear reactions is well established but there exist many challenges associated with production of nuclear fuels and reprocessing their waste. Uranium ore purification prior to use requires extraction based on chemical properties, such as solubility and bonding preference. After fuel is used, separating into recyclable and non-recyclable portions requires chemical understanding of the mixture of elements that are present in used fuel. This complex mixture is not well understood, yet the reprocessing steps must be able to separate these species. This is where a fundamental understanding of the chemistry of the elements in these mixtures is crucial.

Early research of *f*-block elements (lanthanides and actinides) was focused on their physical properties.[1] Since then, the elements have primarily been studied for their characteristic magnetic, luminescent, and Lewis acidic properties giving rise to their essential roles in medicine, energy, and technology.[1] Unfortunately, much less attention has been paid to their chemical properties, in part due to toxicity and radioactivity considerations. For these reasons, the chemistry of the f-block of the periodic table is much less explored when compared to other elements of the periodic table (such as elements in the s-, p- or d-blocks). The top half of the *f*-block, the lanthanides, commonly exist in the trivalent form (Ln^{3+}), and typically do not engage in redox chemistry because of thermodynamic stability. With few exceptions (Ce, Sm, Eu, Dy, Yb), these 14 elements are generally considered redox-restricted.[2] Consequently, lanthanides are typically unable to perform typical two- electron, organometallic transformations such as oxidative addition and

reductive elimination. This limitation has precluded the study of exotic bonding motifs, as the synthetic routes used by transition metal chemists for years do not exist to access them. An effective strategy to circumvent the redox-inactivity of lanthanides is the use redox-active ligands, which have been established to facilitate multi-electron transfer with metals of the p,[3,4] d,[5] and *f* blocks of the periodic table.[6,7]

While redox-active ligands have been proven to impart interesting magnetic[8,9] or electrochemical[10-12] properties to the rare earth elements due to their ability to stabilize ligand radicals,[13,14] fewer examples exist that demonstrate productive electron movement for new bond formation. Mazzanti *et al* reported tetradentate Schiff base complexes of Nd, Eu, Tb, Yb that, upon reduction, store two electrons in a new C-C σ bond.[15] Oxidation of these species can be achieved using AgOTf or I_2, highlighting the reversibility of this redox process, as seen by C-C bond cleavage. Reactivity with 9,10-phenanthrenequinone shows reduction to the corresponding potassium catecholate. Thus, this approach is effective for small molecule activation. Application of redox-active ferrocene diamide ligands has also led to productive polymerization chemistry as demonstrated by Diaconescu and co-workers with their redox switchable rare earth catalysts.[16]

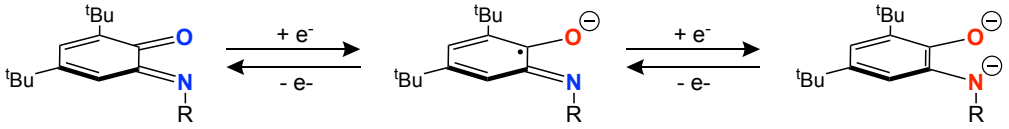

Figure 1.1.: Redox chemistry of the iminoquinone ligand.
Blue denotes neutral atoms while red indicates anionic ones. The iminoquinone (iq^0) (left), iminosemiquinone (isq^{1-}) (middle) and amidophenolate (ap^{2-}) (right).

Based on these exciting examples of ligand mediated redox chemistry for bond formation reactions, we sought to apply this methodology to redox-active ligands that store reducing

equivalents in conjugated π systems. We have recently demonstrated this principle with the synthesis, characterization, and reactivity of uranium(IV) amidophenolate complexes, $(^{R}ap)^{2-}{}_{2}U(THF)_{2}$ [R = *t*-Bu, Ad, dipp (dipp = 2,6-diisopropylphenyl)], supported by two redox-active 4,6-di-*tert*-butyl-2-(R)- amidophenolate ($[ap]^{2-}$) ligands.[17] These species readily undergo oxidative addition with $PhICl_2$, forming the bis-(4,6-di-*tert*-butyl-2-(R)iminosemiquinone) ($[^{R}isq]^{1-}$) uranium(IV) dichloride dimer, $[(^{R}isq)^{1-}{}_{2}UCl]_{2}(\mu^{2}\text{-}Cl)_{2}$. In these cases, the redox chemistry is relegated to the ligands, which act a source of electrons, converting the amidophenolate ligands to iminosemiquinone ligands. This exciting, multi-electron reactivity prompted investigation of these ligands for supporting rare earth complexes. This chapter will present the synthesis and characterization of a family of lanthanide complexes where the redox active ligand is featured in multiple oxidation states. A thorough study of the electronic structure and reactivity of the neodymium analogues is described. Reversible, multi-electron redox chemistry is demonstrated with oxidation of the electron-rich bis(amidophenolate) neodymium derivative by elemental chalcogens and other substrates. In addition, reactivity of ytterbium iminoquinone complexes with aryl azides is discussed, with evidence of transient trivalent lanthanide imido formation.

1.2 Experimental

1.2.1 General Considerations

All air- and moisture-sensitive manipulations were performed using standard Schlenk techniques or in an MBraun inert atmosphere drybox with an atmosphere of purified nitrogen. The MBraun drybox was equipped with two −35 °C freezers for cooling samples and crystallizations. Solvents for sensitive manipulations were dried and deoxygenated using literature procedures with a Seca solvent purification system.[18] Benzene-d_6 was purchased from Cambridge Isotope Laboratories, dried with molecular sieves and sodium, and degassed by three freeze–pump–thaw

cycles. $NdI_3THF_{3.5}$[19] 4,6-di-*tert*-butyl-2-[(2,6-diisopropylphenyl)imino]quinone (^{dipp}iq)[20], KC_8[21] were prepared according to literature procedures. 18-crwon-6, sublimed sulfur and selenium powder were purchased from Sigma Aldrich and dried on a Schlenk line overnight prior to use.

^{1}H NMR spectra were recorded on a Varian Inova 300 spectrometer operating at 299.992 MHz. All chemical shifts are reported relative to the peak for $SiMe_4$, using ^{1}H (residual) chemical shifts of the solvent as a secondary standard. The spectra for all molecules were obtained by using an acquisition time of 0.5 s, thus the peak widths reported have an error of ±2 Hz. For all molecules, the ^{1}H NMR data are reported with the chemical shift, followed by the peak width at half height in Hz, the integration value, and, where possible, the peak assignment. All voltammetric data were obtained under inert atmosphere conditions using external electrical ports of the MBraun inert drybox. All data were obtained using a Gamry Instruments Interface 1000 model potentiostat using the Gamry Instruments Laboratory software. All samples were collected in THF with 0.1 M $[Bu_4N][PF_6]$ supporting electrolyte concentration and a substrate concentration of 2.7 mM. Data were collected using internal resistance compensation of approximately 2000 ohms. Solutions were analyzed in 20 mL vials, consisting of a 3 mm glassy carbon working electrode, a Pt wire counter electrode, and an Ag^0 wire quasi-reference electrode. The Fc/Fc^+ couple was used as an external standard measured under the experimental conditions. Electronic absorption measurements were recorded at 294 K in toluene in sealed 1 cm quartz cuvettes with Cary 100 Scan UV-Visible spectrophotometer. Elemental analyses were performed by Robertson Microlit Laboratories (Ledgewood, NJ).

Single crystals of **Nd-ap** and **Nd-ap crown**, suitable for X-ray diffraction, were coated with poly(isobutylene) oil in a glovebox and quickly transferred to the goniometer head of a Nonius KappaCCD diffractometer equipped with a graphite crystal incident beam monochromator

and examined with Mo Kα radiation (λ = 0.71073 Å). Data from the KappaCCD instrument were collected using the Nonius Collect software.[22] Crystals of **Nd-isq**, **Nd-isq-S_5 crown** and **Nd-isq-Se_5 crown** were coated with poly(isobutylene) and quickly transferred to the goniometer head of a Rigaku Rapid II image plate diffractometer equipped with a MicroMax002+ high intensity copper X-ray source with confocal optics and examined with Cu Kα radiation (λ = 1.54184 Å). Data were collected using the dtrek option of CrystalClear.[23] Data from both the Nonius KappaCCD and the Rigaku Rapid II were processed using HKL3000[24] and data were corrected for absorption and scaling using Scalepack.[24] Single crystals of **Nd-iq** were coated with poly(isobutylene) and quickly transferred to the goniometer head of a Bruker Quest diffractometer with a fixed chi angle, a sealed tube fine focus X-ray tube, single crystal curved graphite incident beam monochromator and a Photon200 CMOS area detector. Examination and data collection were performed with Mo Kα radiation (λ = 0.71073 Å). Data were collected, reflections were indexed and processed, and the files scaled and corrected for absorption using APEX3.[25] All data were collected with Oxford Cryosystems low temperature devices operating at 100 K.

Data for **Nd-iq** were collected, reflections were indexed and processed, and the files scaled and corrected for absorption using APEX3. The space groups were assigned and the structures were solved by direct methods using XPREP within the SHELXTL suite of programs and refined by full matrix least squares against F^2 with all reflections using Shelxl2014[26] using the graphical interface Shelxle.[27] If not specified otherwise, H atoms attached to carbon and nitrogen atoms and hydroxyl hydrogens were positioned geometrically and constrained to ride on their parent atoms, with carbon hydrogen bond distances of 0.95 Å for and aromatic C-H, 1.00, 0.99 and 0.98 Å for aliphatic C-H, CH_2 and CH_3 moieties, respectively. Methyl H atoms were allowed to rotate but not

to tip to best fit the experimental electron density. U_{iso}(H) values were set to a multiple of U_{eq}(C) with 1.5 for CH_3, and 1.2 for CH_2 and C-H units, respectively.

1.2.2 Synthetic Details

Synthesis of (^{dipp}iq)$_2$NdI$_3$ (**Nd-iq**). A 20-mL scintillation vial was charged with $NdI_3(THF)_{3.5}$ (0.100 g, 0.129 mmol) and 10 mL toluene. A separate 20 mL scintillation vial was charged with ^{dipp}iq (0.098 g, 0.257 mmol), dissolved in 5 mL toluene and added dropwise to the pale blue stirring $NdI_3(THF)_{3.5}$ slurry. A reddish-brown solution was observed. After 3 hours, the solution was filtered over Celite and volatiles were removed *in vacuo.* The resulting reddish-brown solid with cold *n*-pentane (3 × 5 mL) to afford red powder (0.093 g, 0.072 mmol, 64% yield) assigned as $NdI_3(^{dipp}iq)_2$ (**Nd-iq**). X-ray quality crystals were obtained from a concentrated diethyl ether solution layered with pentane (5:1) at -35 °C. Elemental analysis of $C_{52}H_{74}N_2I_3NdO_2$: Calculated, C, 48.64; H, 5.81; N, 2.18. Found, C, 48.03; H, 6.51; N, 2.06. ^{1}H NMR (C_6D_6, 25 °C): δ = -6.64 (44, 4H, C*H*$(CH_3)_2$), -0.97 (6, 12H, CH(C*H*$_3$)$_2$), -0.19 (12, 12H, CH(C*H*$_3$)$_2$), 0.71 (3, 18H, C(C*H*$_3$)$_3$), 5.13 (7, 2H, C*H*), 6.25 (8, 18H, C(C*H*$_3$)$_3$), 8.40 (11, 6H, C*H*), 10.59 (6, 2H, C*H*).

Synthesis of (^{dipp}isq)$_2$NdI (**Nd-isq**) from **Nd-iq**. A 20-mL scintillation vial was charged with **Nd-iq** (0.100 g, 0.078 mmol) and 5 mL THF. While stirring, potassium graphite (0.021 g, 0.156 mmol) was added, resulting in a rapid color change from red to dark green. After 1 hour, the solution was filtered over Celite and volatiles were removed *in vacuo*. The crude mixture was recrystallized from *n*-pentane to afford dark green powder (0.071 g, 0.065 mmol, 83%) assigned as (^{dipp}isq)$_2$NdI (**Nd-isq**). Single, X-ray quality crystals were obtained from a concentrated pentane solution at -35 °C. Elemental analysis of $C_{52}H_{74}N_2INdO_2$: Calculated, C, 60.62; H, 7.24; N, 2.72. Found, C, 59.74; H, 7.48; N, 2.48.^{1}H NMR (C_6D_6, 25 ºC): δ = -119.14 (600, 2H, C*H*), -5.42 (189, 6H, CH(C*H*$_3$)$_2$), -3.04 (241, 2H, C*H*$(CH_3)_2$), -2.30 (76, 6H, CH(C*H*$_3$)$_2$), 2.25 (47, 18H, C(C*H*$_3$)$_3$),

3.31 (535, 6H, CH(CH_3)$_2$), 7.93 (395, 2H, C*H*), 8.26 (395, 2H, C*H*), 14.53 (179, 6H, CH(CH_3)$_2$), 16.29 (66, 18H, C(CH_3)$_3$), 37.38 (381, 2H, C*H*), 40.90 (271, 2H, C*H*), 50.71 (387, 2H, C*H*).

Synthesis of [K(THF)$_2$][(^{dipp}ap)$_2$Nd(THF)$_2$] (**Nd-ap**) from **Nd-isq**. A 20-mL scintillation vial was charged with **Nd-isq** (0.100 g, 0.091 mmol) and 5 mL THF. While stirring, potassium graphite (0.025 g, 0.181 mmol) was added resulting in a rapid color change from dark green to faint green. After 1 hour, the solution was filtered over Celite and volatiles were removed *in vacuo*. The crude mixture was washed with cold *n*-pentane to afford pale blue powder (0.097 g, 0.079 mmol, 87%) assigned as [K(THF)$_2$] [(^{dipp}ap)$_2$Nd(THF)$_2$] (**Nd-ap**). Single, X-ray quality crystals were obtained from a concentrated pentane solution at -35 °C. ^{1}H NMR (C_6D_6, 25 °C): δ = -38.27 (82, 4H, K(*THF*)), -22.07 (168, 2H, C*H*(CH_3)$_2$), -15.83 (112, 4H, K(*THF*)), -13.13 (38, 4H, K(*THF*)), -11.53 (23, 6H, CH(CH_3)$_2$), -11.05 (41, 4H, K(*THF*), -9.68 (26, 18H, C(CH_3)$_3$), 1.27 (68, 8H, *THF*)), 3.06 (102, 8H, *THF*), 4.76 (30, 6H, CH(CH_3)$_2$), 4.97 (42, 6H, CH(CH_3)$_2$), 8.41 (4, 18H, C(CH_3)$_3$), 9.14 (25, 2H, C*H*), 10.74 (21, 2H, C*H*), 11.40 (16, 2H, C*H*), 18.53 (27, 6H, CH(CH_3)$_2$), 18.68 (26, 2H, C*H*), 38.92 (38, 2H, C*H*), 71.58 (110, 2H, C*H*).

Synthesis of [K(18-crown-6)(THF)$_2$][(^{dipp}ap)$_2$Nd(THF)$_2$] (**Nd-ap crown**) from **Nd-ap**. A 20-mL scintillation vial was charged with **Nd-ap** (0.100 g, 0.081 mmol) and 5 mL THF. While stirring, 18-crown-6 (0.022 g, 0.081 mmol) was added. After 1 hour, volatiles were removed *in vacuo*. The crude mixture was washed with 10 mL cold *n*-pentane to afford colorless powder (0.112 g, 0.075 mmol, 92%) assigned as [K(18-crown-6)(THF)$_2$][(^{dipp}ap)$_2$Nd(THF)$_2$] (**Nd-ap crown**). Single, X-ray quality crystals were obtained from vapor diffusion of pentane into a concentrated THF solution stored at -35 °C. ^{1}H NMR (C_6D_6, 25 °C): δ = -44.05 (168, 2H, C*H*(CH_3)$_2$), -23.76 (212, 4H, K(*THF*)), -13.13 (264, 4H, K(*THF*)), -12.16 (255, 4H, K(*THF*)), -10.44 (76, 4H, K(*THF*)), -10.44 (76, 6H, CH(CH_3)$_2$), -4.21 (44, 24H, CH_2), -3.70 (15, 18H,

C(CH_3)$_3$), -1.95 (62, 6H, CH(CH_3)$_2$), 4.53 (72, 6H, CH(CH_3)$_2$), 4.88 (71, 2H, C*H*), 7.46 (18, 2H, C*H*), 8.30 (5, 18H, C(CH_3)$_3$), 14.87 (62, 2H, C*H*), 15.32 (10, 2H, C*H*), 19.05 (59, 6H, CH(CH_3)$_2$), 34.35 (25, 2H, C*H*), 72.63 (16, 2H, C*H*).

Synthesis of [K(18-crown-6)][(^{dipp}isq)$_2$Nd(S_5)] (**Nd-isq-S_5 crown**) from **Nd-ap crown**. A 20-mL scintillation vial was charged with **Nd-ap crown** (0.100 g, 0.067 mmol) and 8 mL toluene. While stirring, 5/8 equivalents of S_8 (0.011 g, 0.042 mmol) was weighed by difference and added to the colorless solution. An immediate color change to teal was observed. After 0.5 hours, the solution was filtered over Celite and volatiles were removed *in vacuo*. The teal solid was washed with 8 mL cold *n*-pentane. The teal solid was weighed (0.074 g, 0.054 mmol, 81%) and assigned as [K(18-crown-6)][(^{dipp}isq)$_2$Nd(S_5)] (**Nd-isq-S_5 crown**). Single, X-ray quality crystals were obtained by vapor diffusion of pentane into a concentrated THF solution stored at -35 °C. Elemental analysis of $C_{64}H_{98}N_2NdKO_8S_5$: Calculated, C, 56.23; H,7.23; N, 2.05. Found, C, 55.87; H,7.06; N, 1.97. ^{1}H NMR (C_6D_6, 25 ºC): δ = -97.68 (330, 2H, C*H*(CH_3)$_2$), -18.16 (206, 2H, C*H*(CH_3)$_2$), -2.70 (95, 2H, C*H*(CH_3)$_2$), -2.25 (123, 6H, CH(C*H*$_3$)$_2$), -0.28 (117, 6H, CH(C*H*$_3$)$_2$), 2.77 (9, 24H, C*H*$_2$), 5.33 (65, 18H, C(C*H*$_3$)$_3$), 7.00 (52, 2H, C*H*(CH_3)$_2$), 7.22 (64, 6H, CH(C*H*$_3$)$_2$), 10.53 (19, 6H, CH(C*H*$_3$)$_2$), 13.50 (23, 18H, C(C*H*$_3$)$_3$), 23.12 (184, 2H, C*H*), 28.86 (163, 2H, C*H*), 40.21 (128, 2H, C*H*).

Synthesis of [K(18-crown-6)(THF)][(^{dipp}isq)$_2$Nd(Se_5)] (**Nd-isq-Se_5 crown**) from **Nd-ap crown**. A 20-mL scintillation vial was charged with **Nd-ap crown** (0.100 g, 0.067 mmol) and 8 mL toluene. While stirring, 5 equivalents of selenium powder (0.026 g, 0.334 mmol) was weighed by difference and added to the colorless solution. A gradual color change to teal was observed. After 0.5 hours, the solution was filtered over Celite and volatiles were removed *in vacuo*. The teal solid was washed with 8 mL of cold *n*-pentane The teal solid was dried and weighed (0.101 g,

0.060 mmol, 90%) assigned as [K(18-crown-6)(THF)][(^{dipp}isq)$_2$Nd(Se$_5$)] **(Nd-isq-Se$_5$ crown)**. Single, X-ray quality crystals were obtained by vapor diffusion of pentane into a concentrated toluene solution at -35 °C. Elemental analysis of $C_{68}H_{106}N_2NdKO_9Se_5$: Calculated, C, 48.80; H, 6.38; N, 1.67. Found, C, 48.84; H, 6.57; N, 1.62. ^{1}H NMR (C_6D_6, 25 ºC): δ = -91.16 (161, 2H, C*H*(CH$_3$)$_2$), -18.27 (134, 2H, C*H*(CH$_3$)$_2$), -3.20 (13 6H, CH(C*H*$_3$)$_2$), -2.20 (17, 2H, C*H*(CH$_3$)$_2$), -0.91 (22, 6H, CH(C*H*$_3$)$_2$), 2.88 (12, 24H, C*H*$_2$), 4.87 (11, 18H, C(C*H*$_3$)$_3$), 7.17 (25, 2H, C*H*(CH$_3$)$_2$), 7.54 (12, 6H, CH(C*H*$_3$)$_2$), 11.12 (8, 6H, CH(C*H*$_3$)$_2$), 13.55 (6, 18H, C(C*H*$_3$)$_3$), 26.06 (106, 2H, C*H*), 28.33 (41, 2H, C*H*), 39.68 (20, 2H, C*H*).

1.3 Lanthanide Iminoquinone Complexes

1.3.1 Synthesis of Neodymium Iminoquinone Complexes

To baseline our studies, we sought to coordinate neutral ligands to a lanthanide metal ion. neodymium was chosen as the lanthanide to begin with because of its similar ionic radii to U(IV) and Am(III), allowing for better comparison of bonding. This neutral ligand neodymium species was generated by stirring two equivalents of the dipp-substituted iminoquinone (^{dipp}iq) with NdI$_3$(THF)$_{3.5}$ in diethyl ether. Ligation in THF was unsuccessful, likely due to its coordinating nature. Using the less-coordinating diethyl ether afforded the metallated product, (^{dipp}iq)$_2$NdI$_3$ (**Nd-iq**) as a red powder in moderate yield after workup.

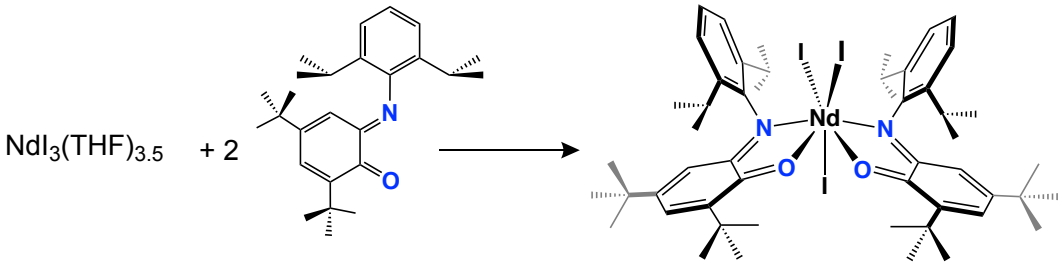

Figure 1.2: Synthesis of the neodymium bis(iminoquinone) complex, **Nd-iq**.

Upon confirming the synthesis of **Nd-iq**, reduction of this species was performed to engage the redox activity of the iminoquinone ligands using two equivalents of KC_8. Workup and isolation of the product of this reaction resulted in the reduced species, $(^{dipp}isq)_2NdI(THF)$ (**Nd-isq**), as a dark green powder. Interestingly, this species can also be generated directly from $NdI_3(THF)_{3.5}$, two equivalents of ligand and two equivalents of KC_8, in a one-pot reaction. The latter synthetic route is more useful, as it is one step and only requires one purification step.

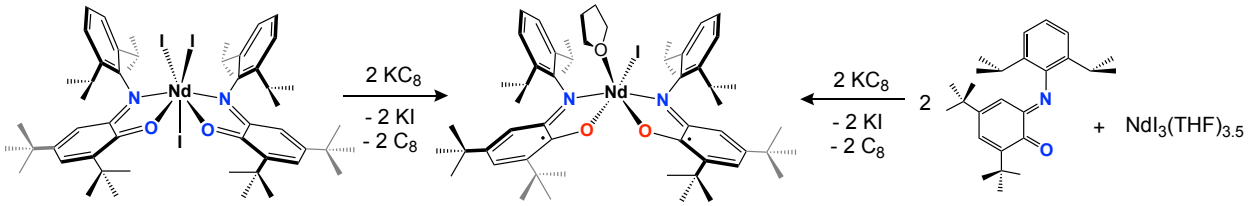

Figure 1.3: Synthesis of the neodymium bis(iminosemiquinone) complex (**Nd-isq).** Synthesis by (1) reduction of **Nd-iq** or (2) *in situ* metalation and reduction.

Further reduction of **Nd-isq** leads to the formation of the bis(amidophenolate) containing, $[K(THF)_2][(^{dipp}ap)_2Nd(THF)_2]$ (**Nd-ap**). The neodymium center remains in the trivalent oxidation state, with two dianionic ligands (4- overall), and a potassium ion to balance the overall charge.

This species can also be generated *via in situ* metalation of ^{dipp}iq to NdI_3 and reduction with KC_8. For **Nd-ap**, filtration and washing of the product resulted in isolation of a pale blue solid. Initial attempts to synthesize this complex were alarming, as the filtrate was colorless (typically, metal complexes are highly colored, thus indicating loss of metal during the reaction).

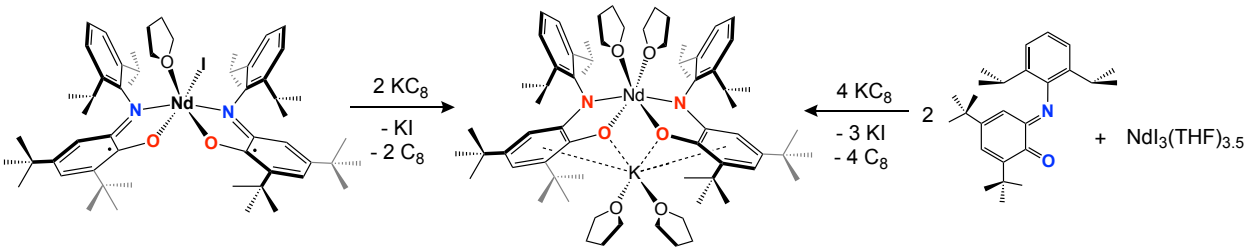

Figure 1.4: Synthesis of the neodymium bis(amidophenolate) species (**Nd-ap).**
Synthesis *via* either (1) reduction of **Nd-isq** using potassium graphite (left) or (2) *in situ* ligation and reduction of $NdI_3THF_{3.5}$ (right).

1.3.2 Synthesis of Lanthanide Iminoquinone Complexes

With the synthesis (*vide supra*) and characterization (*vide infra*) of the neodymium iminoquinone reduction series established, we sought to generalize this synthesis to other neodymium halides besides $NdI_3THF_{3.5}$. While $NdI_3THF_{3.5}$ provides access to the series, it is not commercially available, requiring a multi-step synthesis to prepare. Additionally, it tends to form cation-anion species, leading to an ambiguous solvation sphere that (potentially) affects stoichiometry of reactions. To circumvent these issues, an alternative neodymium source was explored. Neodymium trichloride is an attractive choice, as it is an anhydrous, trivalent neodymium starting material that is commercially available and does not have any bound solvent. Ligation of the neodymium trichloride with the neutral iminoquinone ligand was unsuccessful in a variety of solvents (likely due to the insolubility of neodymium trichloride). This highlights a benefit of the neodymium triiodide material, which is more soluble in organic solvents.

Although the neutral ligand complex was not generated from $NdCl_3$, we aimed to synthesize the iminosemiquinone and amidophenolate-containing complexes. We hypothesized that creating anionic ligands would be the driving force for metalation of the ligands. The iminosemiquinone species, $[(^{dipp}isq)_2Nd(Cl)(THF)]_2$, was successfully generated by *in situ* reduction of $NdCl_3$ and two equivalents of the iminoquinone ligand with KC_8. Interestingly, the smaller, harder chloride ion causes dimerization in the solid state, unlike the monomeric iodide-analog, **Nd-isq**. The amidophenolate complex was generated in a similar way, with loss of KCl, producing **Nd-ap**. Since all halides are removed during this reaction, this material is identical to that from the synthesis using NdI_3.

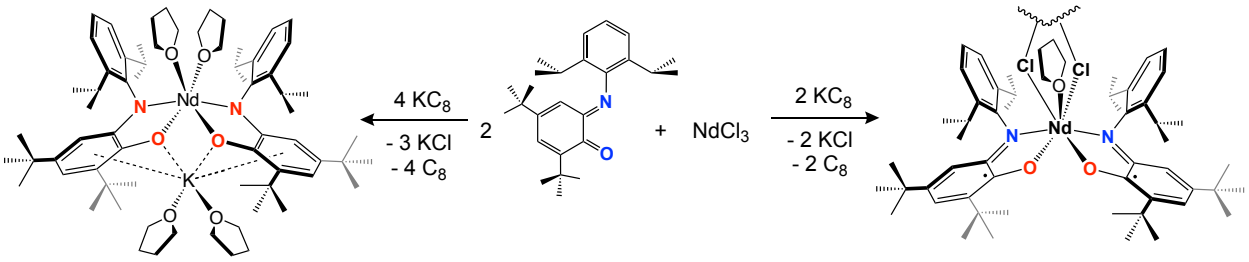

Figure 1.5: Synthesis of $[(^{dipp}isq)_2Nd(Cl)(THF)]_2$ (right) and **Nd-ap** (left) from neodymium trichloride ($NdCl_3$).

By establishing the ability of neodymium chloride to act as a suitable substitute for neodymium iodide in the synthesis of the iminosemiquinone and amidophenolate complexes, we were able to expand our synthesis to a variety of the lanthanides, as the lanthanide trichloride ($LnCl_3$) materials are commercially available. The amidophenolate ligand set displays the most interesting reactivity (*vide infra*) and is, therefore, the most interesting to study. With this in mind, we aimed to synthesize other lanthanide amidophenolate complexes. Namely, we chose gadolinium(III) (f^7) and ytterbium(III) (f^{13}) in addition to our neodymium(III) (f^3) system to round

out this study. This selection provides early, mid and late lanthanides with varying ionic radii and electronic structure, while maintaining the +3 oxidation state. Successful synthesis was achieved by *in situ* metalation of the iminoquinone and reduction with KC_8 of the lanthanide trichloride.

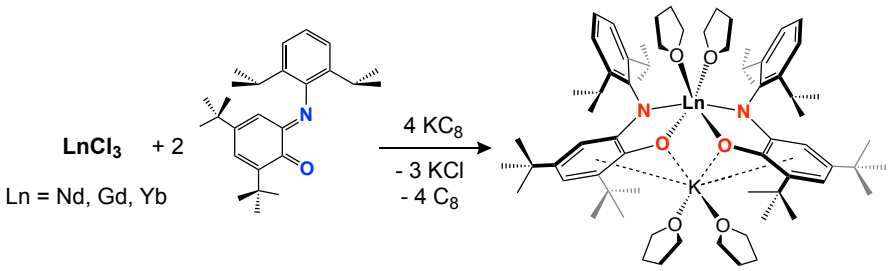

Figure 1.6: Synthesis of **Ln-ap** (Ln = Nd, Gd and Yb) from $LnCl_3$.

1.3.3 Potassium Ion Sequestration

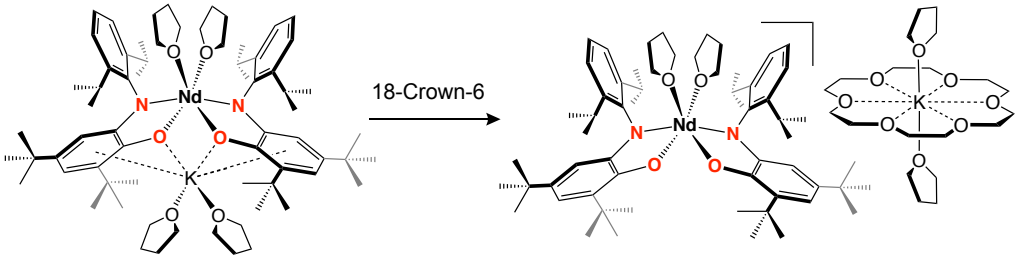

Figure 1.7: Synthesis of **Nd-ap crown** from **Nd-ap**.

As inner-sphere/outer-sphere cation coordination can change characteristics of metal complexes, we sought to create a charge-separated species that prevents any coordination of the potassium ion to the lanthanide complex. To remove the potassium from the coordination sphere, **Nd-ap** was treated with 18-crown-6 (18-C-6), yielding [K(18-C-6)][(^{dipp}ap)$_2$Nd(THF)$_2$] (**Nd-ap crown**). Given that the solution ^{1}H NMR spectra of **Nd-ap** and **Nd-ap crown** are distinct (*vide infra*), the potassium likely retains its coordination to the ligands in the absence of the crown ether.

Analogous reactions with the ytterbium amidophenolate complex (**Yb-ap**) yield a new set of resonances by ^{1}H NMR analysis, suggesting that this method can be generalized to the series of amidophenolate-containing species.

1.4 Characterization of Neodymium Iminoquinone Complexes

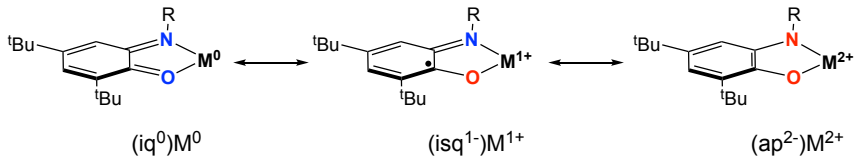

Figure 1.8: Metal-Ligand oxidation state ambiguity with redox-active ligands. The metal oxidation state ranges from 0 to +2, while the ligand balances the charge of the molecule by changing from 0 to -2.

Oxidation state ambiguity (ligand and metal) is commonly discussed when researching organometallic complexes of redox-active ligands. In mid- to late-transition metals, a degree of covalency tends to cloud these discussions. For earlier transition metals such as titanium and zirconium, more polar bonds are favorable, leading to more ionic character and allowing for easier oxidation state assignment. Lanthanides are commonly considered to be most similar to the early transition metals, preferring ionic bonds with hard sigma-donors (nitrogen, oxygen, halides). For all metal complexes, rigorous characterization using a variety of analytical techniques provides the best insight into the electronic structure. We examine our series of lanthanide iminoquinone complexes using NMR, UV-Vis, X-ray crystallography, EPR, electrochemistry and elemental analysis.

1.4.1 Nuclear Magnetic Resonance

For organometallic complexes that can stabilize unpaired electrons, paramagnetism causes shifts and broadening of resonances from the 0-10 ppm range commonly observed. While lanthanides typically exist in the +3 oxidation state, their *f*-electron count varies greatly (from 0-14). Moving from left to right across the lanthanide series, the valence electrons fill the 7 *f*-orbitals, producing species with 0-7 unpaired electrons. Consequently, lanthanides produce NMR spectra with varying degrees of paramagnetism.

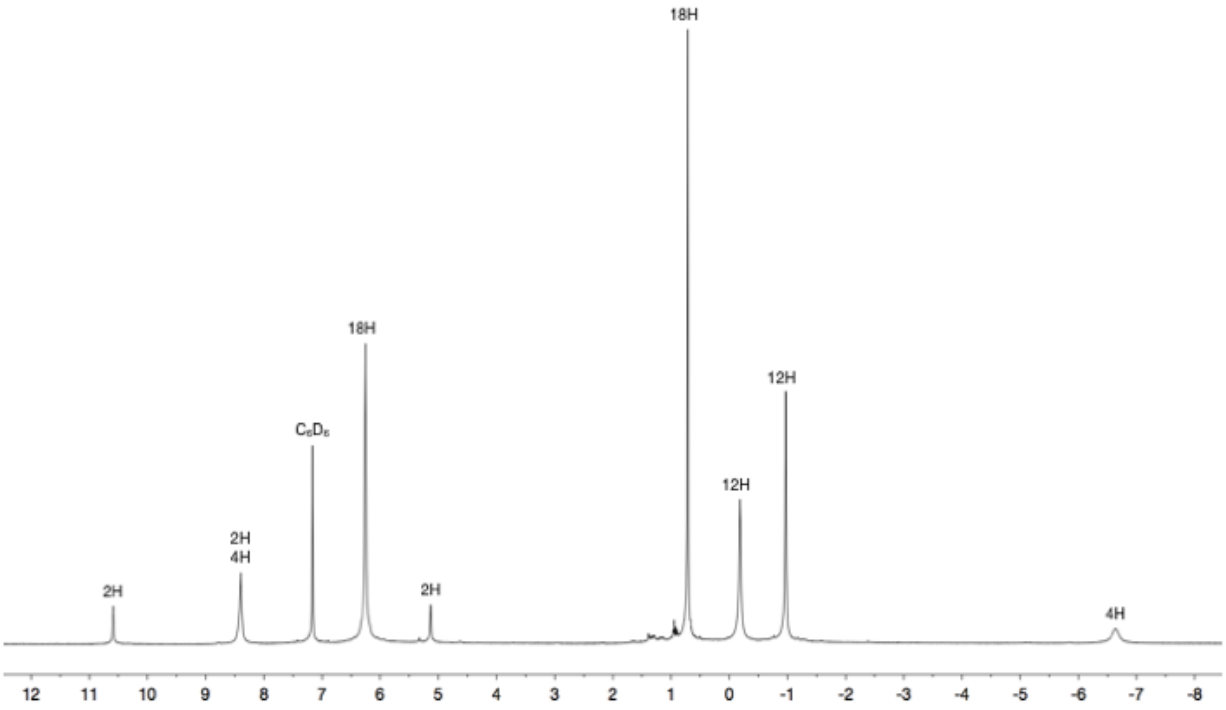

Figure 1.9: ^{1}H NMR spectrum of **Nd-iq** in C_6D_6 at 25 °C.

The NMR spectrum for **Nd-iq** in benzene features slightly broadened signals in the range of -7 to 11 ppm. The number of signals and integration values confirm C_{2v} symmetry in solution. This relatively narrow spread of resonances suggests only a weak interaction with the paramagnetic lanthanide center, especially when compared to the spectrum of **Nd-ap**. The resonances for this species range from -40 to 75 ppm, indicating greater effect of paramagnetism experienced by the protons of the ligands. This is likely a result of tighter binding of the dianion ligands in **Nd-ap** than the neutral ligands in **Nd-iq**.

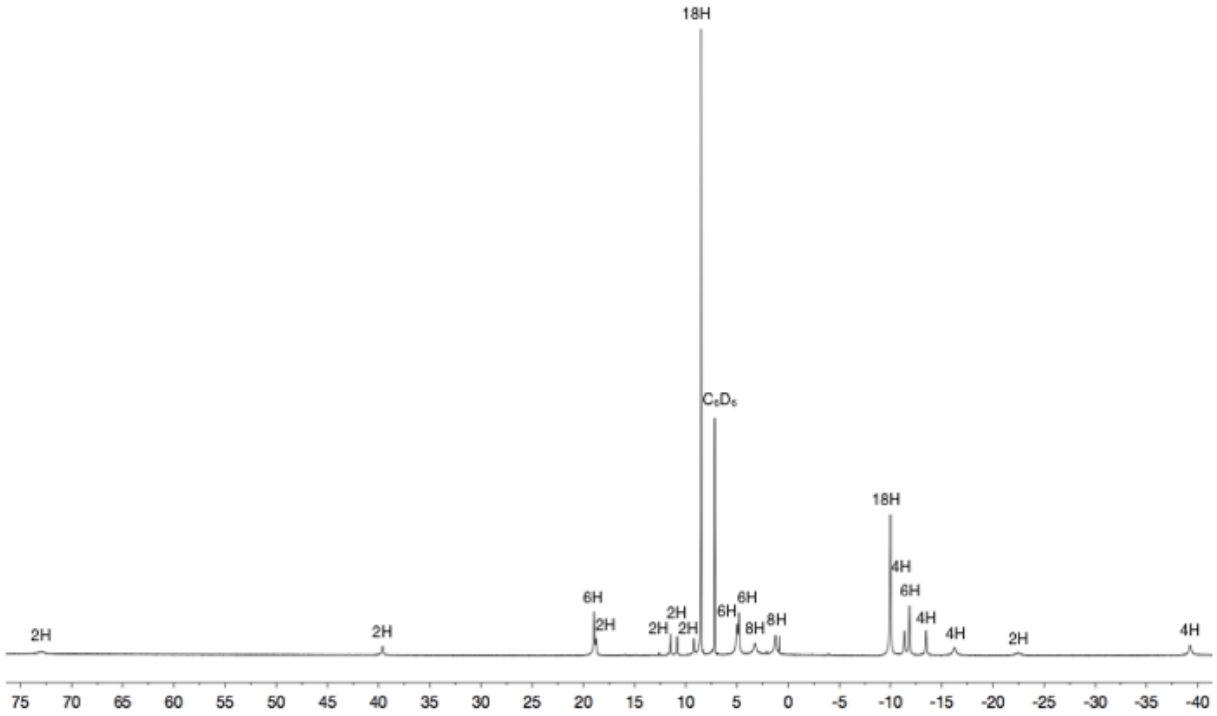

Figure 1.10: ^{1}H NMR spectrum of **Nd-ap** in C_6D_6 at 25 °C.

Further complicating the spectra of these species are the unpaired electrons of the iminosemiquinone ligand. For lanthanide complexes containing the iminosemiquinone ligand, there two sources of paramagnetism. In the spectrum of **Nd-isq**, resonances are extremely broad and range from -120 to 52 ppm. These effects are from a combination of the two unpaired electrons of the ligands and the three unpaired electrons of the Nd^{3+} (f^3) ion.

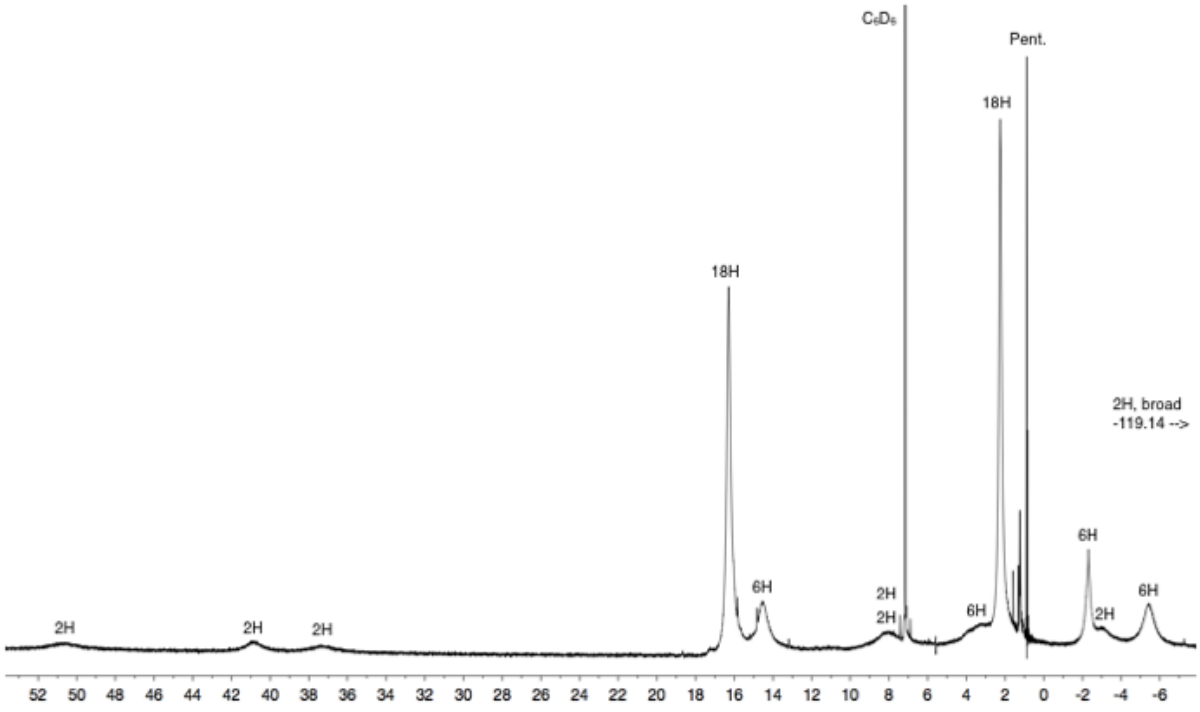

Figure 1.11: ^{1}H NMR spectrum of **Nd-isq** in C_6D_6 at 25 °C.

1.4.2 Single Crystal X-Ray Diffraction

Structural characterization of the neodymium reduction series was performed. This not only provides insight into the geometry and binding modes, but also metrical parameters can be a clear indicator of ligand oxidation state.[18] A discussion of representative distances from **Nd-iq**, **Nd-isq**, and **Nd-ap crown** are presented. Data for **Nd-ap** shows similar trends but intraligand bond distances may be affected by the potassium coordination to the ligands.

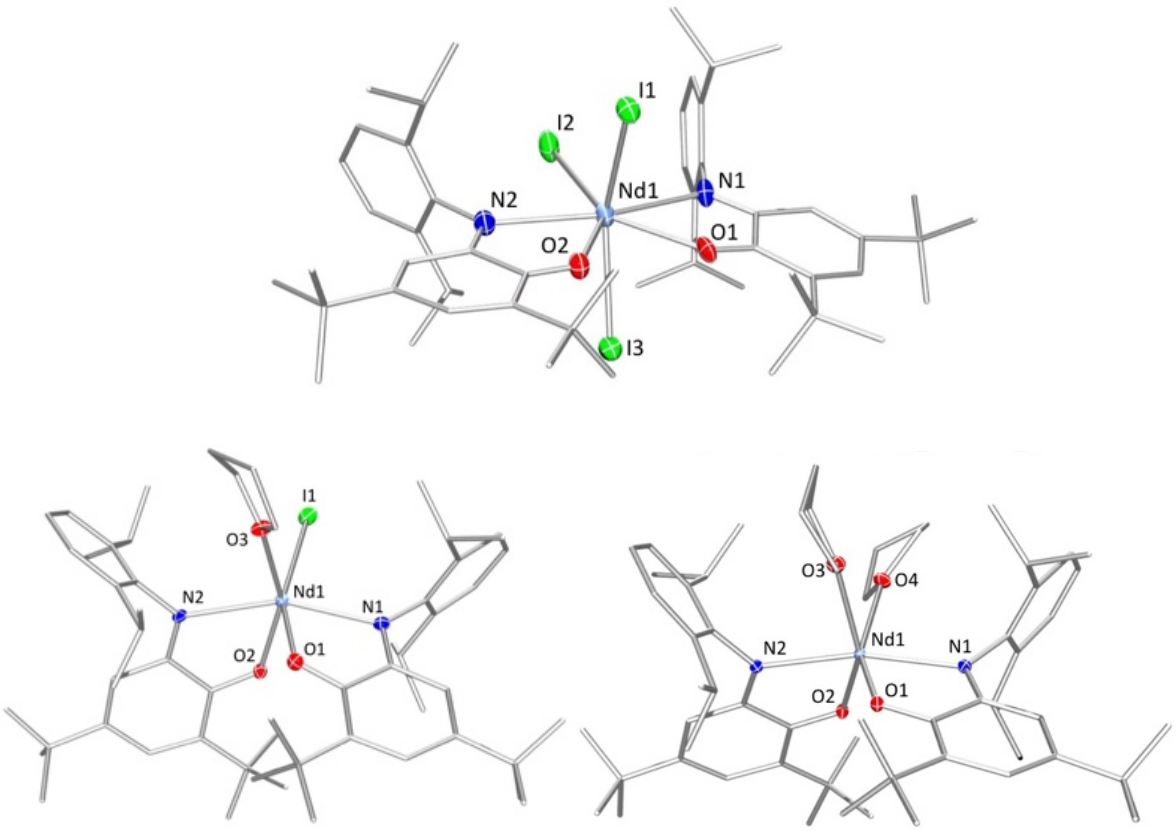

Figure 1.12: Molecular structures of **Nd-iq**, **Nd-isq**, and **Nd-ap crown**.

Nd-iq (top), **Nd-isq** (bottom left), and **Nd-ap crown** (bottom right) are shown at 30% probability ellipsoids with hydrogen atoms, co-crystallized solvent molecules, and the potassium cation with coordinated 18-C-6 removed for clarity.

Compound **Nd-iq** features a 7-coordinate, distorted pentagonal bipyramidal neodymium center. The respective Nd-O and Nd-N of 2.479(3) and 2.702(4) Å are consistent with dative interactions between neodymium and iminoquinone ligand, as expected from the oxidized form. This is corroborated by the C-N (1.300(6) Å) and C-O (1.238(6) Å) bond distances that are on the order of double bonds. Reduction of the ligand in octahedral **Nd-isq** is supported by contraction of the Nd-O bond to 2.317(9) Å as compared to **Nd-iq**, as would be expected from changing a dative bond to an anionic one, and by an elongation of the C-O bond. The Nd-N and C-N bond lengths change very little as compared to **Nd-iq**, since both maintain dative linkages with imine

functionalities. The most reduced species, **Nd-ap crown**, maintains the short Nd-O bond of 2.2648(16) Å, but now displays a short Nd-N bond (2.4378(19) Å) as well, expected for anionic bonds to the distorted octahedral neodymium. Examination of the intraligand distances shows an aromatic ring, with similar distances throughout, and C-O and C-N bond distances that signify single bonds. In **Nd-ap**, where the crown is absent, the ligand distances are similar, but the potassium is bound to the oxygen atoms of the amidophenolate ligand blocking access to the Nd atom.

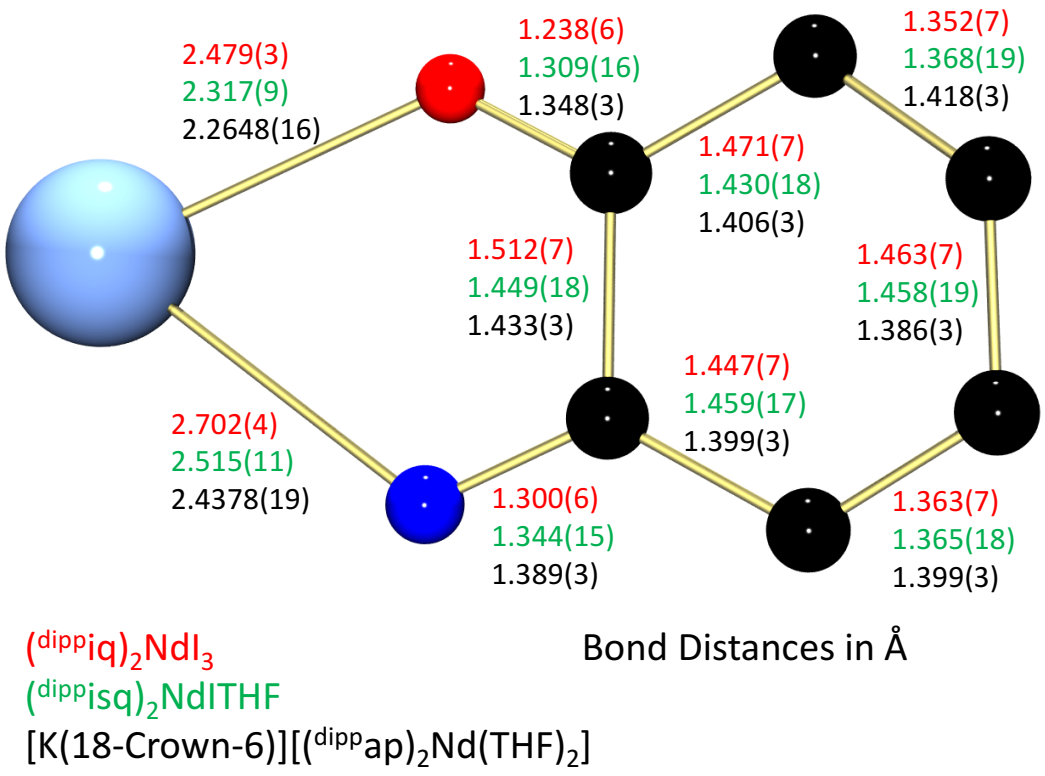

Figure 1.13: Bond distance (Å) comparison for **Nd-iq**, **Nd-isq**, and **Nd-ap crown**.

1.4.3 Electron Paramagnetic Resonance Spectroscopy

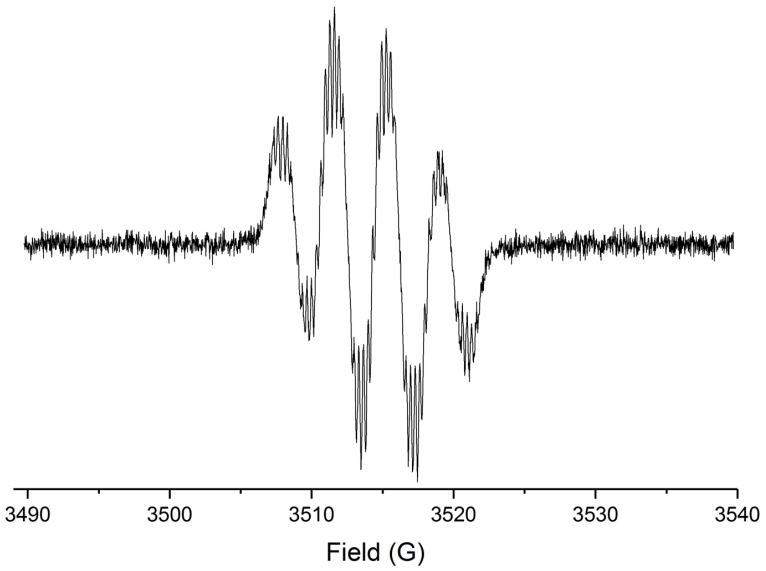

Figure 1.14: EPR Spectrum of **Nd-isq** (toluene, 2.04 mM) recorded at 25 °C. g_{iso}: 2.0026. Frequency: 9.850 GHz. Power: 0.502 mW. Modulation: 0.1 G/100 kHz.

The ligand radical in **Nd-isq** was further confirmed by EPR spectroscopy, which showed a g-value of 2.0026 at 25 °C in toluene solution. This spectrum is reminiscent of that previously observed for 4,6-di-*tert*-butyl-2-*tert*-butyl-iminosemiquinone, an iminosemiquinone organic radical species reported by Heyduk, which featured a g-value of 2.0061 (DMSO, 25° C). The hyperfine splitting is a result of interaction of the unpaired electron with one nitrogen (I = 1) and one hydrogen atom (I = ½) of the ligand. This hyperfine pattern agrees with previously noted results[19]. Thus, these measurements support the presence of an iminosemiquinone ligand radical with only a weak interaction with the neodymium metal center.

1.4.4 UV-Vis Spectroscopy

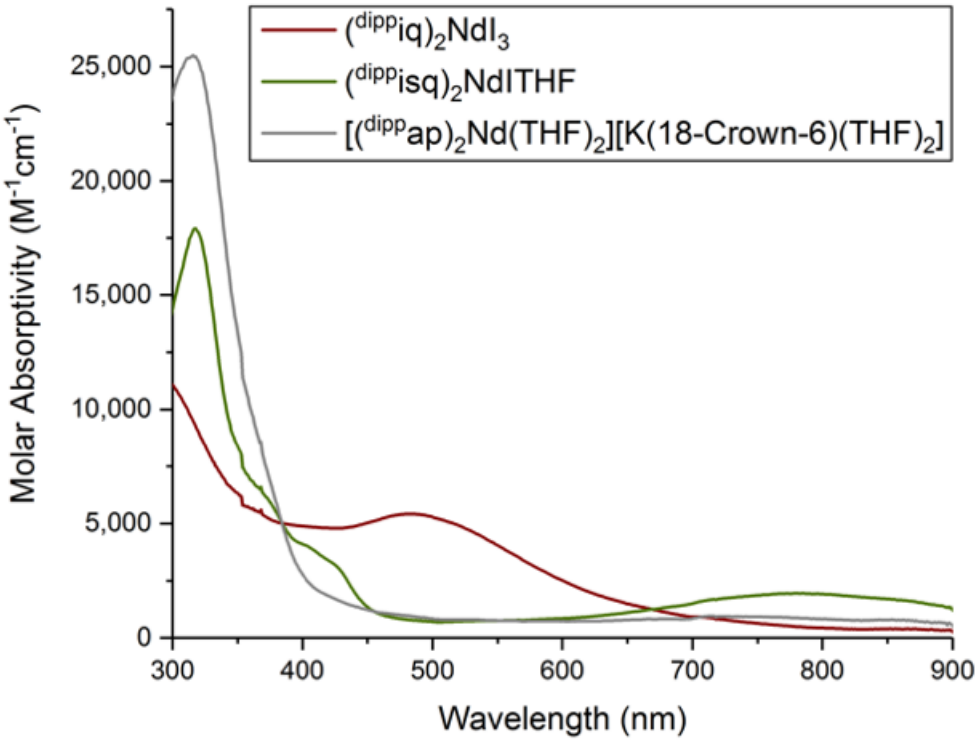

Figure 1.15: Electronic absorption spectra of **Nd-iq**, **Nd-isq**, and **Nd-ap crown** recorded in toluene at 25 °C.

The energies associated with the electronic transitions for the intensely colored family of neodymium complexes were quantified using electronic absorption spectroscopy. Data were collected from 300 to 900 nm in toluene at 25° C. Both **Nd-iq** and **Nd-isq** absorb strongly in the visible region, while colorless **Nd-ap crown** does not. Compound **Nd-iq** shows an intense absorption at 484 nm (6000 $M^{-1}cm^{-1}$), giving rise to the observed deep red color, whereas **Nd-isq** shows a color-producing band at 779 nm (2000 $M^{-1}cm^{-1}$), responsible for the dark green hue. Based on the lack of d electrons and the constant f^3 ground state in this neodymium series, the ligand

oxidation state dictates the appearance, making color a useful metric for ligand oxidation state identification.

1.5 Reactivity with Chalcogenide-Containing Substrates

1.5.1 Introduction

The synthesis and characterization of **Nd-iq**, **Nd-isq**, **Nd-ap,** and **Nd-ap crown** demonstrate that lanthanide-containing molecules can undergo multi-electron reduction chemistry in the appropriate ligand environments. This is facilitated the π*-orbitals of the ligands being able to accept electrons upon reduction. To determine the lability of the ligand and *f*-electrons for the most reduced species, **Nd-ap crown**, the reverse multi-electron oxidation was tested. Elemental chalcogens were chosen to study first, due to their strongly oxidizing nature and the utility of Ln-chalcogen bonds in Ln/An separations. Further investigation of these species revealed that other oxidants, such as diphenyl dichalcogenides and molecular oxygen, are suitable for bond forming reactions with these species.

1.5.2 Reactivity with Elemental Chalcogenides

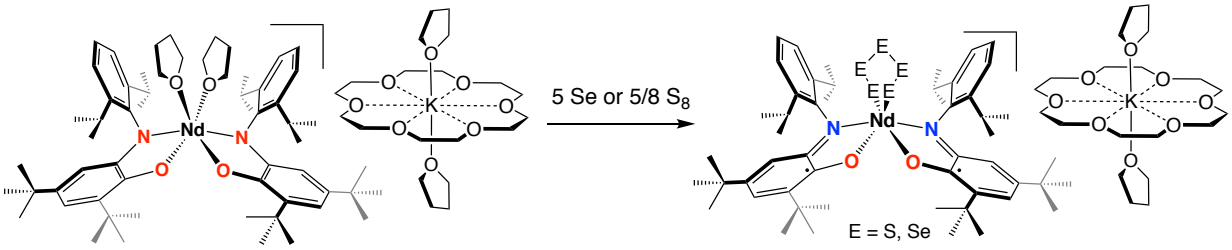

Figure 1.16: Two electron oxidation of **Nd-ap crown** with sulfur or selenium.

Exposure of **Nd-ap crown** to 5/8 equivalents of S_8 or 5 equivalents of Se powder immediately turned the colorless solution to dark blue-green, consistent with formation of iminosemiquinone-containing products. Following workup, the products, identified as [K (18-C-6)][(^{dipp}isq)$_2$Nd(S_5)] (**Nd-isq-S_5 crown**) and [K(18-C-6) (THF)][(^{dipp}isq)$_2$Nd(Se_5)] (**Nd-isq-Se_5 crown**), respectively, were isolated in high yields. Paramagnetically broadened and shifted ^{1}H NMR spectra were observed in the range of -100 to +40 ppm (C_6D_6, 25 ºC); this range is most similar to that observed for **Nd-isq**, suggesting that two ligand-based one-electron oxidations had occurred during the reaction. This formulation is corroborated by EPR spectroscopy, which showed g-values of 2.0026 in the spectra of **Nd-isq-S_5 crown** and **Nd-isq-Se_5 crown**, consistent with the presence of organic radicals.

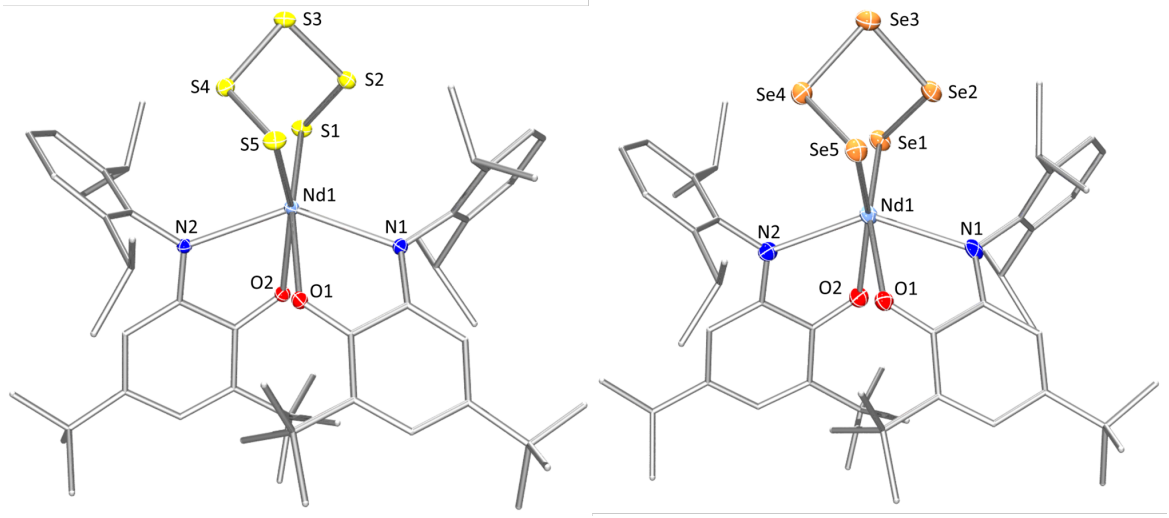

Figure 1.17: Molecular structures of **Nd-isq-S_5 crown** and **Nd-isq-Se_5 crown**. **Nd-isq-S_5 crown** (left) and **Nd-isq-Se_5 crown** (right) shown with 30% probability ellipsoids. Hydrogen atoms, co-crystallized solvent molecules and potassium cations with coordinated 18-C-6 have been omitted for clarity.

Structural support of the iminosemiquinone ligands in **Nd-isq-S_5 crown** and **Nd-isq-Se_5 crown** was obtained using X-ray crystallography. Analysis and refinement of the data showed analogous structures, with the S_5 and Se_5 fragments forming 6-membered twist-boat metallocycles with the neodymium ion. Examination of the ligand distances show average Nd-O bonds of 2.359 Å (**Nd-isq-S_5 crown**) and 2.348 Å (**Nd-isq-Se_5 crown**) as well as average Nd-N bonds of 2.529 Å (**Nd-isq-S_5 crown**) and 2.537 Å (**Nd-isq-Se_5 crown**), all confirming the assignment as iminosemiquinone ligands. The C-N and C-O bond distances track accordingly. Thus, **Nd-isq-S_5 crown** and **Nd-isq-Se_5 crown** are formed from two-electron oxidation of the ligands in **Nd-ap crown**.

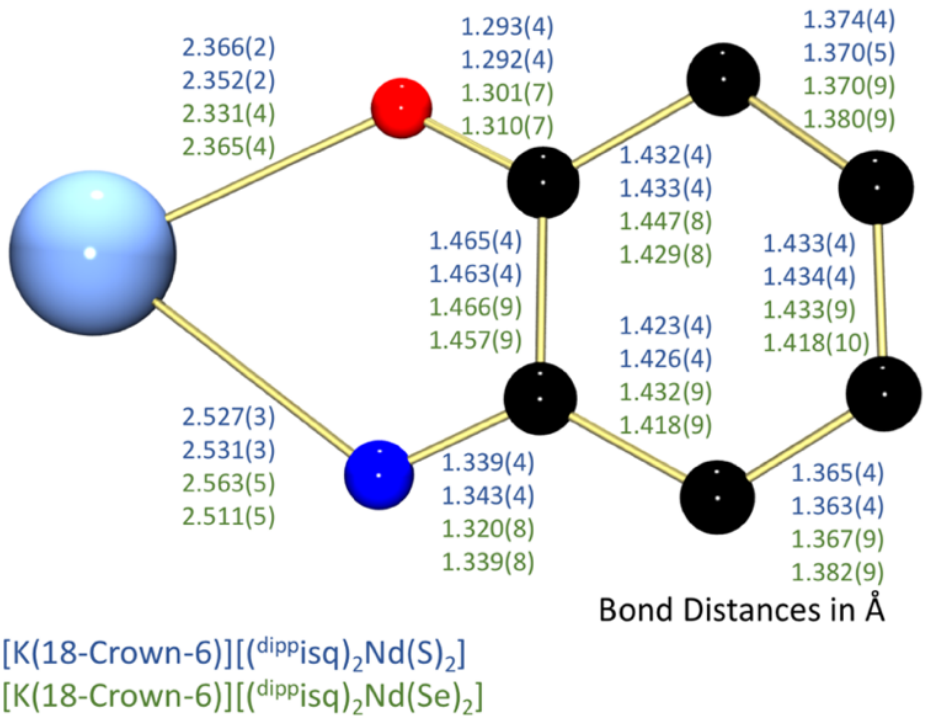

Figure 1.18: Bond distance (Å) comparison for **Nd-isq-S_5 crown** and **Nd-isq-Se_5 crown**.

When compared to similar reactions of *f*-elements with chalcogenides, interesting trends were observed. Elemental chalcogen activation has been previously noted with uranium, but generally persulfide (S_2^{2-}) compounds result.[30,31] Furthermore, the unusual twist-boat metallacycle noted here for Nd is unique to the bottom of the Periodic Table; transition metal counterparts do not display this conformer. Previously, Ryan and co-workers reported formation of twist-boat $Cp^*_2Th(S_5)$ by treating $Cp^*_2ThCl_2$ with Li_2S_5.[32] An analogous Sm(III) derivative, $Tp^{iPr2}Sm(\kappa^1$-3,5-$^{iPr2}Hpz)(S_5)$ (Tp^{iPr2} = hydrotris(3,5-di-isopropylpyrazolyl)borate), was identified by Takats and Edelmann as one of the oxidation products from exposing divalent $(Tp^{iPr2})_2Sm$ to one equivalent of S_8. [33] Surprisingly, the selenium metallacycle reported here is the first for an *f*-element, despite being previously known for the d-block.[24,25] Overall, we have demonstrated the controlled, rational formation of these 6-membered metallocycles *via* 2 e- oxidation–something lanthanides are typically thought to do.

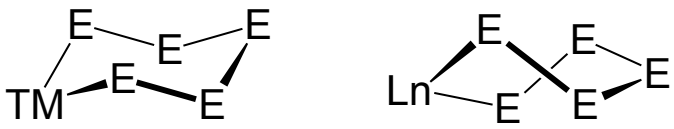

Figure 1.19: Comparison of 6-membered metallocycles for transition metals (TM) and lanthanides (Ln).

Interestingly, reactivity of the neodymium amidophenolate derivatives with Se is only observed in the presence of the crown ether, although both **Nd-ap** and **Nd-ap crown** react with sulfur. Performing the analogous experiment with **Nd-ap** results in no reaction; however, upon addition of the crown ether to the mixture, immediate procession of the reaction is noted. We hypothesized that this is either due to 1) blocking of the neodymium center by the potassium ion that is held in place by interaction with the ligand, or 2) that the oxidation potential of **Nd-ap** was

sufficiently higher such that elemental selenium was not a strong enough oxidant to remove an electron from the ligand π* orbitals. To test the latter idea, electrochemical measurements of **Nd-ap** and **Nd-ap crown** were performed in THF solution with a supporting electrolyte ($[NBu_4][PF_6]$). Cyclic voltammetric data for **Nd-ap** showed a quasi-reversible oxidation, $E_{1/2}$ = -0.864 V (vs Fc/Fc^+), corresponding to formation of **Nd-isq** in solution. Further oxidation showed an irreversible wave, consistent with oxidation of the ligand to iminoquinone. The loss of anionic linkages between the ligand and Nd facilitates ligand substitution with THF, explaining the irreversible nature of this wave. Cyclic voltammetric data for **Nd-ap crown** displayed very similar oxidations with the first quasi-reversible oxidation, $E_{1/2}$ = -0.772 V. These data suggest that **Nd-ap crown** is more difficult to oxidize, thus the lack of reactivity is likely due to blocking of the neodymium by the potassium; thus, sequestration of the potassium ion is necessary for the reaction to proceed.

1.5.3 Reactivity with Diphenyl Dichalcogenides

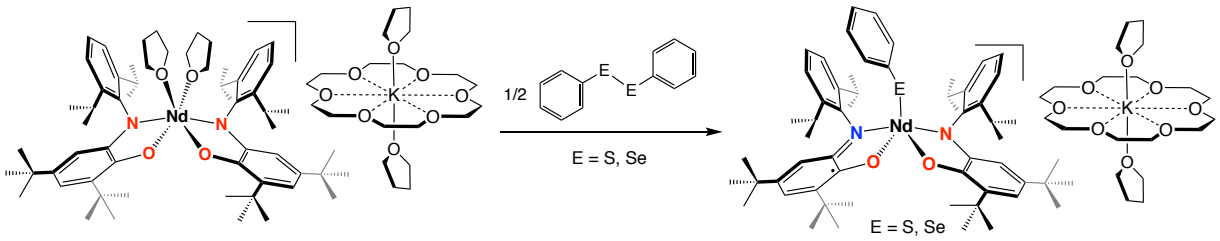

Figure 1.20: Oxidation of **Nd-ap crown** with diphenyl dichalcogenides.

Chalcogen substrates were chosen as substrates due to their oxidizing nature and the utility of Ln-chalcogen bonds in Ln/An separations. One half equivalent of diphenyl disulfide or diphenyl

diselenide were added to **Nd-ap crown**, instantly producing a dark blue-green solution, consistent with formation of iminosemiquinone-containing products. Upon workup, one electron oxidation was confirmed by spectroscopic and crystallographic techniques.

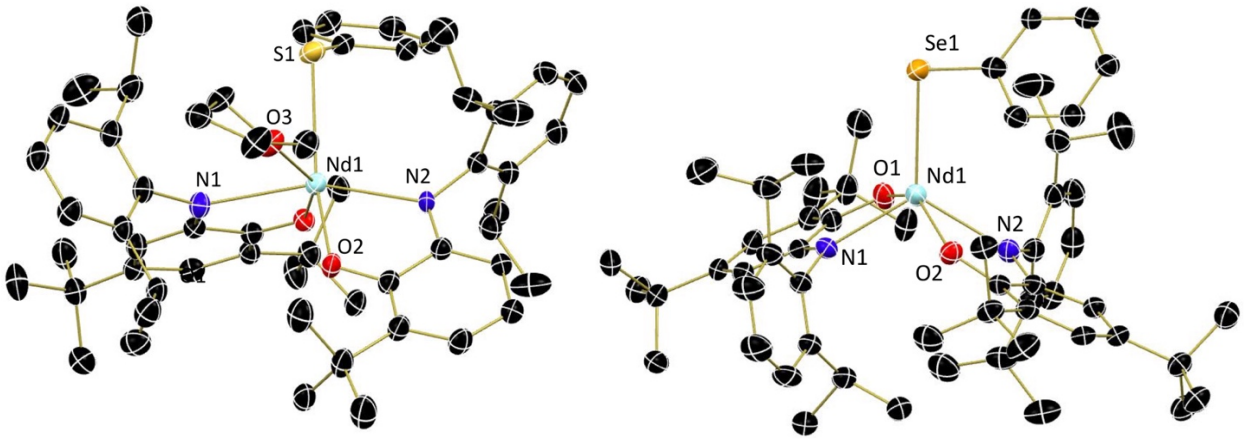

Figure 1.21: Molecular structures of **Nd-iq/isq-SPh crown** and **Nd-iq/isq-SePh crown**. **Nd-iq/isq-SPh crown** (left) and **Nd-iq/isq-SePh crown** (right) shown with 30% probability ellipsoids and hydrogen atoms, co-crystallized solvent molecules and potassium cations with coordinated 18-C-6 have been omitted for clarity.

Crystals of **Nd-iq/isq-SPh crown** and **Nd-iq/isq-SePh crown** were obtained from concentrated toluene solutions stored at -35 ºC. Each structure features the neodymium center bound by two iminoquinone ligands, as well as an "E-Phenyl" fragment. The size of the chalcogen plays a role in the coordination sphere of the neodymium, with **Nd-iq/isq-SPh crown** complex having room for a THF molecule to bind. For the larger **Nd-iq/isq-SePh crown** complex, no THF binding is observed.

The Nd-Se distance of 2.8958(15) Å is quite long, likely due to the large ionic radius of selenium. By comparison, the smaller sulfur atom shortens the bond in **Nd-iq/isq-SPh crown** to 2.8134(18) Å. The Nd-E-Ph (E = S, Se) angles of 100.5(2)º (E = S) 98.2(5)º (E = Se) are rather

acute, considering that the hybridization of the E-atom is sp^3, with expected angles of 109.5. This decrease in angle can be a result of a few factors. According to VSEPR theory, having multiple lone pairs can cause a decrease in the Nd-E-Ph, as the lone pairs are held closer to the E atom, pushing the two bonds together. Another reason could be the ionic nature of the Nd-E bond, which doesn't retain a strong bond angle preference like one would expect for a covalent bond.

Having a closer look at the intraligand bond distances of **Nd-iq/isq-SPh crown** and **Nd-iq/isq-SePh crown** confirm one-electron oxidation of the neodymium complex, with asymmetric ligands in different oxidation states. For example, **Nd-iq/isq-SePh crown** shows two distinct ligand environments. The Nd-N distance of the ap^{2-} is quite short at 2.343(4) Å, especially when compared to the analogous distance of 2.487(4) Å for the isq^{1-} ligand. A similar trend of shorter bonds for the ap^{2-} ligand is observed for the Nd-O distances (2.185(6) Å vs. 2.313(3) Å). The ap^{2-} ligand displays lengthened C-O (1.346(6) Å) and C-N (1.396(6) Å) bonds when compared to the isq^{1-} C-O (1.307(11) Å) and C-N (1.365(11) Å) bonds. Additional evidence can be found in the C-C bonds of the ring, with the similar distances of the ap^{2-} ligand suggesting aromaticity. One can also compare these intraligand distances to those of the reduction series (**Nd-iq**, **Nd-isq** and **Nd-ap crown**) and come to the same conclusion.

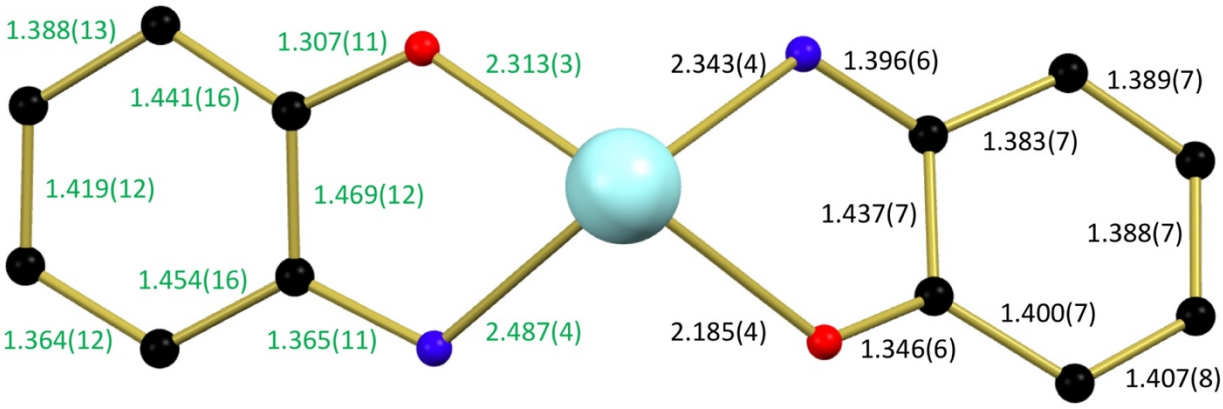

Figure 1.22: Bond distance (Å) comparison for the asymmetric ligands of **Nd-iq/isq-SePh crown**.

The ability to oxidize just one ligand using diphenyl dichalcogenides to create new Nd-E bonds is demonstrated. Corroborating evidence of the one-electron oxidation was provided by single crystal X-ray crystallography. These structures show two distinct ligand environments, with one ligand in the ap^{2-} form and the other in the isq^{1-} form.

1.6 Reactivity with Aryl Azides

1.6.1 Introduction

The chemistry of the *f*-block is underexplored when compared to other elements of the periodic table. The lanthanides commonly exist in the Ln^{3+} form, and typically do not engage in redox chemistry. Consequently, lanthanides are generally unable to perform multi-electron organometallic transformations and support multiply-bonded species. For transition metals, metal-element multiple bonds have proven to be some of the most challenging, yet fruitful interactions to study (i.e. olefin metathesis catalysis). Despite thorough investigation of metal-element multiple bonds, no examples of such bonding motifs exist with the trivalent lanthanides.

The first part of this chapter demonstrates the iminoquinone ligand can mediate multi-electron transformations at a lanthanide metal center. Specifically, the electrons stored in the iminoquinone ligand can be used to activate elemental chalcogenides, displaying multi-electron chemistry is possible with lanthanides through ligand mediation. Building on these results, we sought to construct lanthanide-element multiple bonds through redox-active ligand meditated processes. This novel approach could extend the study of multiple bonds to new elements on the periodic table – allowing for rich comparison of bonding and reactivity of lanthanides to that of the other groups of the periodic table.

To form these metal-ligand multiple bonds, we have activated a variety of small molecules, attempting to form imido, phosphido, oxo and silylene ligands. Thus far, the most promising reactions have been the activation of organic azides. These reactions use the electrons stored in the ligands to produce lanthanide imido complexes. The reactive imido bonding moiety can be trapped using a variety of approaches including cycloaddition, Lewis acid capping and extraction. Trivalent lanthanides, which do not have the ability to undergo the redox processes, have never been examined in this manner. These exciting new reactivity pathways for lanthanides provide promise for the synthesis of a trivalent lanthanide imido complex.

1.6.2 Neodymium Bis(amidophenolate) Reactivity with Aryl Azides

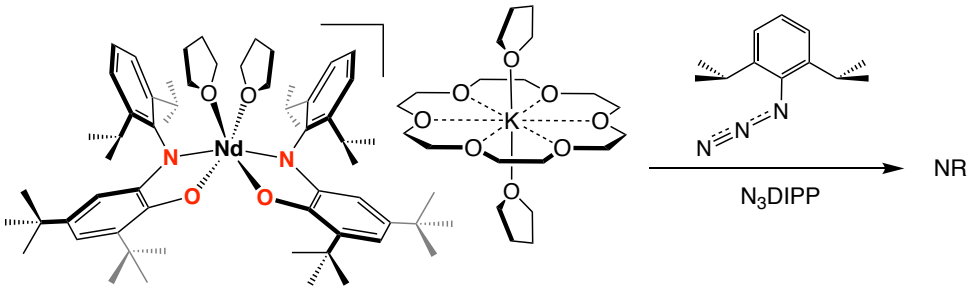

Figure 1.23: Attempted reaction of **Nd-ap crown** with dipp azide.

We initially examined the reactivity of the well-established reduction series of neodymium complexes (**Nd-iq**, **Nd-isq**, **Nd-ap** and **Nd-ap crown**) with aryl azides. **Nd-ap** and **Nd-ap crown** were targeted because of their highly reduced ligands that have shown to be reactive towards chalcogenides. As our group has had success in the past with the stability of the dipp imido fragment, we first screened the reactivity of the DIPP azide with these complexes. Unfortunately, neither of these complexes reacted with the DIPP-substituted azide, N_3DIPP. This is likely a result of steric hindrance preventing the necessary interaction of the Nd center with the nitrogen atom.

We then shifted our focus to the sterically smaller the *p*-tolyl azide. At room temperature, reaction of **Nd-ap** with the azide proceeds slowly and does not consume all of the neodymium starting material. Hypothesizing that an unstable intermediate is being formed, we aimed to stabilize this species by changing the lanthanide to one with a smaller ionic radius.

1.6.3 Ytterbium Bis(amidophenolate) Reactivity with Aryl Azides

The ionic radius of ytterbium(III) is 0.86 Å. That is 14% smaller than the ionic radius of neodymium(III) (1.00 Å). By using the isostructural **Yb-ap** and **Yb-ap crown**, we hoped to help stabilize the reactive intermediates that were being formed during the activation of aryl azides.

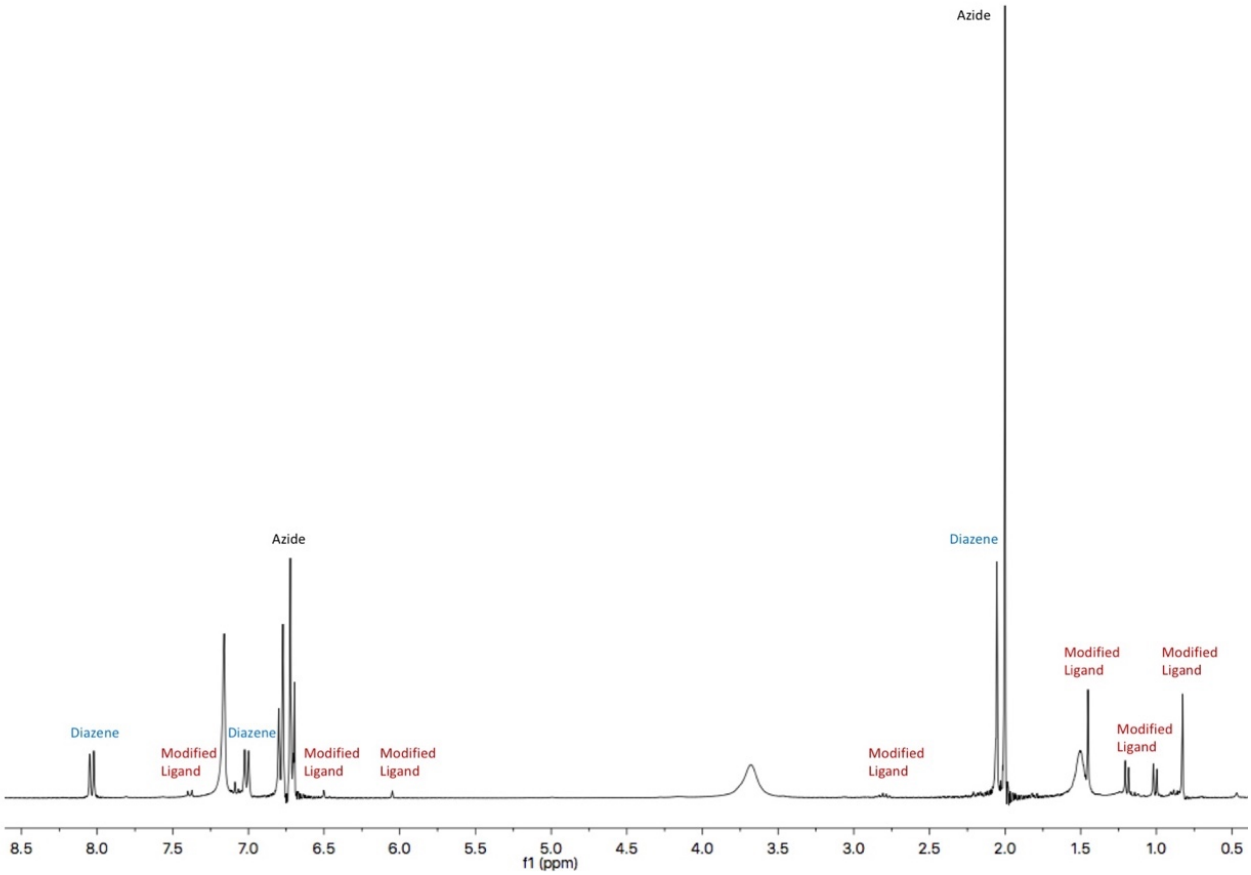

Figure 1.24: ^{1}H NMR spectrum of the crude reaction of **Yb-ap crown** with *p*-tolyl azide.

Addition of *p*-tolyl azide to a solution of the pink **Yb-ap** results in no color change or reaction. However, upon addition of 18-crown-6, an immediate color change from pink to green is observed. ^{1}H NMR spectroscopic analysis in C_6D_6 reveals a mixture of two organic products and one organometallic products. The coupled nitrene product, *p*-tolyl diazene, is observed with three resonances shifted from those of the azide. The second organic product is observed, with resonances assignable as one ^{dipp}iq ligand and one *p*-tolyl group. The assignment of this "modified-ligand product" remained a mystery until X-ray crystallographic data (*vide infra*) proved the connectivity of this species.

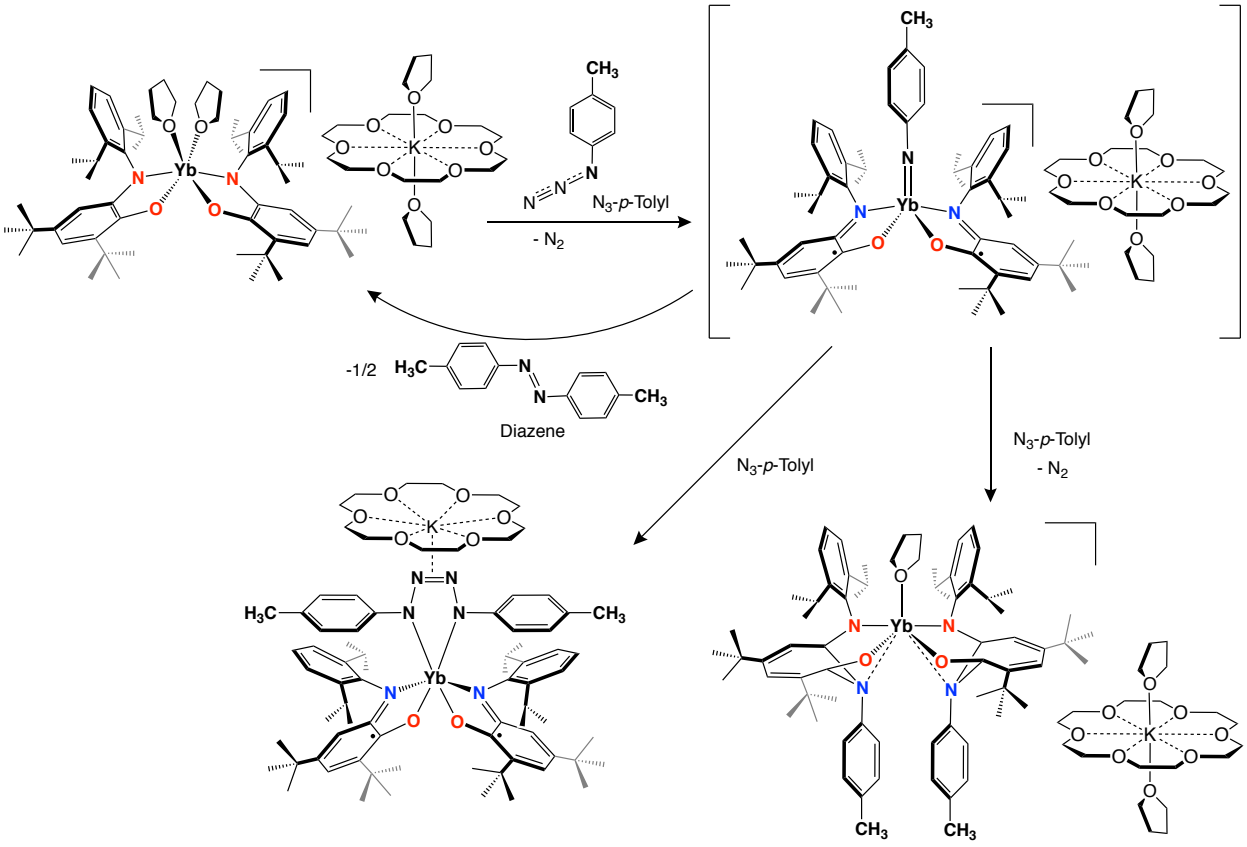

Figure 1.25: Proposed reaction scheme of **Yb-ap crown** with *p*-tolyl azide.

The production of diazene is expected, with previous reports of metal-imidos producing this product catalytically. Notably, typical metal systems use their accessible redox couples to make and break bonds. In our case, the ligand is providing the electrons but can still be produced catalytically. The "modified ligand product" was identified in attempts to crystallize the transient imido. Refinement of the data revealed that the imido fragment had inserted into a C-C bond of the ligand, creating a seven-membered ring. Interestingly, the ligand retains its redox-active nature, still able to shuttle up to two electrons.

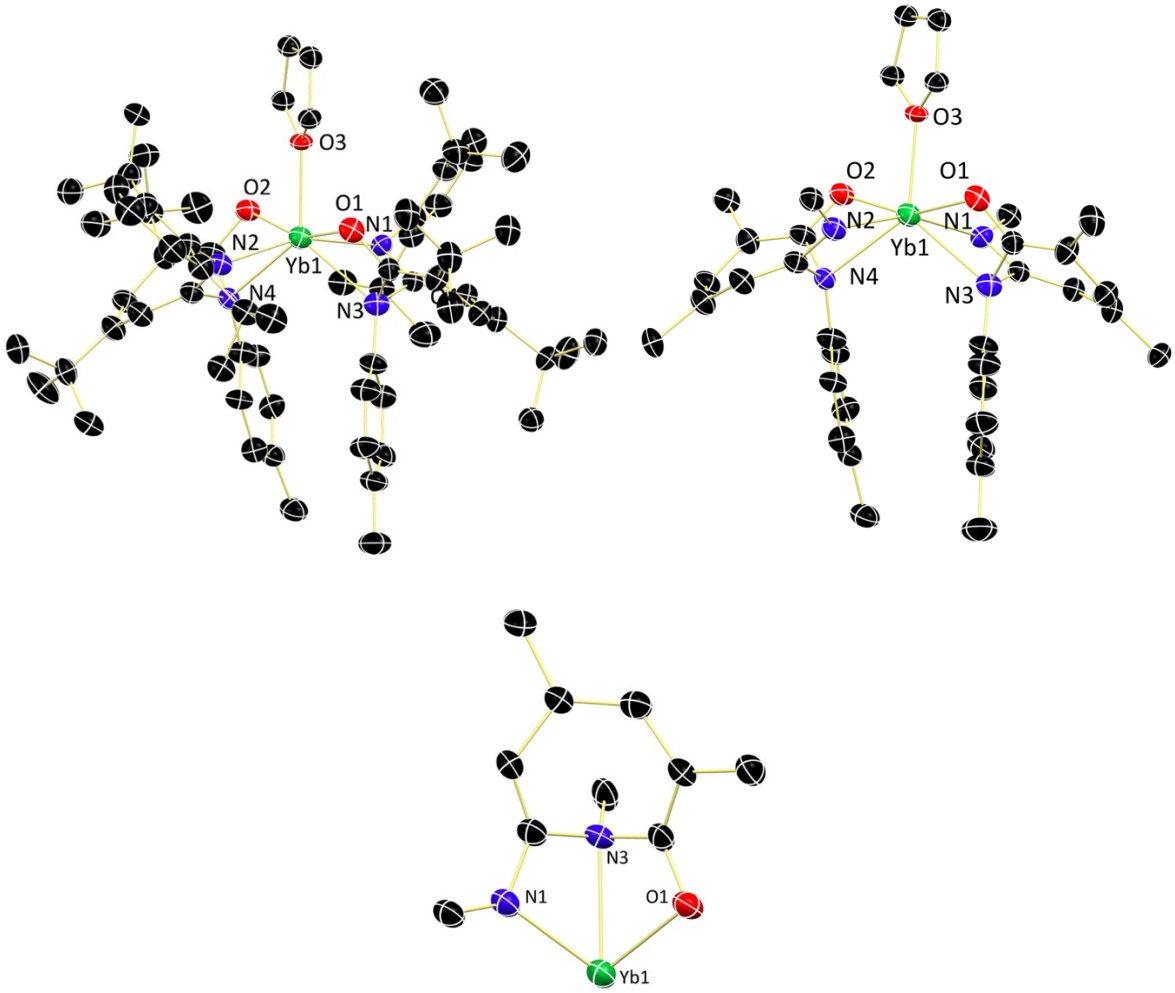

Figure 1.26: Molecular structures of the inserted ligand complex and one of its inserted rings. Inserted ligand complex (left), truncated view (right), and one of its inserted rings (bottom) shown with 30% probability ellipsoids and hydrogen atoms, co-crystallized solvent molecules, tert-butyl groups, dipp groups and potassium cations with coordinated 18-C-6 omitted for clarity.

A closer look at each ligand reveals that the new, seven membered ring has three double bonds and four single bonds, alternating about the ring. The single bonds range in length from 1.450(18) to 1.474(18) Å, while the double bonds are between 1.35(2) to 1.39(2) Å. The C-O distance is 1.319(19) Å and the C-N distance is 1.359(16) Å. These are relatively long bonds and would be considered single bonds, but do not trend well with the distances from the reduction series, possibly because of the transformation of the ring shape.

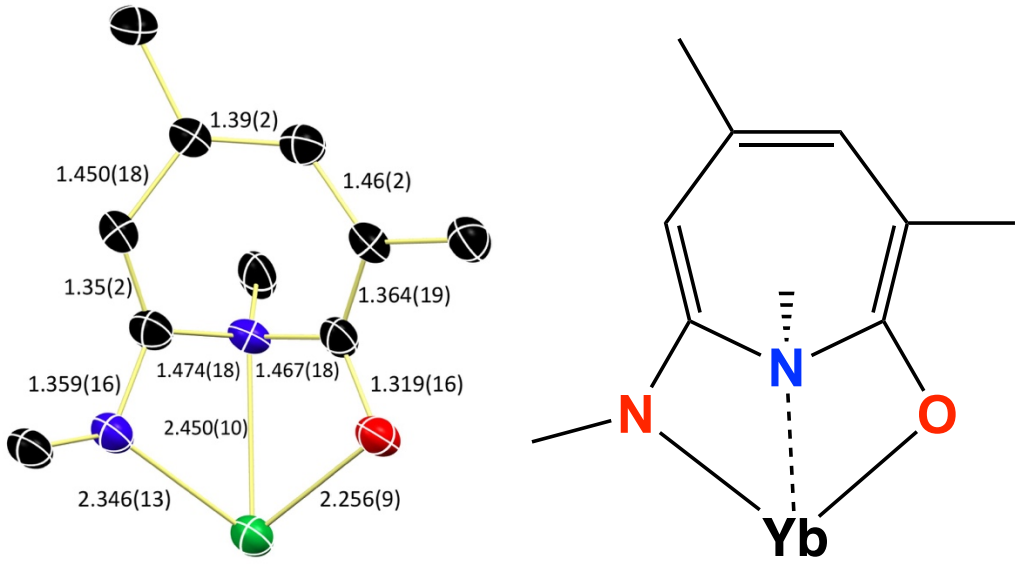

Figure 1.27: Intraligand bond distances and Chemdraw interpretation of the inserted ligand complex.

Inserted ligand ytterbium complex with bond distances(left) and Chemdraw representation (right) shown with 30% probability ellipsoids and hydrogen atoms, co-crystallized solvent molecules, *tert*-butyl groups, dipp groups and potassium cations with coordinated 18-C-6 omitted for clarity.

1.6.4 Ytterbium Tetrazine Synthesis

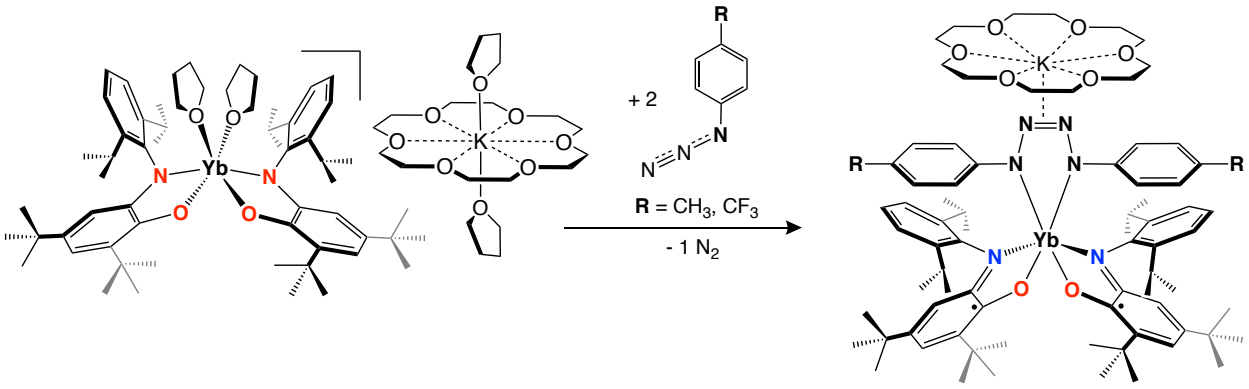

Figure 1.28: Synthesis of ytterbium tetrazine molecules.

Interested in creating a new bonding motif for lanthanides, we sought to trap the transient imido species using a [2+3] dipolar cyclo-addition. After screening a number of molecules with unsaturated pi systems (nitriles, alkenes, alkynes) we found that our transient imido reacted with azides to form a tetrazine moiety. ^{1}H NMR spectroscopic analysis in C_6D_6 shows a C_{2v} symmetric molecule, with resonances ranging from -250 to 250 ppm. Formation of the tetrazine is hypothesized to go through an imido-intermediate, after loss of N_2. As previously observed products (diazene and ligand-inserted products) has shown this intermediate to be quite reactive, careful reaction conditions were developed.

p-Tolyl azide does not react with **Yb-ap crown** below -35 ºC, however, successful conversion can be achieved at 0 ºC for 3 hours. The reaction was found to proceed smoothly in diethyl ether, with THF and toluene giving a mixture of products. Notably, the yield of the tetrazine product was increased by using an excess (~10 equivalents) of azide. This excess of azide increases the chances of the imido fragment interacting with an azide molecule and cycloadding to form the tetrazene before it can find an alternative way to decompose (diazene, ligand insertion).

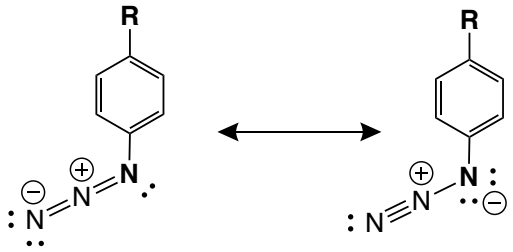

Figure 1.29: Aryl azide resonance structures.
Substitution of the phenyl ring can influence the electronic structure of the N_3 fragment.

It was hypothesized that the thermodynamic barrier of the reaction was azide activation (loss of N_2). To test this theory, an azide that is easier to activate was examined. *p*-CF_3 azide, with

its electron withdrawing group, activates the azide by stabilizing electron density on the nearest nitrogen (the favored resonance structure for loss of N_2). Indeed, the reaction of with **Yb-ap crown** proceeded immediately at -108 ºC, producing a blue/green solution in seconds. Upon workup, a brown material was isolated in good (73%) yield. ^{1}H NMR analysis in C_6D_6 shows a C_{2v} symmetric molecule, with resonances almost identical to that of **Yb-isq-PTol-Tet**. Notably, one resonance at 10.30 ppm is missing, with integration of 6 protons, identified at the *p*-tolyl group. By ^{19}F NMR, a resonance is observed at 52.95 ppm that is assignable as the *p*-CF_3 group of the tetrazine. These spectroscopic data suggest the isostructural product **Yb-isq-PCF$_3$-Tet** is being produced. To confirm this theory, further characterization was carried out.

1.6.5 X-Ray Crystallography of **Yb-isq-*p*Tol-Tet** and **Yb-isq-*p*CF$_3$-Tet**

To aid in product assignment and examine bonding structure, single crystal X-ray diffraction was carried out on **Yb-isq-*p*Tol-Tet** and **Yb-isq-*p*CF$_3$-Tet.** We hypothesized that each ligand was oxidized by one electron to form the iminosemiquinone form, featuring ligand radicals. To confirm this, we examined the intraligand bond distances to help assign the oxidation states of the ligands.

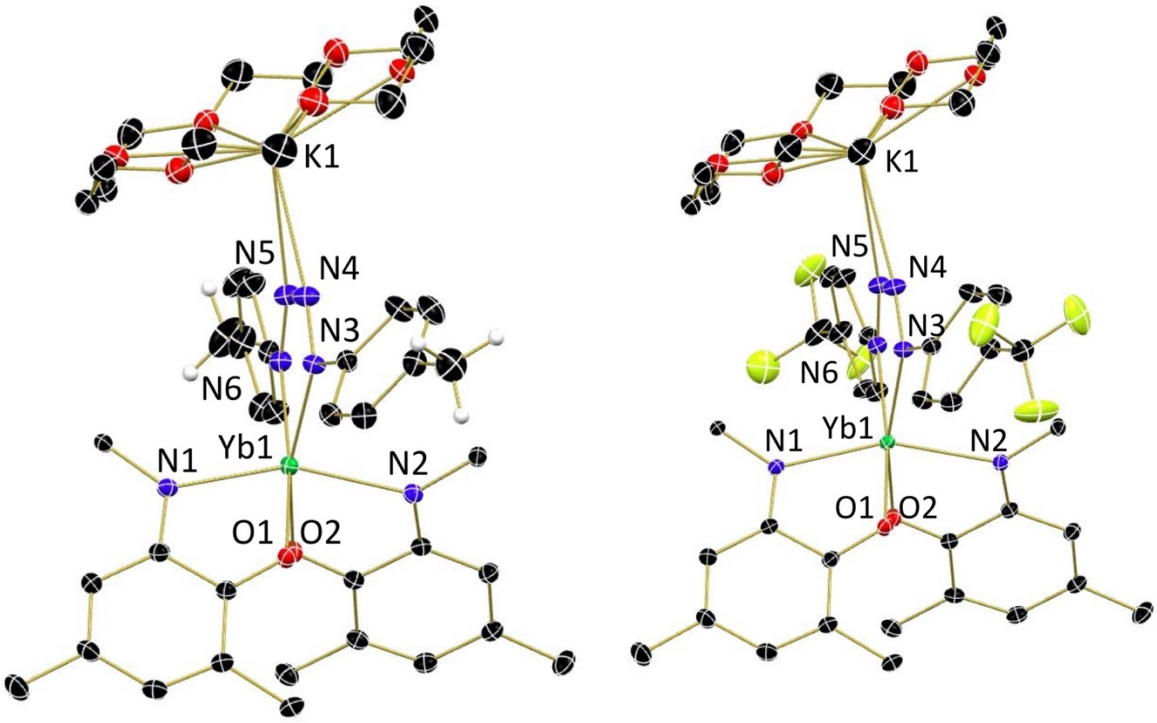

Figure 1.30: Molecular structure of **Yb-isq-PTol-Tet** and **Yb-isq-PCF$_3$-Tet**.

Molecular structure of Yb-isq-PTol-Tet (left) and Yb-isq-PCF3-Tet (right) shown with 30% probability ellipsoids and hydrogen atoms, co-crystallized solvent molecules, *tert*-butyl and dipp groups omitted for clarity.

Single crystals of **Yb-isq-PTol-Tet** and **Yb-isq-PCF$_3$-Tet** were both obtained from concentrated diethyl ether solutions stored at -35 ºC. Both structures crystallize in the P21/n space group with identical unit cell parameters. Each structure features two ligands and a 5 membered metallocycle with 4 nitrogen atoms. The 18-crown-6 chelated potassium ion interacts with the electron rich N-N bond of the tetrazine moiety, literally crowning each complex.

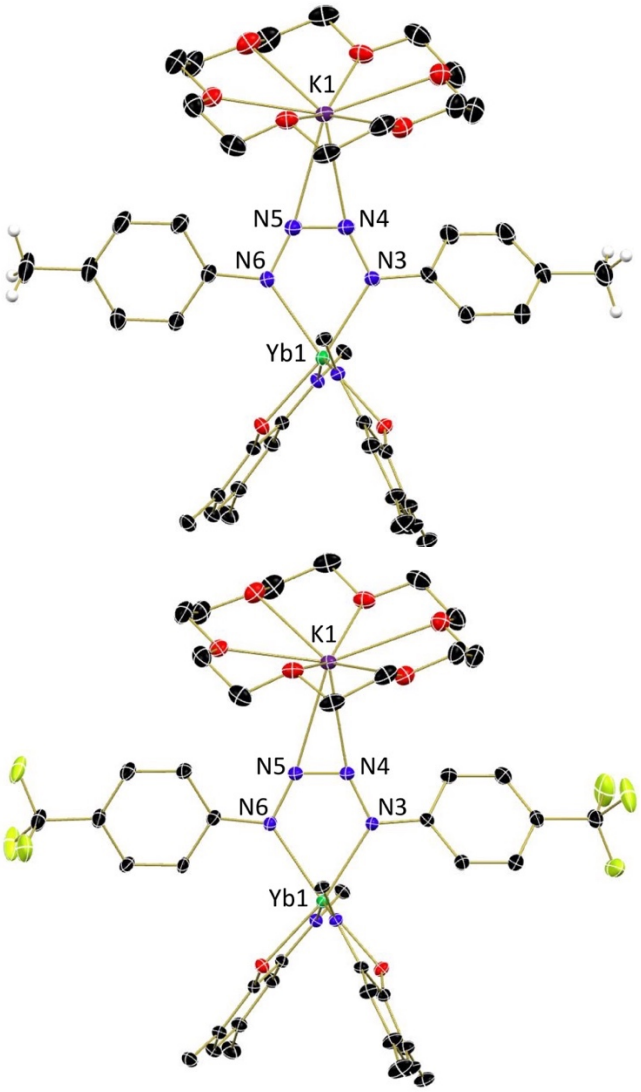

Figure 1.31: Molecular structure of **Yb-isq-pTol-Tet** and **Yb-isq-pCF$_3$-Tet**.

Molecular structure of Yb-isq-PTol-Tet (left) and Yb-isq-PCF$_3$-Tet (right) shown with 30% probability ellipsoids and hydrogen atoms, co-crystallized solvent molecules, *tert*-butyl and dipp groups omitted for clarity.

Of particular interest is the N3-N4, N6-N5 and N4-N5 distances, as these can be used to assign the tetrazine moiety as neutral, mono- or dianionic. For **Yb-isq-PTol-Tet**, the N3-N4 and N5-N6 distances are 1.384(3) and 1.378(3) Å, respectively. These are on the order of single bonds, especially when compared to the shorter N4-N5 distance of 1.280(3) Å, suggesting a double bond.

These distances suggest that the tetrazine motif is dianionic. A similar trend is observed for **Yb-isq-PCF$_3$-Tet**, with only minor differences (within error) between the structures.

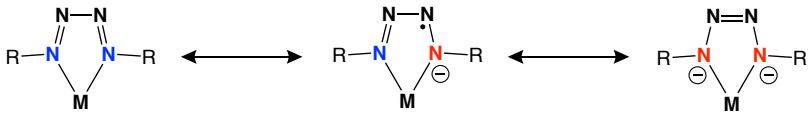

Figure 1.32: Electronic structures of the tetrazine moiety.
Blue denotes neutral bonding atoms while red indicates anionic bonding ones.

As with other iminoquinone containing complexes, intraligand bond distances provide a measure of the oxidation state of the ligand. In **Yb-isq-PTol-Tet** and **Yb-isq-PCF$_3$-Tet**, the ligands appear crystallographically symmetric, with C-O, C-N and C-C bond distances indicating the ligands are in the monoanionic, iminosemiquinone form. One interesting observation in bond lengths in the Yb-O and Yb-N distances. For **Yb-isq-PTol-Tet**, the Yb-N distances for each ligand are 2.4104(19) and 2.3929(19) Å, which are longer than those for the **Yb-isq-PCF$_3$-Tet** (2.3828(18) and 2.3696(19) Å). This shortening of the Yb-N bonds are likely a result of the electron deficient Yb center, as a result of the electron-withdrawing CF_3 groups of the tetrazine fragment. This allows the anionic ligands to get closer to the ytterbium center. A similar shortening is noted for the Yb-O distances of **Yb-isq-PTol-Tet** and **Yb-isq-PCF$_3$-Tet**.

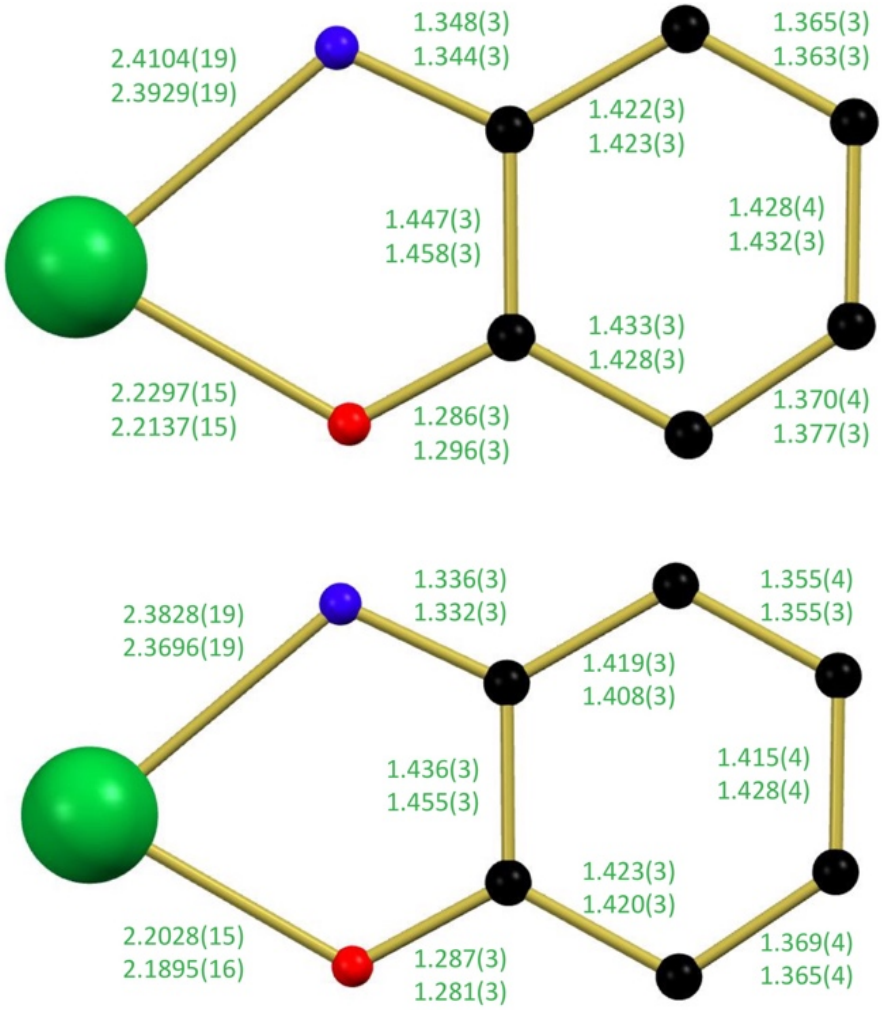

Figure 1.33: Bond distance (Å) comparison for the symmetric ligands of **Yb-isq-PTol-Tet** (top) and **Yb-isq-PCF$_3$-Tet** (bottom).

1.7 Conclusion

In summary, a series of bis(ligand) neodymium complexes was synthesized featuring ligands in three different oxidation states. These species were fully characterized and the most electron-rich derivative, **Nd-ap crown**, was used as a potent reductant towards elemental chalcogens. Products from these reaction are complexes that feature rare 6-membered metallacycles (**Nd-isq-**

S_5 crown and **Nd-isq-Se_5 crown**) in a twist-boat conformation. The selenium example is the first for an *f*-element. The redox chemistry noted here is significant, as rare earth element complexes are not commonly known to participate in multi-electron processes. With this in mind, we expanded our scope to include other lanthanides (Gd and Yb) and examined reactivity with aryl azides. We have isolated the first two lanthanide tetrazine molecules and have evidence for the first trivalent lanthanide imido. These feats highlight the cooperative electron movement using redox-active ligands that has been exploited to facilitate organometallic processes and metal-element multiple bond formation in the d-block and actinide series. Future work will focus on extending this principle to other Rare Earth elements to help expand their utility past their typical Lewis acidic, magnetic, and luminescent properties.

1.8 References

[1] M. Murugesu, E. J. Schelter, *Inorg. Chem.* **2016**, *55*, 9951-9953.

[2] N. N. Greenwood, A. Earnshaw, *Chemistry of the Elements*, 2nd ed., Butterworth Heinemann, Oxford, **1998**.

[3] T. W. Myers, A. L. Holmes, L. A. Berben, *Inorg. Chem.* **2012**, *51*, 8997–9004.

[4] B. E. Cole, J. P. Wolbach, W. G. Dougherty, N. A. Piro, W. S. Kassel, C. R. Graves, *Inorg. Chem.* **2014**, *53*, 3899-3906.

[5] P. J. Chirik, *Acc. Chem. Res.* **2015**, *48*, 1687-1695.

[6] N. H. Anderson, S. O. Odoh, Y. Yao, U. J. Williams, B. A. Schaefer, J. J. Kiernicki, A. J. Lewis, M. D. Goshert, P. E. Fanwick, E. J. Schelter, J. R. Walensky, L. Gagliardi, S. C. Bart, *Nat. Chem.* **2014**, *6*, 919-926.

[7] E. Lu, S. T. Liddle, *Dalton Trans.* **2015**, *44*, 12924-12941.

[8] S. Demir, M. Nippe, M. I. Gonzalez, J. R. Long, *Chem. Sci.* **2014**, *5*, 4701-4711.

[9] H. Sugiyama, I. Korobkov, S. Gambarotta, A. Möller, P. H. M. Budzelaar, *Inorg. Chem.* **2004**, *43*, 5771-5779.

[10] E. J. Schelter, R. Wu, J. M. Veauthier, E. D. Bauer, C. H. Booth, R. K. Thomson, C. R. Graves, K. D. John, B. L. Scott, J. D. Thompson, D. E. Morris, J. L. Kiplinger, *Inorg. Chem.* **2010**, *49*, 1995-2007.

[11] J. A. Bogart, A. J. Lewis, S. A. Medling, N. A. Piro, P. J. Carroll, C. H. Booth, E. J. Schelter, *Inorg. Chem.* **2013**, *52*, 11600-11607.

[12] J. E. Kim, J. A. Bogart, P. J. Carroll, E. J. Schelter, *Inorg. Chem.* **2016**, *55*, 775-784.

[13] I. L. Fedushkin, O. V. Maslova, A. G. Morozov, S. Dechert, S. Demeshko, F. Meyer, *Angew. Chem., Int. Ed.* **2012**, *51*, 10584-10587.

[14] I. L. Fedushkin, O. V. Maslova, E. V. Baranov, A. S. Shavyrin, *Inorg. Chem.* **2009**, *48*, 2355-2357.

[15] C. Camp, V. Guidal, B. Biswas, J. Pecaut, L. Dubois, M. Mazzanti, *Chem. Sci.* **2012**, *3*, 2433-2448.

[16] W. Huang, P. L. Diaconescu, *Inorg. Chem.* **2016**, *55*, 10013-10023.

[17] E. M. Matson, S. R. Opperwall, P. E. Fanwick, S. C. Bart, *Inorg. Chem.* **2013**, *52*, 7295-7304.

[18] A. B. Pangborn; M. A. Giardello, R. H. Grubbs, R. K. Rosen, F. J. Timmers, *Organometallics* **1996**, *15*, 1518.

[19] K. Izod, S. T. Liddle; W. Clegg, *Inorg Chem.* **2004**, *43*, 214.

[20] G. A. Abakumov, V. K. Cherkasov, A. V. Piskunov, I. N. Mescheryakova, A. V. Maleeva, A. I. Poddel'skii, G. K. Fukin, *Doklady Chem.* **2009**, *427*, 168.

[21] S. Chakraborty, J. Chattopadhyay, W. Guo, W. E. Billups, *Angew. Chem., Int. Ed.* **2007**, *46*, 4486.

[22] Nonius. Delft, The Netherlands **1998**.

[23] Rigaku Corp. Rigaku Corporation: The Woodlands, TX **2014**.

[24] Z. Otwinowski, W. Minor, *In Methods in Enzymology*, **1997**, Vol. 276, 326.

[25] Bruker (**2016**). Apex3 v2016.9-0, Saint V8.34A,SAINT V8.37A, Bruker AXS Inc.: Madison (WI), USA 2013/2014.

[26] G. M. Sheldrick. "Crystal structure refinement with SHELXL", *Acta Cryst. C*, **2015**, *71*, 3.

[27] C. B. Hübschle, G. M. Sheldrick, B. Dittrich, *J. Appl. Cryst.*, **2011**, *44*, 1281.

[28] S. C. Bart, K. Chlopek, E. Bill, M. W. Bouwkamp, E. Lobkovsky, F. Neese, K. Wieghardt, P. J. Chirik, *J. Am. Chem. Soc.* **2006**, *128*, 13901-13912.

[29] S. M. Carter, A. Sia, M. J. Shaw, A. F. Heyduk, *J. Am. Chem. Soc.* **2008**, *130*, 5838-5839.

[30] C. Camp, M. A. Antunes, G. Garcia, I. Ciofini, I. C. Santos, J. Pecaut, M. Almeida, J. Marcalo, M. Mazzanti, *Chemical Science* **2014**, *5*, 841-846.

[31] S. M. Franke, F. W. Heinemann, K. Meyer, *Chemical Science* **2014**, *5*, 942-950.

[32] D. A. Wrobleski, D. T. Cromer, J. V. Ortiz, T. B. Rauchfuss, R. R. Ryan, A. P. Sattelberger, *J. Am. Chem. Soc.* **1986**, *108*, 174-175.

[33] M. Kuhling, R. McDonald, P. Liebing, L. Hilfert, M. J. Ferguson, J. Takats, F. T. Edelmann, *Dalton Trans.* **2016**, *45*, 10118-10121.

[34] N. Tzavellas, N. Klouras, C. P. Raptopoulou, *Z. Anorg. Allg. Chem.* **1997**, *623*, 384-388.

[35] A. Kromm, Y. Geldmacher, W. S. Sheldrick, *Z. Anorg. Allg. Chem.* **2008**, *634*, 2191-2198.

CHAPTER 2. ELECTRONIC STRUCTURE AND U-O BOND ACTIVATION OF URANYL (UO_2^{2+}) IMINOQUINONE COMPLEXES

2.1 Introduction

The uranyl ion, $[UO_2]^{2+}$, is the most recognizable actinide containing species due to its prevalence in aqueous environments and in the solid state.[1] Characterized by its robust *trans*-oxo ligands and +6 oxidation state, derivatives of this ion form naturally from interactions of water with uranium ore deposits, as well as anthropogenically from depleted uranium targets,[2] nuclear waste streams,[3] and uranium mining.[4] The high solubility of this ion in water is problematic as its increased mobility in this form causes environmental contamination. In anaerobic environments, uranyl can be reduced to its +5 (unstable) and +4 (stable) forms, greatly reducing its water solubility and facilitating removal from the environment.[5]

The persistence of uranyl is attributed to its strong uranium-oxygen bonds, which are not easily functionalized or cleaved. Taking inspiration from Nature, recent work in non-aqueous uranyl chemistry has demonstrated that transformation of $U\text{-}O_{uranyl}$ bonds may be facilitated by reduction events to generate U(IV) ions, in which pentavalent intermediates are likely involved. One strategy, demonstrated by Duval and co-workers, involves the photochemical reduction of hexavalent $[UO_2(dppmo)_2(OPPh_3)][\ OTf]_2$ (dppmo = $Ph_2P(O)CH_2P(O)Ph_2$) in the presence of BF_4^- anions, producing the corresponding uranium(IV) difluoride species.[6] Reductive silylation of the uranyl ion has also been studied[7-13] and optimized,[7] while strongly Lewis acidic titanium[14] and borane[15] compounds have also proven to be potent reductants for the generation of uranium (IV) *via* $U\text{-}O_{uranyl}$ bond activation. P. Arnold and co-workers have pioneered the use of a specialized dipyrrin ligand and strongly Lewis acidic atoms to facilitate uranyl functionalization by shifting the U(V) – U(IV) reduction into an accessible redox range. More recently, work from their lab has

also demonstrated reduction of the terminal oxos in uranyl using silanes or boranes.[16] In each case, the corresponding silyl and boryl ethers are released, showing full U-O_{uranyl} bond scission.

The Bart lab has reported the utility of redox-active ligands in uranyl functionalization and U-O_{uranyl} bond scission as well. Treating Cp*UO_2(^{Mes}PDI^{Me}) (Cp* = 1,2,3,4,5-pentamethylcyclopentadienide; ^{Mes}PDI^{Me} = 2,6-((Mes)N=CMe)$_2$-C_5H_3N; Mes = 2,4,6-trimethylphenyl), which contains a singly reduced pyridine(diimine) ligand and a hexavalent uranyl ion, with stoichiometric equivalents of Me_3SiI results in stepwise oxo silylation to form tetravalent $(Me_3SiO)_2UI_2$(^{Mes}PDI^{Me}).[17] Additional equivalents of Me_3SiI results in full uranium-oxo bond cleavage and the formation of UI_4(1,4-dioxane)$_2$ with extrusion of hexamethyldisiloxane. The necessary electron equivalents derive from the reduced pyridine(diimine) ligand and loss of the Cp* ring in this example.

Much of the work in uranyl functionalization is based on silylation and borylation of U-O_{uranyl} bonds, with formation of O-Si and O-B bonds acting as a strong thermodynamic driving force. Currently, there are no examples of transformations of U-O_{uranyl} bonds where O-C bonds are formed. We hypothesized that U-O_{uranyl} bonds could undergo such a conversion with electrophilic carbon-containing substrates when mediated by reduced redox-active ligands. The iminoquinone family would be effective for such a task, as this ligand set has mediated multi-electron reactions with low-valent metals[18-23] and would obviate the need for an external reductant by its ability to exist in a reduced state (Figure 1). The most oxidized form of this ligand, the iminoquinone (iq^0), can be reduced to the iminosemiquinone (isq^{1-}), which is characterized by a ligand radical. Further reduction results in the formation of the amidophenolate ligand (ap^{2-}), which stores two electrons in its π^* orbitals.[24]

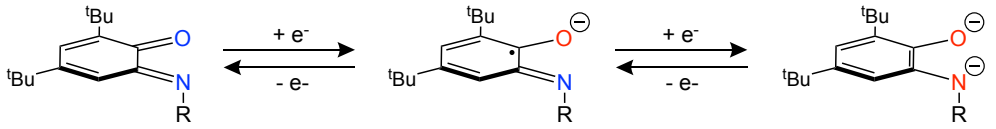

Figure 2.1: Redox chemistry demonstrated by the iminoquinone/amidophenolate ligand. Red atoms denote anionic bonds, while blue atoms engage in dative (neutral) bonding.

Herein, we report a new series of uranyl derivatives containing redox-active iminoquinone/amidophenolate ligands. Storing electrons in this ligand framework generates uranyl complexes with unprecedented electronic structures, including an unusual diradical species. These ligands facilitate multi-electron chemistry at uranyl centers, allowing the complete functionalization and removal of the robust *trans*-oxo ligands through borylation and acylation reactions. Full spectroscopic, structural, and magnetic characterization is provided, as well as isotopic labeling experiments to highlight the transformation of the uranyl moiety.

2.2 Experimental

2.2.1 General Considerations

All air- and moisture-sensitive manipulations were performed using standard Schlenk techniques or in an MBraun inert atmosphere drybox with an atmosphere of purified nitrogen. The MBraun drybox was equipped with a cold well used for freezing samples in liquid nitrogen as well as two -35 °C freezers for cooling samples and crystallizations. Solvents for sensitive manipulations were dried and deoxygenated using literature procedures with a Seca solvent purification system.[25] Water (^{18}O, 97%) was purchased from Cambridge Isotope Laboratories and used as received. Benzene-d_6 was purchased from Cambridge Isotope Laboratories, dried with molecular sieves and sodium and degassed by three freeze–pump–thaw cycles. Chloroform-*d* and pyridine-d_5 were purchased from Cambridge Isotope Laboratories, dried with molecular sieves,

and degassed by three freeze–pump–thaw cycles. 4,6-di-*tert*-butyl-2-[(2,6-diisopropylphenyl)imino]quinone (^{dipp}iq)[23], potassium graphite (KC_8)[26], uranyl dichloride ($[UO_2Cl_2(THF)_2]_2$)[27], uranyl triflate $UO_2(OTf)_2(THF)_3$[28], and uranium tetrachloride (UCl_4)[29] were prepared according to literature procedures. 18-crown-6 (18-C-6) and B-chlorocatecholborane (Cl-BCat) were purchased from Sigma Aldrich and dried under vacuum on a Schlenk line overnight prior to use. Pivaloyl chloride (Piv-Cl) was purchased from Sigma Aldrich, degassed by three freeze–pump–thaw cycles, and dried with molecular sieves prior to use.

^{1}H NMR spectra were recorded on a Varian Inova 300 or Bruker AV-III-400-HD spectrometer operating at 299.99 and 400.13 MHz, respectively. All chemical shifts are reported relative to the peak for $SiMe_4$, using ^{1}H (residual) chemical shifts of the solvent as a secondary standard. ^{13}C{^{1}H} NMR spectra were recorded on a Bruker AV-III-HD spectrometer operating at 100.61 MHz. ^{19}F NMR spectra were recorded on a Bruker AV-III-HD spectrometer operating at 376.50 MHz. ^{11}B NMR spectra were recorded on a Varian Inova 300 spectrometer operating at a frequency of 96.24 MHz. ^{11}B chemical shifts are reported relative to the peak for BF_3•Et_2O (0.0 ppm). The spectra for all paramagnetic molecules were obtained by using an acquisition time of 0.5 s, thus, the peak widths reported have an error of ±2 Hz. For all paramagnetic molecules, the ^{1}H NMR data are reported with the chemical shift, followed by the peak width at half height in Hz, the integration value, and, where possible, the peak assignment. All voltammetric data were obtained under inert atmosphere conditions using external electrical ports of the MBraun inert drybox. All data were obtained using a Gamry Instruments Interface 1000 model potentiostat using the Gamry Instruments Laboratory software. All data were collected on samples in THF with 0.1 M $[Bu_4N][PF_6]$ supporting electrolyte concentration, and using an internal resistance compensation of approximately 2000 ohms. Solutions were analyzed in 10 mL beakers, with a 3

mm glassy carbon working electrode, a Pt wire counter electrode, and an Ag wire quasi-reference electrode. Potential corrections were performed at the end of the experiment using the Fc/Fc^+ couple as an internal standard. X-Band EPR spectra were recorded on a Bruker EMX EPR spectrometer and simulated using the EasySpin toolbox in MATLAB. Electronic absorption measurements were recorded at 294 K in THF in sealed, 1 cm quartz cuvettes with a Cary 6000i UV-vis-NIR spectrophotometer. Elemental analyses were performed by Midwest Microlab (Indianapolis, IN). Solid state infrared spectra were recorded using a Thermo Nicolet 6700 spectrophotometer.

2.2.2 Synthetic Details

Synthesis of (^{dipp}iq)$UO_2(OTf)_2$THF (**UO_2-iq**). A 20-mL scintillation vial was charged with $UO_2(OTf)_2(THF)_3$ (0.100 g, 0.176 mmol) and 5 mL diethyl ether. A separate 20-mL scintillation vial was charged with ^{dipp}iq (0.067 g, 0.176 mmol), dissolved in 5 mL diethyl ether and added dropwise to the stirring $UO_2(OTf)_2(THF)_3$ slurry. A reddish-brown solution was observed. After 6 hours, the volatiles were removed *in vacuo.* The resulting reddish-purple solid was washed with cold diethyl ether (3 × 10 mL) to afford a red powder (0.106 g, 0.132 mmol, 75% yield) assigned as **UO_2-iq**. X-ray quality crystals were obtained from a concentrated toluene solution stored at -35 °C. Elemental analysis of $C_{32}H_{45}NO_{10}F_6S_2U$: Calculated, C, 37.69; H, 4.45; N, 1.37. Found, C, 38.07; H, 4.80; N, 1.29. ^{1}H NMR (C_6D_6, 300MHz, 25 °C): δ = 0.64 (s, 9H, C(C*H*$_3$)$_3$), 0.84 (d, 7, 6H, CH(C*H*$_3$)$_2$), 1.21 (d, 7, 6H, CH(C*H*$_3$)$_2$), 1.44 (s, 9H, C(C*H*$_3$)$_3$), 1.93 (br s, 4H, THF), 2.70 (sept, 7, 2H, C*H*(CH$_3$)$_2$), 5.26 (br s, 4H, THF), 6.17 (d, 2, 1H, C*H*), 7.28 (d, 2, 1H, C*H*), 7.31 (s, 2H, C*H*), 7.28 (s, 1H, C*H*). ^{1}H NMR ($CDCl_3$, 400 MHz, 25 °C): δ = 1.03 (d, 6.8, 6H, CH(C*H*$_3$)$_2$), 1.04 (d, 6.8, 6H, CH(C*H*$_3$)$_2$), 1.19 (s, 9H, C(C*H*$_3$)$_3$), 1.72 (s, 9H, C(C*H*$_3$)$_3$), 2.46 (br s, 4H, THF), 2.53 (sept, 6.8, 2H, C*H*(CH$_3$)$_2$), 5.21 (br s, 4H, THF), 6.21 (s, 1H, C*H*), 7.45 (d, 7.7, 2H, C*H*), 7.53 (t,

7.7, 2H, C*H*), 7.28 (s, 1H, C*H*). $^{13}C\{^{1}H\}$ NMR ($CDCl_3$, 100 MHz, 25 °C): δ = 22.66, 24.99, 26.35, 27.89, 29.10, 36.16, 36.50, 116.36, 124.85, 129.64, 138.11, 143.90, 145.39, 150.40, 160.90, 169.15, 195.99. ^{19}F NMR ($CDCl_3$, 376.5 MHz, 25 °C): δ = -78.10.

Synthesis of $(^{dipp}isq)_2UO_2THF$ (**UO_2-isq**). A 20-mL scintillation vial was charged with $[UO_2Cl_2(THF)_2]_2$ (0.100 g, 0.103 mmol) and 5 mL THF. A separate 20-mL scintillation vial was charged with ^{dipp}iq (0.156 g, 0.412 mmol), dissolved in 5 mL THF and added dropwise to the stirring $[UO_2Cl_2(THF)_2]_2$ slurry. After stirring for 15 minutes, KC_8 (0.056 g, 0.412 mmol) was weighed by difference and added over 5 minutes, resulting in a rapid color change from red to dark green. After 2 hours, the slurry was filtered through Celite and volatiles were removed *in vacuo*. The remaining mixture was recrystallized from *n*-pentane to afford a green powder (0.152 g, 0.138 mmol, 67% yield) assigned as **UO_2-isq**. Single, X-ray quality crystals were obtained from a concentrated diethyl ether solution at -35 °C. Elemental analysis of $C_{56}H_{82}N_2O_5U$: Calculated, C, 61.07; H, 7.51; N, 2.54. Found, C, 60.94; H, 7.70; N, 2.22. ^{1}H NMR (C_6D_6, 300MHz, 25 °C): δ = 0.05 (br s), 1.50 (br s), 2.47 (br s), 3.68 (br s), 3.89 (br s), 6.86 (br s), 7.70 (br s), 16.47 (br s), 53.64 (br s).

Synthesis of $[[(^{dipp}ap)_2U][K(THF)_2]_2]_2$ (**UO_2-ap**) from **UO_2-isq**. A 20-mL scintillation vial was charged with **UO_2-isq** (0.100 g, 0.091 mmol) and 10 mL THF. While stirring, KC_8 (0.025 g, 0.181 mmol) was weighed by difference and added over 5 minutes, resulting in a rapid color change from dark green to black. After 1 hour, the solution was filtered through Celite and volatiles were removed *in vacuo*. The crude mixture was washed with 10 mL cold *n*-pentane to afford a tan powder (0.140 g, 0.056 mmol, 62% yield) assigned as **UO_2-ap**. Single, X-ray quality crystals were obtained from a concentrated diethyl ether solution at -35 °C. Elemental analysis of $C_{120}H_{180}N_4O_{12}K_4U_2$: Calculated, C, 57.58; H, 7.25; N, 2.24. Found, C, 57.84; H, 7.34; N, 2.34. ^{1}H

NMR (NC_5D_5, 300MHz, 25 °C): δ = 0.82 (d, 7, 12H, CH(C*H*$_3$)$_2$), 1.29 (d, 7, 12H, CH(C*H*$_3$)$_2$), 1.40 (s, 18H, C(C*H*$_3$)$_3$), 1.83 (s, 18H, C(C*H*$_3$)$_3$), 4.37 (sept, 7, 4H, C*H*(CH$_3$)$_2$), 5.73 (s, 2H, C*H*), 6.49 (s, 2H, C*H*), 6.80 (t, 8, 2H, C*H*), 7.02 (d, 8, 4H, C*H*). $^{13}C\{^1H\}$ NMR (NC_5D_5, 100 MHz, 25 °C): δ = 23.28, 25.48, 26.20, 26.95, 30.80, 32.39, 34.26, 34.81, 67.50, 107.69, 110.48, 122.19, 122.78, 130.77, 137.50, 148.31, 154.09, 156.96.

Synthesis of [(^{dipp}ap)$_2$UO$_2$THF][K(18-crown-6)(THF)$_2$]$_2$ (**UO$_2$-ap crown**) from **UO$_2$-ap**. A 20-mL scintillation vial was charged with **UO$_2$-ap** (0.100 g, 0.040 mmol) and 5 mL THF. While stirring, 18-crown-6 (0.042 g, 0.160 mmol) was weighed by difference and added. After 1 hour, volatiles were removed *in vacuo*. The crude mixture was washed with 10 mL cold diethyl ether to afford a white powder (0.121 g, 0.061 mmol, 76% yield) assigned as **UO$_2$-ap crown**. Single, X-ray quality crystals were obtained from a concentrated THF/toluene (1:1) solution stored at -35 °C. Elemental analysis of $C_{96}H_{162}N_2O_{21}K_2U$: Calculated, C, 57.75; H, 8.18; N, 1.40. Found, C, 57.27; H, 8.07; N, 2.14. The EA values for C and N are off by more than 0.4%, which may be an indication of decomposition as a result of the reactive nature of this complex. ^1H NMR (NC_5D_5, 300MHz, 25 °C): δ = 1.24 (d, 7, 12H, CH(C*H*$_3$)$_2$), 1.37 (d, 7, 12H, CH(C*H*$_3$)$_2$), 1.44 (s, 18H, C(C*H*$_3$)$_3$), 1.55 (s, 18H, C(C*H*$_3$)$_3$), 3.43 (s, 24H, C*H*$_2$), 4.87 (sept, 7, 4H, C*H*(CH$_3$)$_2$), 5.90 (d, 2, 2H, C*H*), 6.56 (d, 3, 2H, C*H*), 7.06 (t, 8, 2H, C*H*), 7.38 (d, 8, 4H, C*H*). $^{13}C\{^1H\}$ NMR (NC_5D_5, 100 MHz, 25 °C): δ = 23.74, 24.67, 25.49, 26.53, 26.90, 30.92, 31.33, 32.63, 33.94, 34.27, 34.96, 67.50, 70.08, 106.69, 108.35, 121.58, 122.64, 130.49, 135.82, 148.59, 153.97, 156.48, 159.31.

Synthesis of (^{dipp}iq)(^{dipp}isq)UO$_2$Cl (**UO$_2$-iq/isq**). A 20-mL scintillation vial was charged with [UO$_2$Cl$_2$(THF)$_2$]$_2$ (0.275 g, 0.283 mmol) and 8 mL THF. A separate 20-mL scintillation vial was charged with ^{dipp}iq (0.430 g, 1.133 mmol), dissolved in 10 mL THF and added dropwise to the stirring [UO$_2$Cl$_2$(THF)$_2$]$_2$ slurry. After stirring for 15 minutes, KC_8 (0.077 g, 0.567 mmol) was

weighed by difference and added over 5 minutes, resulting in a rapid color change from red to brown. After 2 hours, the slurry was filtered through Celite and volatiles were removed *in vacuo*. The brown solid was triturated with diethyl ether (2 × 10 mL) and *n*-pentane (2 × 10 mL) then dried *in vacuo*. The resulting black powder was washed with cold *n*-pentane (3 × 10 mL) to afford a greenish brown powder (0.400 g, 0.376 mmol, 66% yield) assigned as **UO_2-iq/isq**. Single, X-ray quality crystals were obtained from a concentrated diethyl ether solution at -35 °C. Elemental analysis of $C_{52}H_{74}N_2O_4ClU$: Calculated, C, 58.66; H, 7.01; N, 2.63. Found, C, 58.91; H, 7.13; N, 2.53. ^{1}H NMR (C_6D_6, 300MHz, 25 °C): δ = 2.09 (br s), 3.10 (br s), 4.90 (br s).

Reaction of **UO_2-isq** with 4 eq. Cl-BCat. A 20-mL scintillation vial was charged with **UO_2-isq** (0.100 g, 0.091 mmol) and 10 mL of THF. The vial was placed in the coldwell and the solution was frozen. Upon thawing, Cl-BCat (0.056 g, 0.363 mmol) was weighed by difference and added to the stirring solution. After warming to room temperature for 1 hour, volatiles were removed *in vacuo*. The products of the reaction were identified to be $UCl_4{}^{dipp}iq_2(THF)_2$ and $BOBCat_2$ by ^{1}H and ^{11}B NMR. The reaction mixture was washed with cold *n*-pentane (2 × 5 mL) to separate organics from the uranium product, producing a black powder (0.057 g, 0.063 mmol, 69% yield).

Independent synthesis of $^{dipp}iqUCl_4(THF)_2$ (**UCl_4-iq**). A 20-mL scintillation vial was charged with UCl_4 (0.100 g, 0.263 mmol) and 10 mL THF. In a separate vial, ^{dipp}iq (0.100 g, 0.263 mmol) was dissolved in 5 mL of THF and added dropwise to the stirring UCl_4 solution. The solution immediately changed color from green to black. After 8 hours the solvent was removed *in vacuo* and washed with *n*-pentane (2 × 5 mL) to yield a black powder (0.184 g, 242 mmol, 92% yield). This sample was submitted for elemental analysis. Single, X-ray quality crystals were obtained from a concentrated THF solution at -35 °C. Elemental analysis of $C_{26}H_{37}N_1O_1Cl_4U$ (solvent free): Calculated, C, 41.12; H, 4.91; N, 1.84. Found, C, 40.83; H, 5.02; N, 1.64. ^{1}H NMR

(C_6D_6, 300MHz, 25 °C): δ = -14.89 (4, 1H, C*H*), -6.49 (3, 9H, C(C*H*$_3$)$_3$), -5.16 (103, 3H, CH(C*H*$_3$)), -5.07 (35, 4H, THF), -3.79 (106, 3H, CH(C*H*$_3$)),-3.61 (35, 4H, THF), -1.07 (4, 9H, C(C*H*$_3$)$_3$), -0.54 (4, 1H, C*H*), 1.98 (32, 2H, C*H*), 9.11 (t, *J* = 7 Hz, 1H, C*H*), 10.87 (37, 4H, THF), 11.65 (36, 4H, THF), 12.29 (115, 3H, CH(C*H*$_3$)), 13.99 (118, 3H, CH(C*H*$_3$)), 19.44 (10, 2H, C*H*).

Reaction of **UO_2-isq** with 4 eq. Piv-Cl. A 20-mL scintillation vial was charged with **UO_2-isq** (0.080 g, 0.073 mmol), dissolved in 10 mL benzene and transferred to a 25 mL receiving flask. Pivaloyl chloride (0.035 g, 0.290 mmol) was weighed by difference and added to the green, stirring solution. The flask was sealed and then heated to 50 °C for 8 hours, producing a red solution. After cooling to room temperature for 1 hour, volatiles were removed *in vacuo*. The products of the reaction were identified by ^{1}H NMR to be pivaloyl anhydride, and **UCl_4-iq$_2$**. The reaction mixture was washed with cold *n*-pentane (2 × 5 mL) to separate organics from the uranium product, producing a brown powder (0.061 g, 0.053 mmol, 73% yield).

Independent synthesis of ^{dipp}iq$_2$UCl$_4$ (**UCl_4-iq$_2$**). A 20-mL vial was charged with UCl_4 (0.056 g, 0.142 mmol) and 8 mL benzene. In a separate vial, ^{dipp}iq (0.119 g, 0.312 mmol) was dissolved in benzene (8 mL) and added dropwise to the stirring UCl_4 slurry. The reddish-brown mixture was then transferred to a receiving flask, sealed, and heated to 50 °C for 16 hours. The solvent was removed *in vacuo* and the resulting brown powder washed with *n*-pentane (2 × 10 mL), leaving **UCl_4-iq$_2$** (0.144 g, 0.126 mmol, 89% yield). Elemental analysis of $C_{52}H_{74}N_2O_2Cl_4U$: Calculated, C, 54.83; H, 6.55; N, 2.46. Found, C, 55.64; H, 6.37; N, 2.59. ^{1}H NMR (C_6D_6, 300MHz, 25 °C): δ = -75.30 (19, 2H, C*H*), -5.66 (t, *J* = 7 Hz, 2H, C*H*), -2.36 (12, 18H, C(C*H*$_3$)$_3$), 7.03 (8, 12H, CH(C*H*$_3$)$_2$), 7.25 (8, 2H, C*H*), 8.81 (10, 12H, CH(C*H*$_3$)$_2$), 19.07 (7, 18H, C(C*H*$_3$)$_3$), 28.96 (27, 4H, C*H*(CH$_3$)$_2$), 56.68 (d, *J* = 7 Hz, 4H, C*H*).

Synthesis of ^{18}O-Labeled $[UO_2Cl_2(THF)_2]_2$. This procedure was developed by adapting literature procedures.[27, 30] A 25-mL, borosilicate glass Schlenk flask was charged with approximately 1 g of $UO_2Cl_2(H_2O)_x$ (x = 1-3) and purged with argon. Against a flow of argon, 1 mL of $H_2{}^{18}O$ was added via pipette. After 1 minute of purging with argon, the flask was sealed. The yellow solution was gently stirred in front of a UV lamp (365 nm). *Note, using* [UO2Cl2(THF)2]2 as the uranium source leads to decomposition of the material, as evidenced *by color change from yellow to green and precipitation*. After 12 days, the water was removed from the yellow slurry *in vacuo*, yielding a yellow powder. From this material, anhydrous ^{18}O-labeled $[UO_2Cl_2(THF)_2]_2$ was obtained via a previously published procedure.[27] IR spectroscopy was employed to confirm the incorporation of ^{18}O into the U-O_{uranyl} (Figure S20).

2.3 Uranyl Iminoquinone Complex

2.3.1 Synthesis of **UO_2-iq**

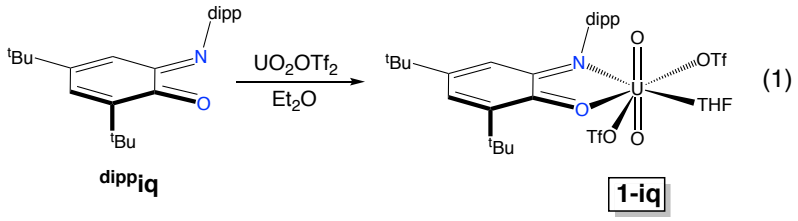

Figure 2.2: Synthesis of the uranyl iminoquinone complex **UO_2-iq**.

Initially, a neutral ^{dipp}iq U(VI) complex was synthesized to provide a baseline for studies of more reduced species and allow comparison of spectroscopic data. Ligation of uranyl triflate, $UO_2(OTf)_2(THF)_3$, was accomplished by stirring with an equimolar amount of ^{dipp}iq in diethyl ether (Eq. 1). Upon workup, a red-purple powder was obtained in good yield (76%). The ^{1}H NMR

spectrum (Figure S1) displayed 9 resonances slightly shifted from those observed for the free ligand, indicative of binding to the diamagnetic, U(VI), f^0 ion. Two additional, broad resonances, assignable as one bound THF molecule, were also observed at 1.93 and 5.26 ppm.

2.3.2 X-Ray Crystallography of **UO_2-iq**

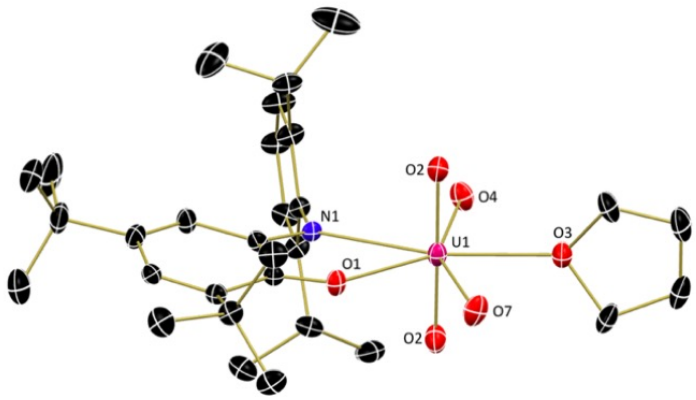

Figure 2.3: Molecular structure of **UO_2-iq**.
Sturcture shown with 30% probability ellipsoids and hydrogen atoms, co-crystallized solvent molecules, and bound triflate ions (except coordinated oxygen atoms) are omitted for clarity.

To unequivocally determine the number of coordinated ligands and examine the structural parameters of the complex, single crystals of **UO_2-iq**, grown from toluene, were analyzed using X-ray diffraction. Refinement of the data revealed a seven-coordinate pentagonal bipyramidal uranyl coordination complex with one ^{dipp}iq ligand, one THF molecule, and two bound triflate anions in the equatorial plane along with the oxo ligands in axial positions (Figure 2, left; Table 1). The U-O_{uranyl} distance of 1.745(5) Å and O_{uranyl}-U-O_{uranyl} angle of 179.1(2)° are as expected based on similar uranyl compounds.[31] If the reaction is performed with excess ^{dipp}iq ligand,

formation of **UO_2-iq** is still observed, suggesting the triflate anions are not subject to substitution by neutral ^{dipp}iq despite the chelation effect of the bidentate ligand.

Table 2.1 Selected uranyl bond distances (Å) and angles (°) for **UO_2-iq**, **UO_2-isq**, **UO_2-ap**, **UO_2-ap crown** and **UO_2-iq/isq**.

	UO_2-iq	**UO_2-isq**	**UO_2-ap**	**UO_2-ap crown**	**UO_2-iq/isq**
U-O_{Uranyl}	1.745(5)	1.762(4)	1.824(3)	1.812(2)	1.757(3)
U-O_{Uranyl}	1.745(5)	1.786(3)	1.834(3)	1.814(2)	1.758(3)
O_{Uranyl}-U-O_{Uranyl}	179.1(2)	175.42(17)	172.22(12)	174.54(10)	175.09(13)

2.4 Uranyl Iminosemiquinone Complex

2.4.1 Synthesis of **UO_2-isq**

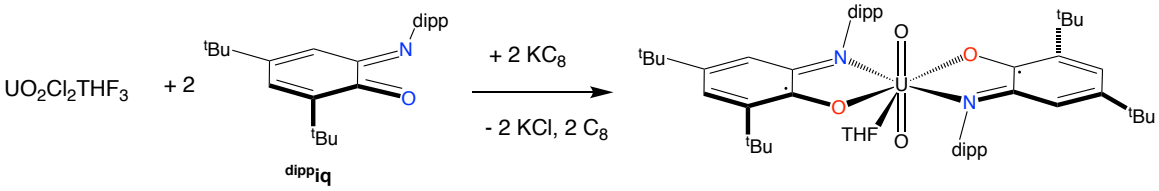

Figure 2.4: Synthesis of the bis(iminosemiquinone) complex **UO_2-isq**.

After successful metalation of the neutral ^{dipp}iq ligand, the redox-active nature of the ligand was engaged by stirring two equivalents of ^{dipp}iq with one equivalent of $UO_2Cl_2(THF)_3$ followed by slow addition of two equivalents of potassium graphite (Scheme 1), causing a color change from red/brown to dark green. After workup, a green powder was isolated in moderate yield (67%). The ^{1}H NMR spectrum (Figure S5) displays broad, paramagnetically-shifted signals ranging from

0 – 55 ppm. In this case, the paramagnetism can arise either from 1) reduction of the uranium (VI) (f^0) center to uranium (V) (f^1) while maintaining a neutral iminoquinone ligand, or 2) from ligand reduction to generate two radical-containing iminosemiquinone ligands.

2.4.2 X-Ray Crystallography of **UO_2-isq**

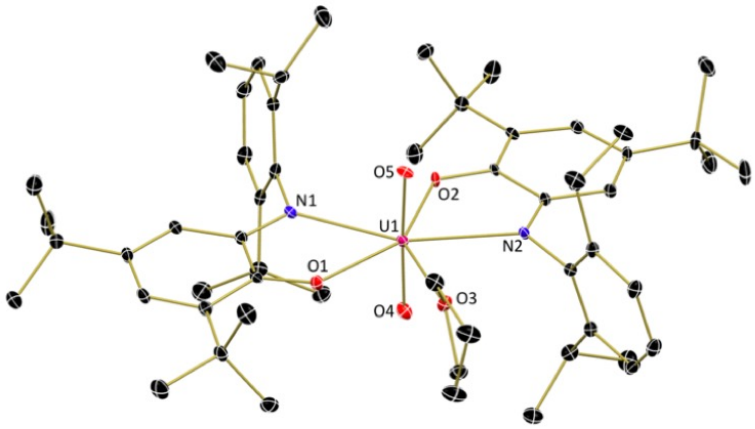

Figure 2.5: Molecular structure **UO_2-isq.**
Structure shown with 30% probability ellipsoids and hydrogen atoms and co-crystallized solvent molecules are omitted for clarity.

To further elucidate the electronic structure of **UO_2-isq**,[17, 32, 33] X-ray crystallography was employed as structural parameters, including intraligand bond distances, can often aid in ligand oxidation state assignment.[34] Crystals of **UO_2-isq** grown from diethyl ether at -35 °C were analyzed. Refinement of the data revealed a seven coordinate uranyl species, with two ^{dipp}iq ligands and a THF molecule coordinated in the equatorial plane (Figure 2, middle). As with **UO_2-iq**, a pentagonal bipyramidal geometry with the uranyl oxygen atoms in axial positions was observed. Additionally, the U-O_{uranyl} bond distances of 1.762(4) and 1.786(3) Å are within the range of 1.76

– 1.79 Å observed for U(VI) uranyl molecules.[31, 32, 35] These U-O_{uranyl} distances suggest the reduction is ligand-based rather than occurring at the uranium.

2.4.3 EPR of **UO_2-isq**

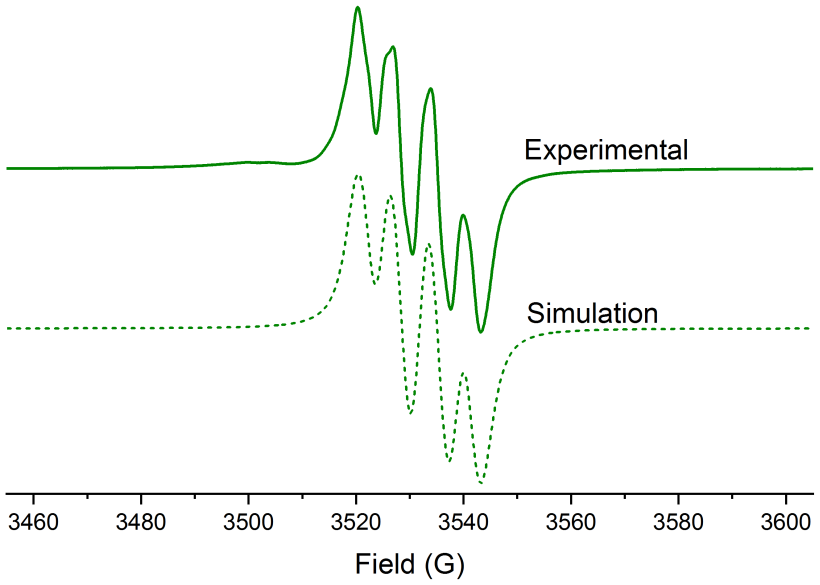

Figure 2.6: EPR spectrum of **UO_2-isq**.
Solution sample (*n*-pentane, 5.8 mM) recorded at 25 °C. g_{iso} = 1.993. Frequency: 9.852 GHz. Power: 10 mW. Modulation: 0.5 G/100 kHz.

To further confirm the presence of ligand radicals, EPR spectroscopy was performed. The EPR spectrum of **UO_2-isq** (Figure 3) displays an isotropic signal at g = 1.993, which is shifted from that of 2.0061 observed for 4,6-di-*tert*-butyl-2-*tert*-butyl-iminosemiquinone (H^{tBu}isq•)[36]. This value agrees well with the g-value previously observed for hexavalent uranyl species featuring redox-active ligands, such as Cp*UO_2(^{Mes}PDI^{Me}) (g_{iso} = 1.974), Cp*UO_2(^{t}Bu-^{Mes}PDI^{Me}) (g_{iso} =1.936) and [UO_2(salophen)^{tBu}(H_2O)]$^+$ (g_{av} =1.997) (^{t}Bu-^{Mes}PDI^{Me} = 2,6-((Mes)-N=CMe)$_2$-*p*-C(CH_3)$_3$$C_5H_2N$; salophen = *N*,*N*'-bis(3-^{t}Bu-(5^{t}Bu)-salicylidene)-1,2-phenylenediamine).[17] Spin-

orbit coupling of the ligand-based radical with the empty *f*-orbitals of the uranium center is likely the cause of the high-field shift from the g-value observed for H^{tBu}isq•. Simulation of the spectrum was accomplished with one nitrogen (I = 1) and one hydrogen atom (I = ½) of the ligand, yielding hyperfine coupling constants of A_N = 19.48 and A_H = 13.97 MHz. These values suggest a stronger interaction with the nitrogen atom than the hydrogen atom of the ligand. This hyperfine pattern agrees with previously noted results[18, 36]. Thus, these measurements support the presence of an iminosemiquinone ligand radical with only a weak interaction with uranium. 4,6-di-*tert*-butyl-2-*tert*-butyl-iminosemiquinone (H^{tBu}isq•)

2.4.4 SQUID Magnetometry of **UO_2-isq**

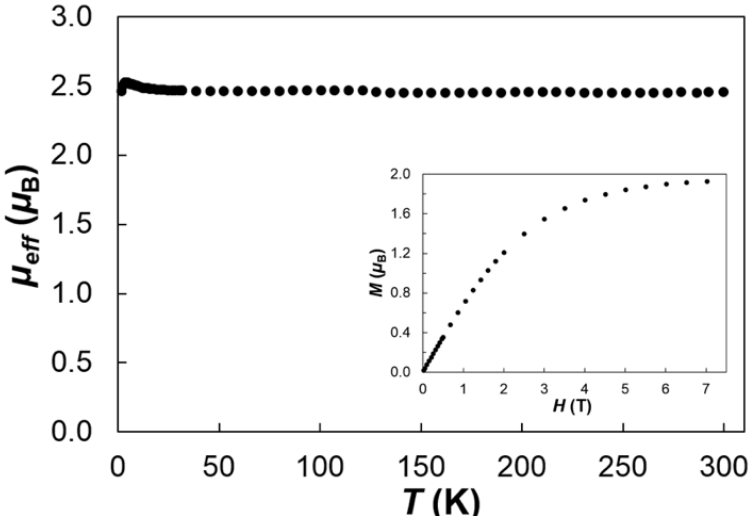

Figure 2.7: Variable temperature molar magnetic data (μ_{eff}) for **UO_2-isq** and variable field data collected at 2 K (inset)

Variable-temperature and field-dependent magnetic measurements were performed to elucidate the uranium and ligand oxidation states in **UO_2-isq** (Figure 4). At room temperature, the μ_{eff} value (2.45 μ_B) was consistent with that expected for two isolated, unpaired electrons with g =

2.0 (theoretical μ_{eff} value = 2.45 μ_B).[37] Upon cooling, the μ_{eff} value slightly increased to 2.52 μ_B at 4 K. The increase in moment resulted from the ferromagnetic coupling of the two unpaired electrons. The data were fitted by the Bleaney−Bowers equation[38] with g = 2.00 and exchange coupling constant J = 0.4 cm^{-1} (see the supporting information for details). The magnetization in the field dependent measurement saturated at 1.94 μ_B at 2 K, also characteristic of two isolated S = 1/2 spins.[37] Overall, these magnetic data indicated the presence of one U(VI) cation and two ligand-centered radicals with negligible ferromagnetic coupling in **UO_2-isq**. This value supports the presence of two non-communicating ligand radicals that were measured by EPR and predicted with the metrical parameters deduced by X-ray crystallography (*vide infra*). The radicals in **UO_2-isq** are relegated to the ligand at all temperatures, with little interaction with the uranium. This rules out alternate potential electronic structures for **UO_2-isq**. These magnetic data also eliminate formation of pentavalent $(isq^{1-})(iq^0)U^VO_2$, which would have both uranium based and ligand based radicals, as well as $(iq^0)_2U^{IV}O_2$, which would have closed-shell ligands with only uranium based electrons unpaired.

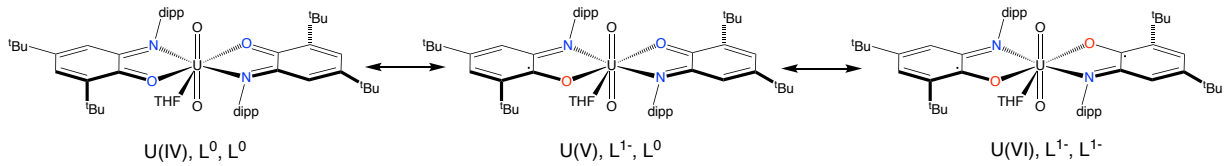

Figure 2.8:Possible electronic structures of **UO_2-isq**.

2.5 Uranyl Amidophenolate Complexes

2.5.1 Synthesis of **UO_2-ap**

To probe the ability of our system to accommodate additional electrons beyond monoreduction of both ligands, electrochemical measurements of **UO_2-isq** were performed in THF

(Figure S19). The cyclic voltammetric data for **UO_2-isq** showed a quasi-reversible reduction at -1.58 V, which could be attributed to the reduction of the two ligands from isq^{1-} to ap^{2-} or reduction of uranium from +6 to +5.

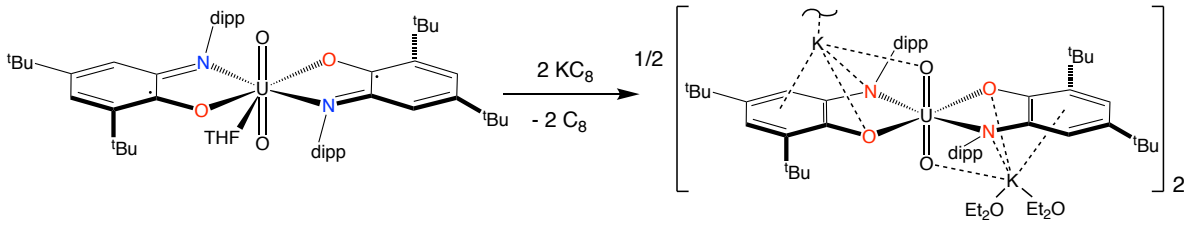

Figure 2.9: Synthesis of the bis(amidophenolate) complex, **UO_2-ap.**

Encouraged by the electrochemical results, **UO_2-isq** was reduced chemically by stirring with two equivalents of KC_8 in THF. Following workup, a tan powder that is poorly soluble in hydrocarbon solvents was isolated. ^{1}H NMR spectroscopic analysis (pyridine-d_5) showed a spectrum (Figure S6) with 11 resonances. Of these, nine signals were assigned to the ligand and two signals as bound THF, none of which were drastically shifted from the diamagnetic region. These data suggest a closed-shell U(VI), f^0 ion with ^{dipp}ap ligands bound to uranium.

2.5.2 Synthesis of **UO_2-ap crown**

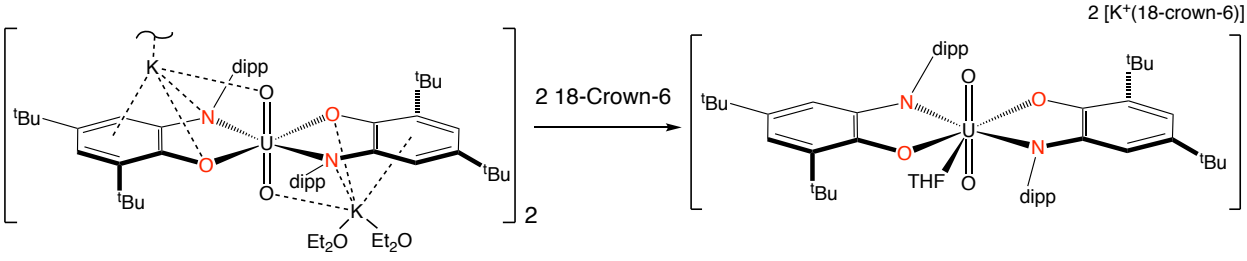

Figure 2.10: Synthesis of the bis(amidophenolate) complex, **UO_2-ap crown**.

Because solution behavior can be complicated by dynamic inner-sphere and outer-sphere cation exchange, a crown ether was employed to encapsulate the potassium ion for further studies.[18, 39, 40] To achieve this, two equivalents of 18-crown-6 were added to a stirring solution of **UO_2-ap** in THF. After workup, a white powder was isolated in good yield (76%). The ^{1}H NMR spectrum is quite similar to that of **UO_2-ap**, with minor differences, including an additional resonance at 3.43 ppm corresponding to the 24 protons associated with 18-crown-6.

2.5.3 X-Ray Crystallography of **UO_2-ap** and **UO_2-ap crown**

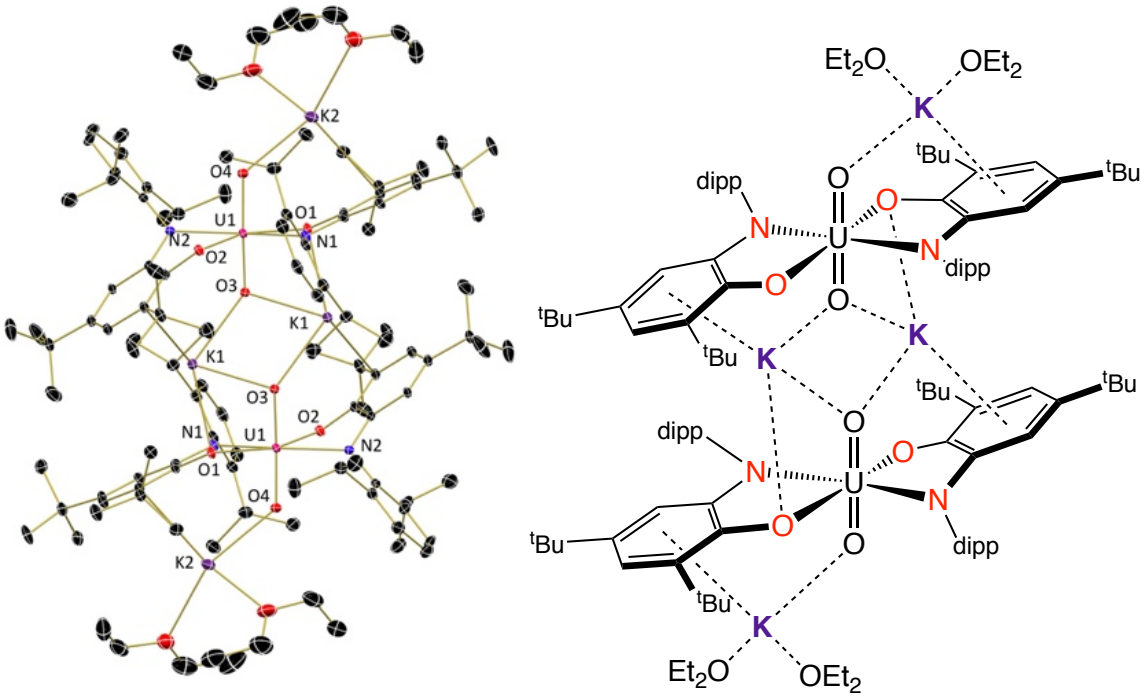

Figure 2.11: Molecular structure and Chemdraw representation of **UO_2-ap**.
Structure shown with 30% probability ellipsoids and co-crystallized solvent molecules and H atoms are omitted for clarity. Schematic representation of **UO_2-ap** (right), with interactions between potassium ions and various parts of the molecule shown as dashed lines.

Comparison of the structural changes that accompany reduction and examination of the effect of potassium ion sequestration in **UO_2-ap** and **UO_2-ap crown** were examined using X-ray

crystallography. **UO_2-ap** crystallizes as a dimer from diethyl ether or toluene at -35 °C with the oxygen atom and aromatic ring of the ^{dipp}iq ligand, and uranyl oxygen atoms interacting with the potassium ions. This dimerization causes out of plane bending of the ligand with the N and O atoms appearing to be sp^3 hybridized to allow for lone pair interaction with the nearby potassium ions. Additionally, the uranyl bond distances of 1.824(3) and 1.834(3) Å (Table 1) are quite long,[31] appearing to result from the potassium binding to the O_{uranyl}. This cation-capping effect has been thoroughly studied by P. Arnold and coworkers who employed a large, compartmental, N_8-macrocyclic ligand.[41] In these studies, reduction of uranyl was facilitated by coordination of a cation, held in place by the specialized "Pacman" type ligand, to the O_{uranyl}.

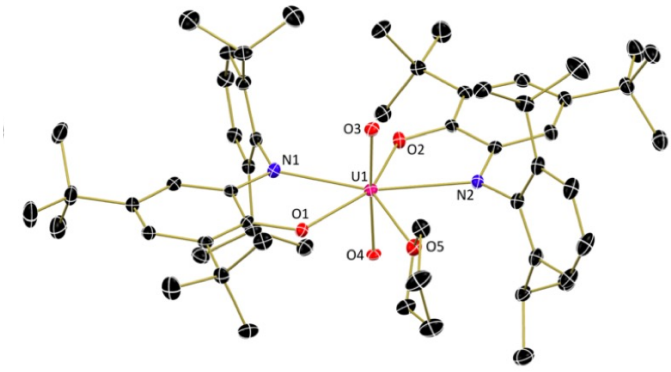

Figure 2.12: Molecular structure of **UO_2-ap crown.**

Structure shown with 30% probability ellipsoids and hydrogen atoms, co-crystallized solvent molecules, potassium ions and crown ether molecules are omitted for clarity.

The structure of **UO_2-ap crown** shows that sequestering the potassium ions with crown ethers permits the amidophenolate ligands to return to their planar geometry, isostructural to **UO_2-isq**. Interestingly, despite the absence of the interaction of potassium atoms with the uranyl moiety in **UO_2-ap crown**, the U-O_{uranyl} bond distances remain long (1.814(2) and 1.812(2) Å), suggesting

ligand reduction plays a role in the elongation of the U-O_{uranyl} bond. This implies that cation coordination is not the only contributing factor in the U-O_{uranyl} bond elongation observed in **UO_2-ap**. U-O_{uranyl} bond lengthening has been previously observed by Hayton and co-workers when they described tris- and tetrakis-ketimide complexes [Li(THF)(TMEDA)][UO_2(N=C^{t}BuPh)$_3$] and [Li(THF)(Et_2O)]$_2$[UO_2(N=C^{t}BuPh)$_4$].[42] These ketimide uranyl molecules display U-O_{uranyl} bond lengths of 1.830(5) and 1.804(5) Å (tris-ketimide) and 1.838(4) Å (tetrakis-ketimide). The authors attribute this elongation to the presence of four strong donors in the equatorial plane, which act to weaken the U-O_{uranyl} bonds via electrostatic repulsion and π-donation to the uranium center. Further evidence of this elongation can be found in the imido family of uranyl analogues. Studies of uranium tris-[43] and tetrakis(imidos)[44] – featuring strong π-donating imido groups in the equatorial plane – have shown that imido bonds lengthen and weaken with each additional π-donor. The $^{dipp}ap^{2-}$ ligand has been studied as a π-donating ligand for high valent metals previously.[24] As its high-lying π orbitals have the appropriate symmetry to donate electron density to the uranium VI center, this is likely a factor in U-O_{uranyl} bond elongation and activation in **UO_2-ap crown**.

2.6 Uranyl Reduction Series Comparison

2.6.1 Bond Distance Comparison of **UO_2-iq**, **UO_2-isq**, **UO_2-ap**, and **UO_2-ap crown**

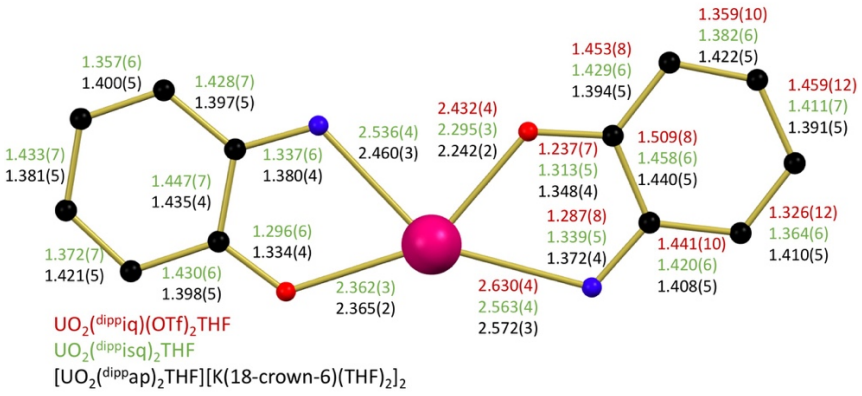

Figure 2.13: Bond distance comparison (Å) for **UO_2-iq**, **UO_2-isq**, and **UO_2-ap crown**. Carbon atoms shown in black, nitrogen atoms shown in blue, oxygen atoms shown in red, and uranium atom shown in magenta.

The bond metrics vary based on the ligand oxidation state and can therefore provide insight into the electronic structure of **UO_2-iq**, **UO_2-isq**, and **UO_2-ap crown** (Figure 7). The neutral ^{dipp}iq ligand of **UO_2-iq** displays relatively long uranium-oxygen (2.432(4) Å) and uranium-nitrogen (2.630(4) Å) bonds that are indicative of a datively bound ligand. Furthermore, the short C-O (1.237(7) Å) and C-N (1.287(8) Å) bonds suggest the ligand retains double bond character. In contrast, the iminosemiquinone ligands of **UO_2-isq** feature shortened U-O bonds (2.295(3) and 2.362(3) Å) and U-N bonds (2.563(4) and 2.536(4)) accompanied by longer C-O (1.313(5) and 1.296(6) Å) and C-N bonds (1.339(5) and 1.337(6) Å), indicating reduction of the ligand.

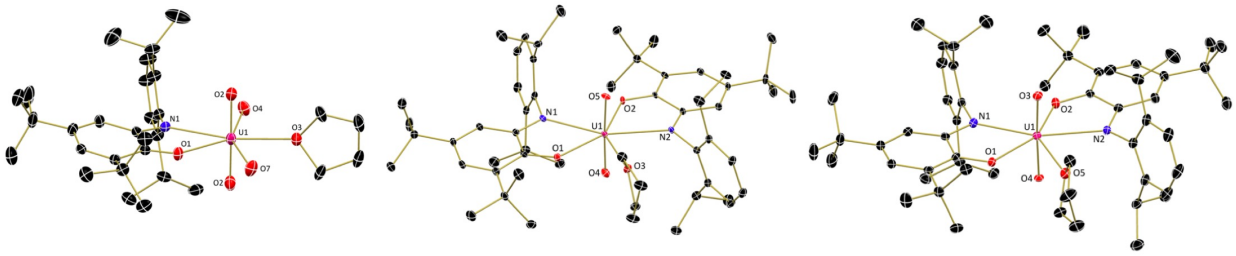

Figure 2.14: Structural comparison of **UO_2-iq**, **UO_2-isq** and **UO_2-ap crown**. **UO_2-iq** (left), **UO_2-isq** (middle) and **UO_2-ap crown** (right) shown with 30% probability ellipsoids and hydrogen atoms, co-crystallized solvent molecules, potassium ions, crown ether molecules and bound triflate ions (except coordinated oxygen atoms) are omitted for clarity.

The bond distances of **UO_2-ap crown** are not as simple to analyze as those of the other compounds of the series. While the expected shortening trend of the U-E (E = O, N) bond is observed for one "E" atom of each ligand, the other "E" atom bond distance is nearly identical to that of **UO_2-isq**. This could be attributed to steric hindrance with the bulky dipp or ^{t}Bu groups that prevent the U-E bonds from contracting towards the metal center upon reduction. In this case, a stronger indication of reduction can be found in the intraligand bond distances (Figure 7). The C-O and C-N bonds in each ligand lengthen, signifying the conversion from a double bond to a single bond. Corroborating evidence can also be found in the C-C bond distances of the rings in the ligands. As the ligand is reduced, the distances throughout the ring become more similar, suggesting aromaticity is present.

2.6.2 Bond Angle Comparison of **UO_2-iq**, **UO_2-isq**, and **UO_2-ap crown**

As the bond distances in molecules **UO_2-iq**, **UO_2-isq** and **UO_2-ap crown** change with ligand oxidation state, the bond angles also indicate ligand reduction. In particular, this effect is noticeable in the N_{iq}-U-O_{iq} angles of the iminoquinone ligand. As the ligand becomes more

reduced, the shortening of the U-O_{iq} and U-N_{iq} bonds causes the N_{iq}-U-O_{iq} bite angle of the ligand to increase from 61.83° (**UO_2-iq**) to 64.44° (**UO_2-isq**) and finally to 65.26° (**UO_2-ap crown**).

2.6.3 UV-Vis/NIR spectroscopy of **UO_2-iq**, **UO_2-isq**, **UO_2-iq/isq,** and **UO_2-ap**

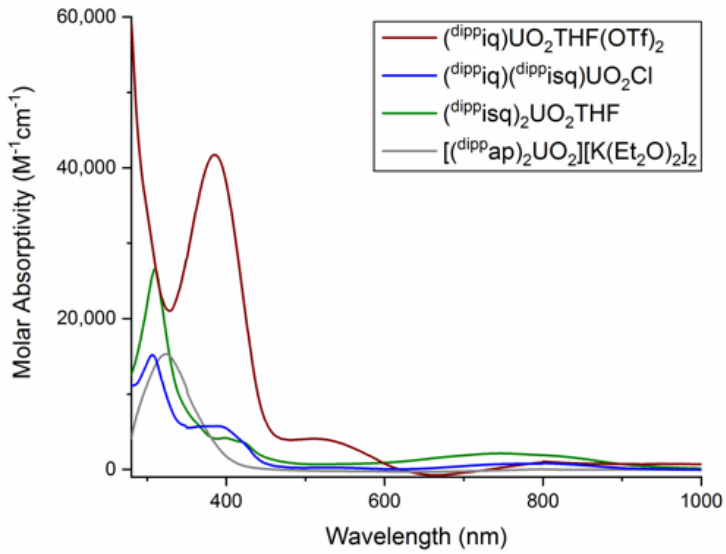

Figure 2.15: Electronic absorption spectra (UV-Vis region) of **UO_2-iq**, **UO_2-isq**, **UO_2-ap** and **UO_2-iq/isq**.

Data recorded in THF at 25 °C

Another useful technique for examining the ligand and metal oxidation states in uranium/uranyl systems is electronic absorption spectroscopy. For the current study, this technique is particularly advantageous as **UO_2-iq**, **UO_2-isq**, and **UO_2-ap** all exhibit distinctly different colors (Figure S16 and S17). Spectra were recorded in THF at 25 °C from 375 – 1800 nm. The spectrum of **UO_2-iq** displays an intense absorption at 385 nm (41,711 $M^{-1}cm^{-1}$) with a weaker absorption at 511 nm (4,075 $M^{-1}cm^{-1}$), giving rise to the observed red-purple color. **UO_2-isq** shows an intense absorption at 310 nm (26,600 $M^{-1}cm^{-1}$) and a much less intense, broad absorption at 747 nm (2,130 $M^{-1}cm^{-1}$), responsible for the observed green color. Finally, **UO_2-ap** shows only one absorption at

313 nm (15,313 $M^{-1}cm^{-1}$) and does not absorb significantly in the visible region, consistent with its pale color. Interpretation of these data suggests that the major, color-producing peaks of the spectra can be attributed to the ligand oxidation state, as similar colors have been observed for complexes of early transition metals[20], lanthanides[18], and low valent uranium.[21]

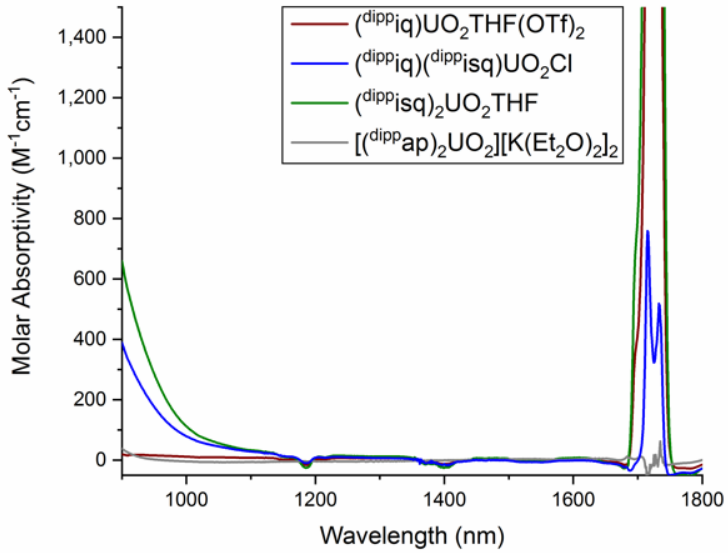

Figure 2.16: Electronic absorption spectra (NIR region) of **UO_2-iq**, **UO_2-isq**, **UO_2-ap** and **UO_2-iq/isq**.

Data recorded in THF at 25 °C THF overtones and blank subtraction errors observed at 1200, 1400 and 1700 nm. Notably, sharp *f-f* transitions are absent, corroborating the assignment of a U(VI) oxidation state for each molecule. **UO_2-isq** and **UO_2-iq/isq** display absorbance beginning around 1000 nm, which contribute to their green colors.

2.7 A Uranyl Mixed Ligand Species

2.7.1 Synthesis

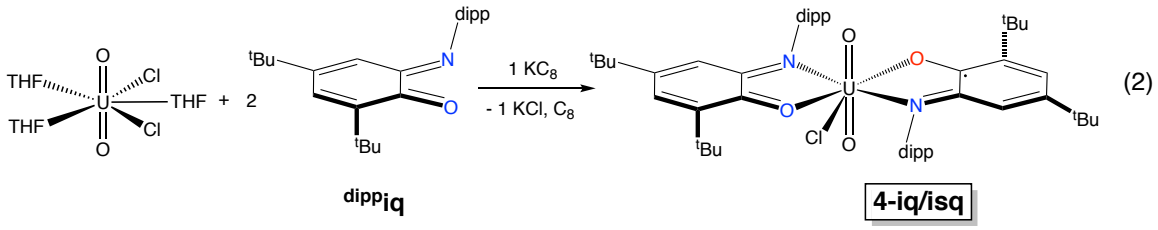

Figure 2.17: Synthesis of the mixed ligand species, **UO_2-iq/isq**.

The extent of radical delocalization in the uranyl iminoquinone complexes was tested by synthesizing a mixed iminoquinone/iminosemiquinone ligand species. We hypothesized that rather than full delocalization of the radical across both ligands, the radical would remain localized on one of the iminosemiquinone ligands and not the other. Preparation of (dippiq)(dippisq)UO2Cl (**UO_2-iq/isq**) was achieved by stirring two equivalents of the iminoquinone ligand with one equivalent of uranyl chloride in the presence of one equivalent of potassium graphite (Eq. 2). Upon workup, a greenish-brown powder was isolated in moderate yield (66%).

2.7.2 X-Ray Crystallography of **UO_2-iq/isq**

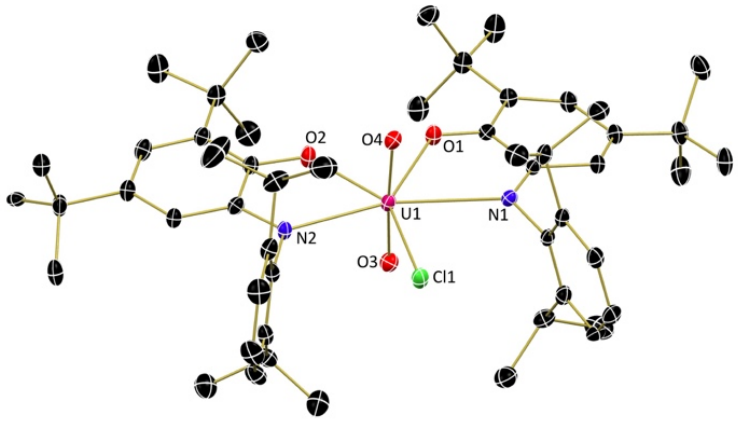

Figure 2.18: Molecular structure of **UO_2-iq/isq.**
Structure shown with 30% probability ellipsoids and co-crystallized solvent molecules and H atoms are omitted for clarity.

X-ray crystallographic analysis of green-brown crystals grown from diethyl ether show a pentagonal bipyramidal uranium center similar to that of **UO_2-isq** but with a chloride atom instead of a THF molecule (Figure 8, Table 1). Compound **UO_2-iq/isq** shows asymmetric ligands in the solid state, with each ligand's oxidation state undoubtedly assignable based on bond distances (Figure 9). The U-O distances of 2.493(3) and 2.312(3) Å and U-N distances of 2.670(3) and 2.498(3) Å highlight the asymmetric nature of the two ligands, with the shorter contact belonging to the isq ligand and the longer to the iq ligand. Further evidence can be found in the C-O and C-N distances, as well as the intraligand C-C distances. For the iminoquinone ligand, C-O and C-N bonds of 1.230(5) and 1.290(5) Å are indicative of double bond character, as observed for **UO_2-iq**. However, the C-O and C-N bonds of the other ligand are significantly longer at 1.297(5) and 1.341(5) Å, agreeing well with the ligands of **UO_2-isq**. Additional evidence can be found in the C-C bonds of each ring, with the iminoquinone ligand featuring two short bonds and three long ones,

whereas the iminosemiquinone ligand has bonds more similar in length. Both of these trends match well with the ligands of compounds **UO_2-iq** and **UO_2-isq**, respectively.

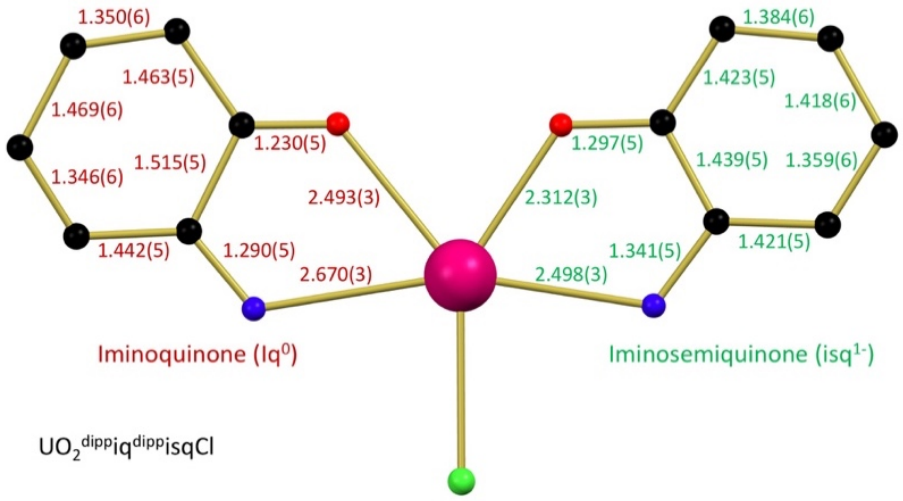

Figure 2.19: Bond distance comparison (Å) for **UO_2-iq/isq**.

Carbon atoms shown in black, nitrogen atoms shown in blue, oxygen atoms shown in red, chloride atoms shown in green and uranium atom shown in magenta.

2.7.3 EPR, SQUID and UV-Vis of **UO_2-iq/isq**

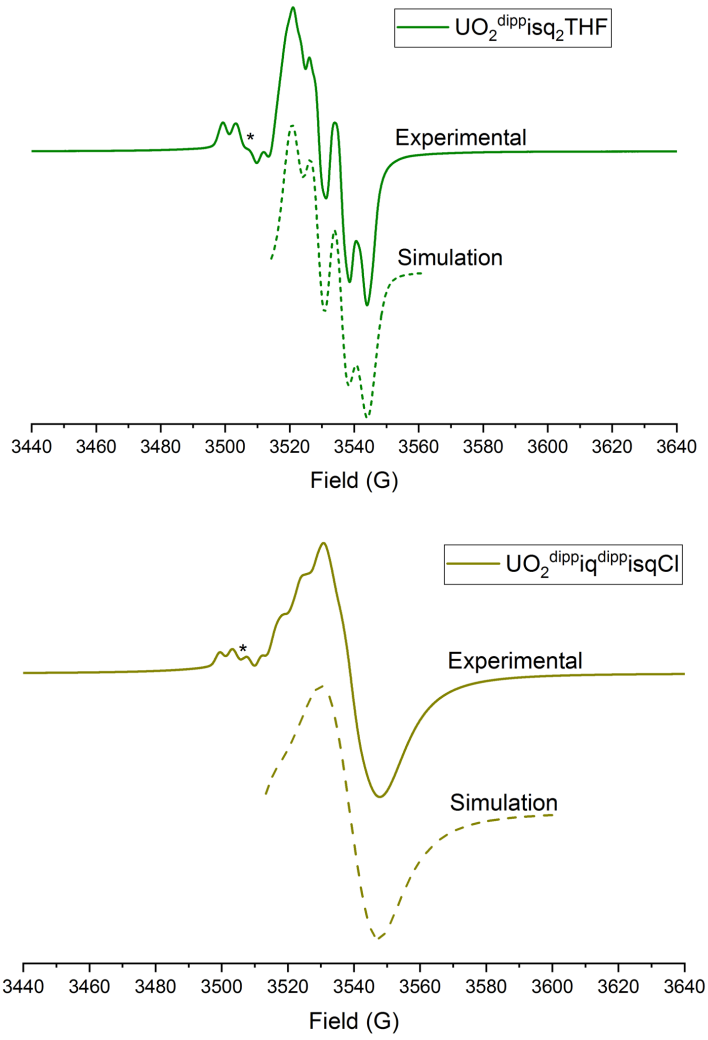

Figure 2.20: EPR spectra of **UO_2-isq** and **UO_2-iq/isq**.

Solution samples recorded in toluene at 25 °C Spectrum of **UO_2-isq** (top) (2.2 mM) displays a g-value of 1.993 and hyperfine (AN = 14.205, AH = 19.147 MHz) similar to that observed in pentane (Figure 3). Spectrum of **UO_2-iq/isq** (bottom) (2.2 mM) displays a g-value of 1.989. Frequency: 9.852 GHz. Power: 10 mW. Modulation: 5.0 G/100 kHz. Small organic radical observed at approximately 3505 G is attributed to decomposition to $H^{dipp}isq\bullet$.

The presence of a ligand radical in **UO_2-iq/isq** was confirmed using EPR spectroscopy (Figure S18). In a toluene solution, an isotropic signal is observed at g = 1.989. This is comparable to the g-value of **UO_2-isq** (1.993). Variable temperature SQUID magnetometry provides additional

evidence of the ligand radical, which establishes a room temperature μ_{eff} value of 1.86 μ_B. The UV-Vis/NIR spectrum of **UO_2-iq/isq** displays absorbance in multiple regions, which explains the observed brown color. Intense absorbances are noted at 307 nm (15,188 $M^{-1}cm^{-1}$) and 388 nm (5759 $M^{-1}cm^{-1}$), while signals at 528 nm (259 $M^{-1}cm^{-1}$) and 800 nm (839 $M^{-1}cm^{-1}$) are broad and less intense. The number of absorbance maxima is likely the product of the ligands existing in two oxidation states, absorbing at different wavelengths.

2.8 Uranyl Functionalization

2.8.1 Reactivity of **UO_2-isq** with B-Chlorocatecholborane

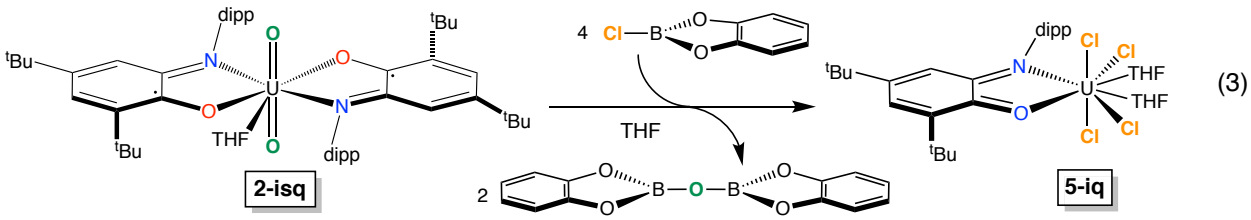

(3)

Figure 2.21: Reductive borylation of **UO_2-isq** with Cl-BCat.

Boron is well-known for its Lewis acidic properties, making it an excellent candidate to examine reactivity with electron-rich **UO_2-isq**. B-chlorocatecholborane (Cl-BCat) features a B-Cl bond that can be heterolytically cleaved by the chlorophilic uranium. Treating **UO_2-isq** with four equivalents of Cl-BCat causes the solution to change color from green to brown immediately. Resonances in the ^{1}H NMR spectrum of the reaction mixture (Figure S11) range from -20 to +20 ppm, suggesting that the uranyl was reduced to paramagnetic U(IV), f^2, a transformation that likely involves uranyl U-O_{uranyl} bond activation (Eq. 3). Further inspection of the data, coupled with ^{11}B NMR data (Figure S12), revealed that dicatecholatobisborylether ($BOBCat_2$) was produced during

the reaction. In sealed-tube NMR experiments in benzene-d_6 and THF-d_8, free ligand is also observed, but does not integrate to one full equivalent. Based on the stoichiometry of Cl-BCat and the number and integration values of resonances in the ^{1}H NMR spectrum, the resulting uranium product was hypothesized to be $UCl_4(^{dipp}iq^0)_n$ (n = 1, 2).

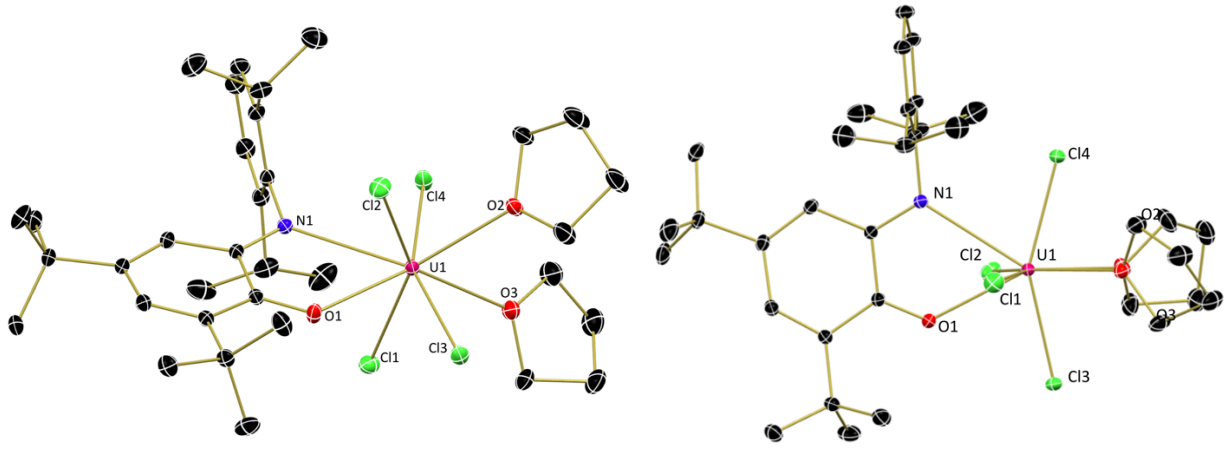

Figure 2.22: Molecular structure of **UCl_4-iq**.
Structure shown with 30% probability ellipsoids and co-crystallized solvent molecules and hydrogen atoms are omitted for clarity. Isometric view (left) and top view (right). Light green blocks were grown from a concentrated THF solution stored at -35° C.

Identification of the U(IV) product from borylation of **UO_2-isq** was achieved by an independent synthesis. Treating UCl_4 with an equivalent of ^{dipp}iq in THF produced a dark green solution (Eq. 4), and ^{1}H NMR data confirmed the product was the same as that observed in the uranyl borylation reaction (Figure S14). The material from the independent synthesis was crystallized from THF and subsequent X-ray analysis revealed the identity to be $UCl_4{}^{dipp}iq(THF)_2$ (**UCl_4-iq**) (Figure S23). The ligands are confirmed to be in the iminoquinone form with C-O and C-N distances of 1.234(3) and 1.298(3) Å, signifying double bonds and matching the distances observed in **UO_2-iq** and **UO_2-iq/isq**. Further evidence can be found in the U-O and U-N distances

of 2.4878(16) and 2.8283(18) Å, which are longer than the contacts reported for iminosemiquinone-containing U(IV) complexes (^{tBu}isq)$_2$UI$_2$(THF) (U-O = 2.160(10) and 2.164(10), U-N = 2.514(12) and 2.567(14) Å).[21] These longer contacts highlight the dative nature of the ligand binding in **UCl$_4$-iq**. The U(IV) metal center has U-Cl bond distances ranging from 2.0651(5) to 2.6257(6) Å. The geometry is best described as trigonal dodecahedral, with the chloride ions in sterically favored sites (None of the Cl-U-Cl bond angles are less than 90°).

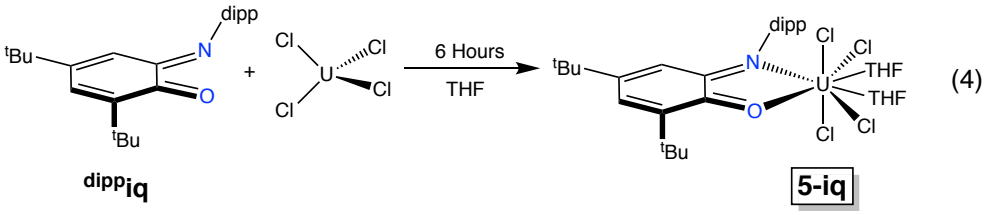

(4)

Figure 2.23: Independent synthesis of **UCl$_4$-iq** from U(IV)Cl$_4$.

2.8.2 ^{18}O Labeling of **UO_2-isq**

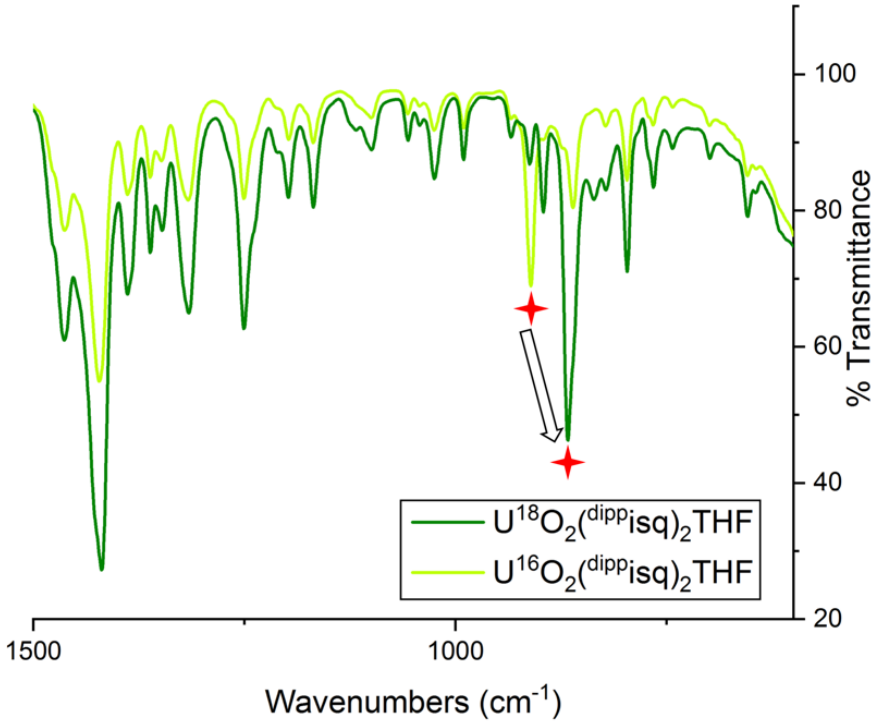

Figure 2.24: Solid state infrared (IR) spectra of $U^{16}O_2{}^{dipp}isq_2THF$ and $U^{18}O_2{}^{dipp}isq_2THF$. Data recorded from benzene solutions evaporated onto on KBr salt plates at 25 °C.

To corroborate that the organic products observed were the result of U-O_{uranyl} bond cleavage and that the extracted oxygen atoms had originated from the U-O_{uranyl}, isotopic labeling studies were performed. ^{18}O-labeled uranyl dichloride ($[U^{18}O_2Cl_2(THF)_2]_2$) was synthesized through photolysis of uranyl chloride hydrate in ^{18}O-labeled water.[31] ^{18}O incorporation was confirmed by IR spectroscopy, with the expected OUO asymmetric stretching frequency reducing from 942.4 cm^{-1} ($[U^{16}O_2Cl_2(THF)_2]_2$) to 892.3 cm^{-1} ($[U^{18}O_2Cl_2(THF)_2]_2$) (Figure S20). Synthesis of $(^{dipp}isq)_2U^{18}O_2THF$ (**UO_2-isq^{18}**) was accomplished in an analogous manner to **UO_2-isq**, using $[U^{18}O_2Cl_2(THF)_2]_2$ as the uranyl source. Successful incorporation was confirmed by IR

spectroscopy. All corresponding absorption maxima are within 1 cm^{-1} between each sample except one. For the ^{18}O labeled sample, the ν_3 asymmetric O-U-O absorption band is observed at 866.9 cm^{-1}. This absorption is shifted from the value of 910.6 cm^{-1} for the unlabeled uranyl. This shift in the ν_3 asymmetric absorption is indicative of isotopic incorporation.

2.8.3 ^{18}O Labeling of $BOBCat_2$

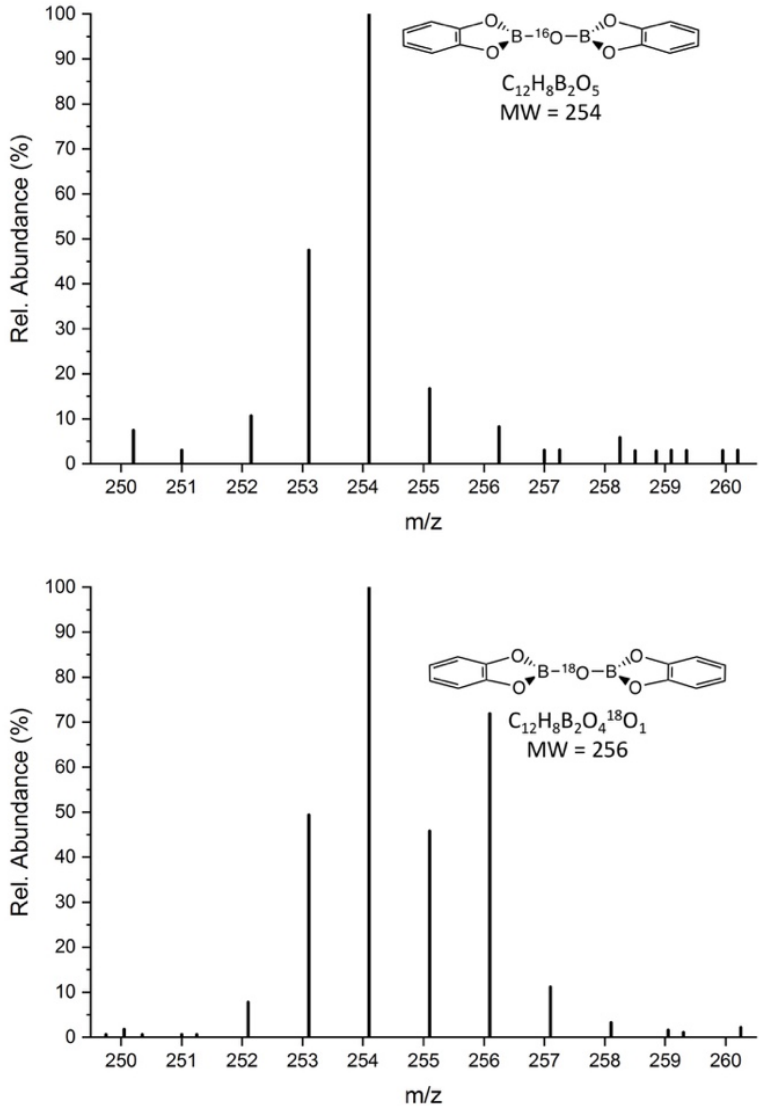

Figure 2.25: Electron ionization mass spectra (EI-MS) of $BOBCat_2$.
Data from the reaction mixtures of ClBCat and **UO_2-isq** (top) and **UO_2-isq^{18}** (bottom).

Treating **UO_2-isq^{18}** with Cl-BCat under the same conditions as previously described for the unlabeled isotopomer yielded analogous results as identified by ^{1}H and ^{11}B NMR spectroscopies. Analysis of the organic bisborylether, $B^{18}OBCat_2$, by EI-MS gave an increase in

the $M^{\bullet+}$ peak appearing at m/z = 256, corresponding to the incorporation of one ^{18}O-labeled oxygen atom. $BOBCat_2$, obtained from the borylation of **UO_2-isq**, shows an analogous peak at m/z = 254 (Figure 10, top). The shift from m/z of 254 to 256 is indicative of ^{18}O incorporation and supports that the source of the oxygen atom in $BOBCat_2$ is from the labeled uranyl U-O_{uranyl}.

2.8.4 Reactivity of **UO_2-isq** with Pivaloyl Chloride

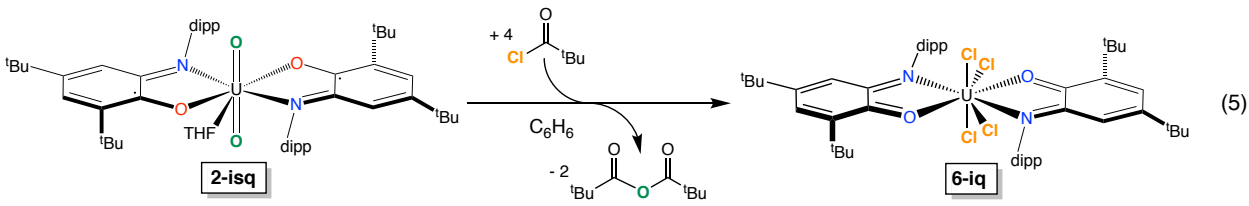

(5)

Figure 2.26: Reductive acylation of **UO_2-isq** with pivaloyl chloride.

Upon establishing that **UO_2-isq** could mediate U-O_{uranyl} bond cleavage with Cl-BCat, we hypothesized that an analogous electrophilic carbon could be used to activate the uranyl ion. Pivaloyl chloride (Piv-Cl) was an attractive choice, as the *tert*-butyl group provides steric pressure to aid product dissociation. Treating **UO_2-isq** with four equivalents of pivaloyl chloride in benzene results in no observable reaction. Heating this solution to 50 °C for four hours causes a color change from green to brown. Analysis of the reaction mixture by ^1H NMR revealed a singlet at 1.04 ppm and disappearance of the resonance at 0.89 ppm, suggesting conversion of pivaloyl chloride to pivalic anhydride. Additionally, resonances ranging from -80 to +60 ppm (Figure S13) show that a paramagnetic product is formed; however, these resonances do not match that of **UCl_4-iq**. We hypothesized that in the non-coordinating benzene solution, ligand displacement would not occur as in the borylation, which was performed in THF. To confirm this, UCl_4 was treated with two equivalents of iminoquinone in benzene and heating to 50 °C for 18 hours yields an NMR

spectrum matching that of the acylation reaction, with no free ligand observed. In the absence of THF, a bis-ligand U(IV) complex, $UCl_4(^{dipp}iq^0)_2$ (**UCl_4-iq_2**), is formed. These spectroscopic results suggest that the two pivaloyl chloride molecules were able to exchange their chloride atoms for the oxygen atom of a uranyl ion, producing pivalic anhydride (Eq. 5), which is then displaced from the uranium ion.

2.8.5 ^{18}O Labeling of Pivalic Anhydride

Reactions of **UO_2-isq** and **UO_2-isq^{18}** were performed with pivaloyl chloride, and the organic anhydrides isolated and examined using CI-MS. The labile nature of the C-O bonds in pivalic anhydride causes dissociation in the mass spectrometer, thus, only the protonated carboxylic acid was detected. In the case of the unlabeled sample, a $[M+H]^+$ peak at m/z = 103 was observed. The data for the ^{18}O-labeled sample display an additional $[M+H]^+$ peak m/z = 105, assignable as the ^{18}O-labeled isotopomer. Based on the ratio of these peaks in the labeled sample, the percent incorporation of ^{18}O was calculated to be about 35%. These results, along with the spectroscopic data (*vide supra*), support that $U\text{-}O_{uranyl}$ bonds are broken in the process of borylation and acylation, and the oxygen atoms in the organic byproducts originate from the $U\text{-}O_{uranyl}$ bond.

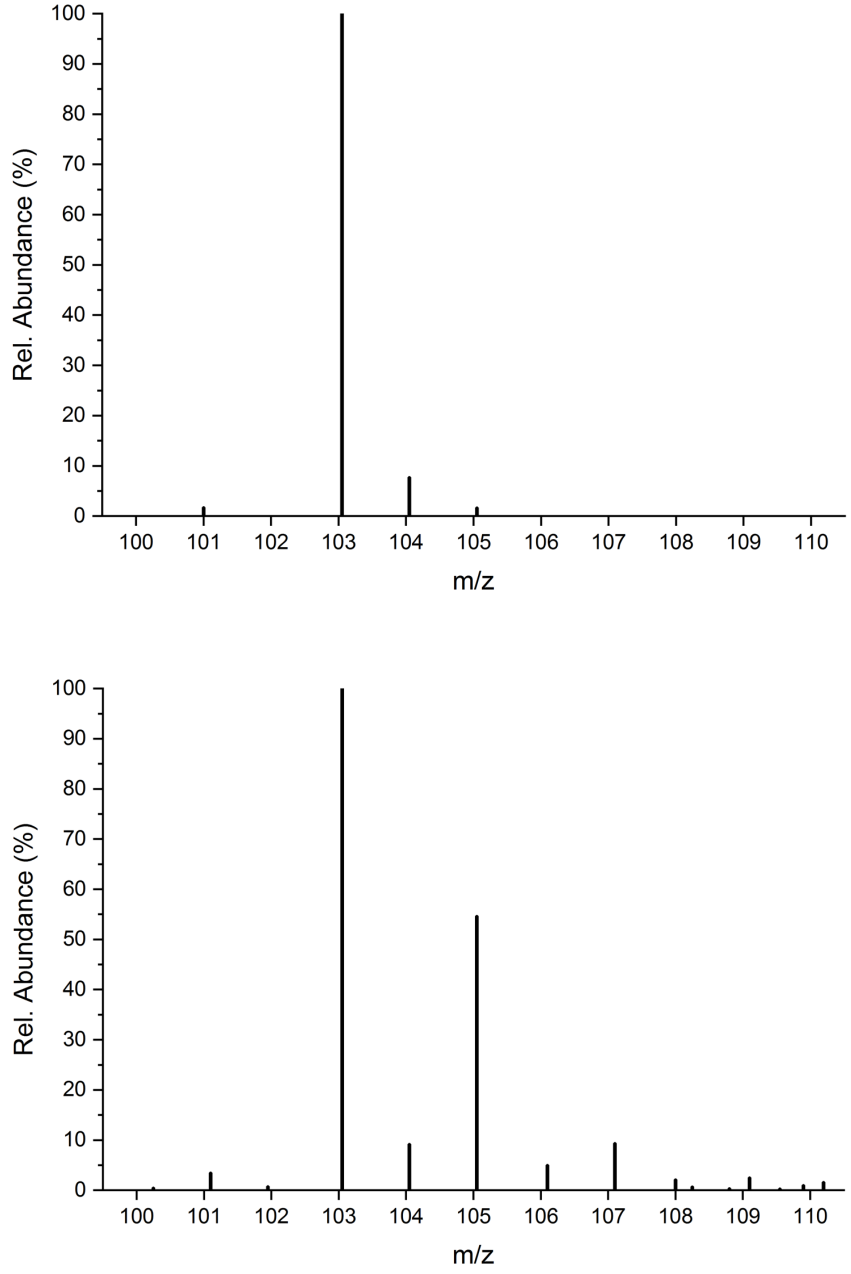

Figure 2.27: CI-MS of Pivalic Anhydride.

Samples from Sigma Aldrich (top) and from the reaction mixture of Cl-Piv and $U^{18}O_2{}^{dipp}isq_2THF$ (bottom).

2.9 Conclusion

In summary, a family of uranyl complexes bearing redox-active ligands has been isolated in three different oxidation states. Thorough characterization has provided insight into their electronic structures. Upon reduction, electrons are stored in the ligand π* orbitals rather than in uranium-based orbitals, retaining the U(VI) oxidation state throughout the series. Notably, **UO_2-isq** has two isolated, ligand-based radicals that can be harnessed for U-O_{uranyl} bond activation. U-O_{uranyl} bond functionalization and scission was carried out with B-chlorocatecholborane or pivaloyl chloride, furnishing either mono- or bis-iminoquinone U(IV) products and the corresponding organic ethers. The origin of the oxygen atom was established by isotopic labeling experiments. Formation of a C-O bond followed by complete U-O cleavage from a uranyl species is unprecedented, with previous examples limited to typical Lewis acidic atoms.

The expansion and understanding of ligand bonding and electronic structure in uranyl compounds is a crucial part of the processing and remediation of uranium in the environment. We have examined this bonding thoroughly with a variety of analytical techniques and exploited the activation of U-O_{uranyl} bonds to convert U(VI) to U(IV) with electrons stored in the iminoquinone ligand. The ability to convert U(VI) to U(IV) is an important requirement in manipulating uranium in the environment and would be a fundamental step in any catalytic cycle featuring high valent uranium. Future experiments will aim to generalize the coordination environment and expand the family of reagents capable of U-O_{uranyl} bond functionalization.

2.10 References

[1] Greenwood, N. N.; Earnshaw, A., *Chemistry of the Elements*. 2nd ed.; Butterworth Heinemann: Oxford, 1998.

[2] Briner, W. E. "The Evolution of Depleted Uranium as an Environmental Risk Factor: Lessons from Other Metals" *Int. J. Environ. Res. Public Health* **2006,** 3, 129-135.

[3] Amme, M.; Wiss, T.; Thiele, H.; Boulet, P.; Lang, H. "Uranium Secondary Phase Formation During Anoxic Hydrothermal Leaching Processes of UO_2 Nuclear Fuel" *J. Nucl. Mater.* **2005,** 341, 209-223.

[4] DeLemos, J. L.; Bostick, B. C.; Quicksall, A. N.; Landis, J. D.; George, C. C.; Slagowski, N. L.; Rock, T.; Brugge, D.; Lewis, J.; Durant, J. L. "Rapid Dissolution of Soluble Uranyl Phases in Arid, Mine-Impacted Catchments near Church Rock, Nm" *Environ. Sci. Technol.* **2008,** 42, 3951-3957.

[5] Arnold, P. L.; Love, J. B.; Patel, D. "Pentavalent Uranyl Complexes" *Coord. Chem. Rev.* **2009,** 253, 1973-1978.

[6] Kannan, S.; Moody, M. A.; Barnes, C. L.; Duval, P. B. "Fluoride Abstraction and Reversible Photochemical Reduction of Cationic Uranyl(VI) Phosphine Oxide Complexes" *Inorg. Chem.* **2006,** 45, 9206-9212.

[7] Kiernicki, J. J.; Zeller, M.; Bart, S. C. "Facile Reductive Silylation of UO_2^{2+} to Uranium(IV) Chloride" *Angew. Chem. Int. Ed.* **2017,** 56, 1097-1100.

[8] Arnold, P. L.; Jones, G. M.; Odoh, S. O.; Schreckenbach, G.; Magnani, N.; Love, J. B. "Strongly Coupled Binuclear Uranium-Oxo Complexes from Uranyl Oxo Rearrangement and Reductive Silylation" *Nat Chem* **2012,** 4, 221-227.

[9] Arnold, P. L.; Pecharman, A.-F.; Lord, R. M.; Jones, G. M.; Hollis, E.; Nichol, G. S.; Maron, L.; Fang, J.; Davin, T.; Love, J. B. "Control of Oxo-Group Functionalization and Reduction of the Uranyl Ion" *Inorg Chem* **2015,** 54, 3702-3710.

[10] Brown, J. L.; Mokhtarzadeh, C. C.; Lever, J. M.; Wu, G.; Hayton, T. W. "Facile Reduction of a Uranyl(VI) Beta-Ketoiminate Complex to U(IV) Upon Oxo Silylation" *Inorg. Chem.* **2011,** 50, 5105-5112.

[11] Kiernicki, J. J.; Harwood, J. S.; Fanwick, P. E.; Bart, S. C. "Reductive Silylation of Cp*UO_2(^{Mes}PDI^{Me}) Promoted by Lewis Bases" *Dalton Trans.* **2016,** 45, 3111-3119.

[12] Pedrick, E. A.; Wu, G.; Hayton, T. W. "Reductive Silylation of the Uranyl Ion with Ph_3SiOTf" *Inorg. Chem.* **2014,** 53, 12237-12239.

[13] Pedrick, E. A.; Wu, G.; Kaltsoyannis, N.; Hayton, T. W. "Reductive Silylation of a Uranyl Dibenzoylmethanate Complex: An Example of Controlled Uranyl Oxo Ligand Cleavage" *Chem. Sci.* **2014,** 5, 3204-3213.

[14] Jones, G. M.; Arnold, P. L.; Love, J. B. "Oxo–Group-14-Element Bond Formation in Binuclear Uranium(V) Pacman Complexes" *Chem. – Eur. J.* **2013,** 19, 10287-10294.

[15] Arnold, P. L.; Mansell, S. M.; Maron, L.; McKay, D. "Spontaneous Reduction and C-H Borylation of Arenes Mediated by Uranium(III) Disproportionation" *Nature Chem* **2012,** 4, 668-674.

[16] Cowie, B. E.; Nichol, G. S.; Love, J. B.; Arnold, P. L. "Double Uranium Oxo Cations Derived from Uranyl by Borane or Silane Reduction" *Chemical Communications* **2018,** 54, 3839-3842.

[17] Kiernicki, J. J.; Cladis, D. P.; Fanwick, P. E.; Zeller, M.; Bart, S. C. "Synthesis, Characterization, and Stoichiometric U=O Bond Scission in Uranyl Species Supported by Pyridine(Diimine) Ligand Radicals" *J. Am. Chem. Soc.* **2015,** 137, 11115-11125.

[18] Coughlin Ezra, J.; Zeller, M.; Bart Suzanne, C. "Neodymium(III) Complexes Capable of Multi-Electron Redox Chemistry" *Angew. Chem.* **2017,** 129, 12310-12313.

[19] Blackmore, K. J.; Ziller, J. W.; Heyduk, A. F. ""Oxidative Addition" to a Zirconium(IV) Redox-Active Ligand Complex" *Inorg. Chem.* **2005,** 44, 5559-5561.

[20] Blackmore, K. J.; Sly, M. B.; Haneline, M. R.; Ziller, J. W.; Heyduk, A. F. "Group IV Imino-Semiquinone Complexes Obtained by Oxidative Addition of Halogens" *Inorg. Chem.* **2008,** 47, 10522-10532.

[21] Matson, E. M.; Opperwall, S. R.; Fanwick, P. E.; Bart, S. C. ""Oxidative Addition" of Halogens to Uranium(IV) Bis(Amidophenolate) Complexes" *Inorg. Chem.* **2013,** 52, 7295-7304.

[22] Matson, E. M.; Franke, S. M.; Anderson, N. H.; Cook, T. D.; Fanwick, P. E.; Bart, S. C. "Radical Reductive Elimination from Tetrabenzyluranium Mediated by an Iminoquinone Ligand" *Organometallics* **2014,** 33, 1964-1971.

[23] Abakumov, G. A.; Cherkasov, V. K.; Piskunov, A. V.; Meshcheryakova, I. N.; Maleeva, A. V.; Poddel'skii, A. I.; Fukin, G. K. "Zinc Molecular Complexes with Sterically Hindered O-Quinone and O-Iminoquinone" *Dokl. Chem.* **2009,** 427, 168-171.

[24] Ranis, L. G.; Werellapatha, K.; Pietrini, N. J.; Bunker, B. A.; Brown, S. N. "Metal and Ligand Effects on Bonding in Group 6 Complexes of Redox-Active Amidodiphenoxides" *Inorg. Chem.* **2014,** 53, 10203-10216.

[25] Pangborn, A. B.; Giardello, M. A.; Grubbs, R. H.; Rosen, R. K.; Timmers, F. J. "Safe and Convenient Procedure for Solvent Purification" *Organometallics* **1996,** 15, 1518-1520.

[26] Chakraborty, S.; Chattopadhyay, J.; Guo, W.; Billups, W. E. *Angew. Chem. Int. Ed.* **2007,** 46, 4486-4488.

[27] Wilkerson, M. P.; Burns, C. J.; Paine, R. T.; Blosch, L. L.; Andersen, R. A. "Organometallic and Coordination Complexes. Di(M-Chloro)Bis{Chlorodioxobis(Tetrahydrofuran)Uranium(VI)}, $[UO_2Cl_2(THF)_2]_2$" *Inorg. Synth.* **2004,** 34, 93-95.

[28] Berthet, J. C.; Lance, M.; Nierlich, M.; Ephritikhine, M. "Simple Preparations of the Anhydrous and Solvent-Free Uranyl and Cerium(IV) Triflates $UO_2(OTf)_2$ and $Ce(OTf)_4$ - Crystal Structures of $UO_2(OTf)_2(Py)_3$ and $[\{UO_2(Py)_4\}_2(m\text{-}O)][OTf]_2$" *Eur. J. Inorg. Chem.* **2000**, 1969-1973.

[29] Kiplinger, J. L.; Morris, D. E.; Scott, B. L.; Burns, C. J. "Convenient Synthesis, Structure, and Reactivity of $(C_5Me_5)U(CH_2C_6H_5)_3$: A Simple Strategy for the Preparation of Monopentamethylcyclopentadienyl Uranium(Iv) Complexes" *Organometallics* **2002,** 21, 5978-5982.

[30] Abergel, R. J.; de Jong, W. A.; Deblonde, G. J. P.; Dau, P. D.; Captain, I.; Eaton, T. M.; Jian, J.; van Stipdonk, M. J.; Martens, J.; Berden, G.; Oomens, J.; Gibson, J. K. "Cleaving Off Uranyl Oxygens through Chelation: A Mechanistic Study in the Gas Phase" *Inorg. Chem.* **2017,** 56, 12930-12937.

[31] Fortier, S.; Hayton, T. W. "Oxo Ligand Functionalization in the Uranyl Ion (UO_2^{2+})" *Coord. Chem. Rev.* **2010,** 254, 197-214.

[32] Herasymchuk, K.; Chiang, L.; Hayes, C. E.; Brown, M. L.; Ovens, J.; Patrick, B. O.; Leznoff, D. B.; Storr, T. "Synthesis and Electronic Structure Determination of Uranium(VI) Ligand Radical Complexes" *Dalton Trans.* **2016,** 45, 12576-12586

[33] Takao, K.; Tsushima, S.; Ogura, T.; Tsubomura, T.; Ikeda, Y. "Experimental and Theoretical Approaches to Redox Innocence of Ligands in Uranyl Complexes: What Is Formal Oxidation State of Uranium in Reductant of Uranyl(VI)?" *Inorg. Chem.* **2014,** 53, 5772-5780.

[34] Budzelaar, P. H. M.; de Bruin, B.; Gal, A. W.; Wieghardt, K.; van Lenthe, J. H. "Metal-to-Ligand Electron Transfer in Diiminopyridine Complexes of Mn-Zn. A Theoretical Study" *Inorg. Chem.* **2001,** 40, 4649-4655.

[35] Azam, M.; Al-Resayes, S. I.; Velmurugan, G.; Venuvanalingam, P.; Wagler, J.; Kroke, E. "Novel Uranyl(VI) Complexes Incorporating Propylene-Bridged Salen-Type N_2O_2-Ligands: A Structural and Computational Approach" *Dalton Trans.* **2015,** 44, 568-577.

[36] Carter, S. M.; Sia, A.; Shaw, M. J.; Heyduk, A. F. "Isolation and Characterization of a Neutral Imino-Semiquinone Radical" *J. Am. Chem. Soc.* **2008,** 130, 5838-5839.

[37] Kahn, O., *Molecular Magnetism*. Wiley-VCH: New York, NY, 1993; p 396.

[38] Bleaney, B.; Bowers, K. D. "Anomalous Paramagnetism of Copper Acetate" *Proc. R. Soc. London, Ser. A: Mathematical and Physical Sciences* **1952,** 214, 451.

[39] Cobb, P. J.; Moulding, D. J.; Ortu, F.; Randall, S.; Wooles, A. J.; Natrajan, L. S.; Liddle, S. T. "Uranyl-Tri-Bis(Silyl)Amide Alkali Metal Contact and Separated Ion Pair Complexes" *Inorg. Chem.* **2018,** 57, 6571-6583.

[40] Arnold, P. L.; Stevens, C. J.; Bell, N. L.; Lord, R. M.; Goldberg, J. M.; Nichol, G. S.; Love, J. B. "Multi-Electron Reduction of Sulfur and Carbon Disulfide Using Binuclear Uranium(III) Borohydride Complexes" *Chem. Sci.* **2017,** 8, 3609-3617.

[41] Arnold, P. L.; Patel, D.; Wilson, C.; Love, J. B. "Reduction and Selective Oxo Group Silylation of the Uranyl Dication" *Nature* **2008,** 451, 315-317.

[42] Seaman, L. A.; Pedrick, E. A.; Wu, G.; Hayton, T. W. "Promoting Oxo Functionalization in the Uranyl Ion by Ligation to Ketimides" *J. Organomet. Chem.* **2018,** 857, 34-37.

[43] Anderson, N. H.; Odoh, S. O.; Yao, Y.; Williams, U. J.; Schaefer, B. A.; Kiernicki, J. J.; Lewis, A. J.; Goshert, M. D.; Fanwick, P. E.; Schelter, E. J.; Walensky, J. R.; Gagliardi, L.; Bart, S. C. "Harnessing Redox Activity for the Formation of Uranium Tris(Imido) Compounds" *Nat. Chem.* **2014,** 6, 919-926.

[44] Anderson, N. H.; Xie, J.; Ray, D.; Zeller, M.; Gagliardi, L.; Bart, S. C. "Elucidating Bonding Preferences in Tetrakis(Imido)Uranate(VI) Dianions" *Nat. Chem.* **2017,** 9, 850-855.

CHAPTER 3. SYNTHESIS, CHARACTERIZATION, AND ELECTRONIC STRUCTURE OF COPPER IMINOQUINONE COMPLEXES

3.1 Introduction

Copper iminoquinone complexes have come to the forefront of redox-active ligand research over the past 20 years, with interest in their electronic structure[1-4], reactivity[5-9] and bonding[2,10]. While these studies have provided good evidence for the neutral (iminoquinone) and monoanionic (iminosemiquinone) complexes, little attention has been paid to the dianionic ligand (amidophenolate) bound to copper. This is likely a result of its highly reduced nature, and thus instability. One study by Wieghardt and co-workers electrochemically generated a copper amidophenolate species *in situ.*[4] They measured the electronic absorption spectrum of the species and compared it to other copper complexes with the same ligand in different oxidation states. While other studies have advanced the understanding of reactivity and bonding preferences for the neutral and monoanionic forms of the ligand, these aspects of the copper amidophenolate species have not been examined. Herein, we present a study of the ^{dipp}iq ligand on copper, isolated in 3 oxidation states. To study the electronic structure, bonding preferences, and reactivity of these complexes, characterization including multinuclear NMR, EPR, UV-Vis, and X-ray crystallography is discussed. In particular, the effect of potassium binding to the complexes was evaluated, showing that interactions have drastic effect on the color of the complexes.

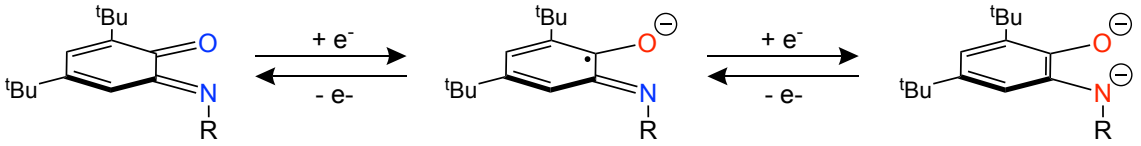

Figure 3.1: Redox chemistry of the iminoquinone ligand.

Blue denotes neutral atoms while red indicates anionic ones. The iminoquinone (iq^0) (left), iminosemiquinone (isq^{1-}) (middle) and amidophenolate (ap^{2-}) (right) exists in three oxidation states.

3.2 Experimental

3.2.1 General Considerations

All air- and moisture-sensitive manipulations were performed using standard Schlenk techniques or in an MBraun inert atmosphere drybox with an atmosphere of purified nitrogen. The MBraun drybox was equipped with two –35 °C freezers for cooling samples and crystallizations. Solvents for sensitive manipulations were dried and deoxygenated using literature procedures with a Seca solvent purification system.[11] Benzene-d_6 and pyridine-d_5 were purchased from Cambridge Isotope Laboratories, dried with molecular sieves and sodium, and degassed by three freeze–pump–thaw cycles. 4,6-di-*tert*-butyl-2-[(2,6-diisopropylphenyl)imino]quinone (^{dipp}iq)[12], potassium graphite (KC_8)[13], were prepared according to literature procedures. CuI, $[(CuOTf)_2tol]_2$ 18-crown-6 (18-C-6) was purchased from Sigma Aldrich and dried on a Schlenk line overnight prior to use.

^{1}H NMR spectra were recorded on a Varian Inova 300 spectrometer operating at 299.992 MHz. All chemical shifts are reported relative to the peak for $SiMe_4$, using ^{1}H (residual) chemical shifts of the solvent as a secondary standard. The spectra for all paramagnetic molecules were obtained by using an acquisition time of 0.5 s, thus the peak widths reported have an error of ±2 Hz. For all diamagnetic molecules, the ^{1}H NMR data are reported with the chemical shift, followed by the multiplicity, coupling constant in Hz, the integration value, and, where possible, the peak

assignment. For all paramagnetic molecules, the ^{1}H NMR data are reported with the chemical shift, followed by the peak width at half height in Hz, the integration value, and, where possible, the peak assignment. ^{11}B NMR spectra were recorded on a Varian Inova 300 spectrometer operating at a frequency of 96.24 MHz. ^{11}B chemical shifts are reported relative to the peak for BF_3Et_2O (0.0 ppm). All voltammetric data were obtained under inert atmosphere conditions using external electrical ports of the MBraun inert drybox. All data were obtained using a Gamry Instruments Interface 1000 model potentiostat using the Gamry Instruments Laboratory software. All data were collected on samples in THF with 0.1 M $[Bu_4N][PF_6]$ supporting electrolyte concentration, and using an internal resistance compensation of approximately 2000 ohms. Solutions were analyzed in 10 mL beakers, with a 3 mm glassy carbon working electrode, a Pt wire counter electrode, and an Ag wire quasi-reference electrode. Potential corrections were performed at the end of the experiment using the Fc/Fc^{+} couple as an internal standard. X-Band EPR spectra were recorded on a Bruker EMX EPR spectrometer. Electronic absorption measurements were recorded at 294 K in THF in sealed, 1 cm quartz cuvettes with a Cary 6000i UV-vis-NIR spectrophotometer. Elemental analyses were performed by Midwest Microlab (Indianapolis, IN). Solid state infrared spectra were recorded using a Thermo Nicolet 6700 spectrophotometer.

Crystals of **Cu-isq** suitable for X-ray diffraction, were coated with poly(isobutylene) oil in a glovebox and quickly transferred to the goniometer head of a Bruker Quest diffractometer with a fixed chi angle, a sealed tube fine focus X-ray tube, single crystal curved graphite incident beam monochromator and a Photon100 CMOS area detector. Examination and data collection were performed with Mo Kα radiation (λ = 0.71073 Å). Crystals of **Cu-iq, Cu-ap** and **Cu-ap crown** suitable for X-ray diffraction, were coated with poly(isobutylene) oil in a glovebox and quickly transferred to the goniometer head of a Bruker Quest diffractometer with kappa geometry, an I-μ-

S microsource X-ray tube, laterally graded multilayer (Goebel) mirror single crystal for monochromatization, a Photon2 CMOS area detector and an Oxford Cryosystems low temperature device. Examination and data collection were performed with Cu Kα radiation (λ = 1.54184 Å). Data were collected, reflections were indexed and processed, and the files scaled and corrected for absorption using APEX3.[14] All data were collected with Oxford Cryosystems low temperature devices operating at 100 or 150 K.

Data were collected, reflections were indexed and processed, and the files scaled and corrected for absorption using APEX3. The space groups were assigned and the structures were solved by direct methods using XPREP within the SHELXTL suite of programs and refined by full matrix least squares against F^2 with all reflections using Shelxl2014[15] using the graphical interface Shelxle.[16] If not specified otherwise, H atoms attached to carbon and nitrogen atoms were positioned geometrically and constrained to ride on their parent atoms, with carbon hydrogen bond distances of 0.95 Å for and aromatic C-H, 1.00, 0.99 and 0.98 Å for aliphatic C-H, CH_2 and CH_3 moieties, respectively. Methyl H atoms were allowed to rotate, but not to tip, to best fit the experimental electron density. U_{iso}(H) values were set to a multiple of U_{eq}(C) with 1.5 for CH_3, and 1.2 for CH_2 and C-H units, respectively.

3.2.2 Synthetic Details

Synthesis of (^{dipp}iq)$_2$Cu(OTf) (**Cu-iq**). A 20-mL scintillation vial was charged with [(CuOTf)$_2$Tol]$_2$ (0.075 g, 0.145 mmol) and 10 mL diethyl ether. A separate 20-mL scintillation vial was charged with ^{dipp}iq (0.220 g, 0.580 mmol), dissolved in 8 mL diethyl ether and added dropwise to the stirring [CuOTf)Tol]$_2$ slurry. A reddish-brown solution was observed. After 24 hours, the solution was filtered over Celite and volatiles were removed *in vacuo.* The resulting reddish-black solid was washed with cold pentane (3 × 10 mL) to afford a dark red powder (0.209

g, 0.215 mmol, 74% yield) assigned as **Cu-iq**. X-ray quality crystals were obtained from a concentrated toluene solution stored at -35 °C. Elemental analysis of $C_{53}H_{74}N_2O_5F_3S_1Cu_1$: Calculated, C, 65.51; H, 7.68; N, 2.88. Found, C, 64.88; H, 7.83; N, 2.73. ^{1}H NMR (C_6D_6, 25 °C): δ = 1.09 (s, 18H, C(C*H*$_3$)$_3$), 1.24 (s, 18H, C(C*H*$_3$)$_3$), 1.34 (s, 12H, CH(C*H*$_3$)$_2$), 1.49 (s, 12H, CH(C*H*$_3$)$_2$), 3.97 (s, 4H, C*H*(CH$_3$)$_2$), 4.29 (s, 2H, C*H*), 6.06 (t, 7, 2H, C*H*), 7.31 (d, 6 4H, C*H*). ^{19}F NMR (C_6D_6, 25 °C): δ = -78.47 (s, 3F, -OTf).

Synthesis of (^{dipp}isq)$_2$Cu (**Cu-isq**). A 20-mL scintillation vial was charged with CuI (0.140 g, 0.735 mmol) and 10 mL THF. A separate 20-mL scintillation vial was charged with ^{dipp}iq (0.558 g, 1.470 mmol), dissolved in 8 mL THF and added dropwise to the stirring CuI slurry. After stirring for 15 minutes, KC_8 (0.099 g, 0.735 mmol) was weighed by difference and added, resulting in a rapid color change from brown to dark green. After 2 hours, the solution was filtered over Celite and volatiles were removed *in vacuo*. The remaining mixture was washed with cold *n*-pentane (1 × 10 mL) to afford a green powder (0.526 g, 0.639 mmol, 87% yield) assigned as **Cu-isq**. Single, X-ray quality crystals were obtained from a concentrated toluene solution at -35 °C. Elemental analysis of $C_{52}H_{74}N_2O_2Cu$: Calculated, C, 75.92; H, 9.07; N, 3.41. Found, C, 75.42; H, 9.28; N, 3.52. ^{1}H NMR (C_6D_6, 25 °C): δ = -107.77 (1023, 2H, C*H*), -29.68 (34, 2H, C*H*), -6.13 (32, 2H, C*H*), 1.90 (37, 18H, C(C*H*$_3$)$_3$), 3.59 (37, 12H, CH(C*H*$_3$)$_2$), 3.96 (22, 12H, CH(C*H*$_3$)$_2$), 6.51 (22, 18H, C(C*H*$_3$)$_3$), 13.08 (152, 4H, C*H*(CH$_3$)$_2$), 28.33 (43, 4H, C*H*).

Synthesis of [(^{dipp}ap)$_2$Cu][K(THF)$_2$]$_2$ (**Cu-ap**) from **Cu-isq**. A 20-mL scintillation vial was charged with **Cu-isq** (0.100 g, 0.122 mmol) and 10 mL THF. While stirring, KC_8 (0.033 g, 0.243 mmol) was weighed by difference and added, resulting in a rapid color change from dark green to purple. After 1 hour, the solution was filtered over Celite and volatiles were removed *in vacuo*. The crude mixture was washed with cold *n*-pentane (2 × 5 mL) to afford a purple powder (0.099

g, 0.095 mmol, 78% yield) assigned as **Cu-ap**. Single, X-ray quality crystals were obtained from a concentrated diethyl ether solution at -35 °C. Elemental analysis of $C_{60}H_{90}N_2O_4K_2Cu_1$: Calculated, C, 68.95; H, 8.68; N, 2.68. Found, C, 68.44; H, 8.54; N, 2.57.

Synthesis of $[(^{dipp}ap)_2Cu][K(18\text{-crown-6})(THF)_2]_2$ (**Cu-ap crown**) from **Cu-ap**. A 20-mL scintillation vial was charged with **Cu-ap** (0.330 g, 0.316 mmol) and 15 mL THF forming a red solution. While stirring, 18-crown-6 (0.167 g, 0.632 mmol) was weighed by difference and added. Immediately, A tan precipitate forms, suspended in the THF solution. After stirring the slurry for 3 hours, volatiles were removed *in vacuo*. The crude mixture was washed with cold diethyl ether (2 × 10 mL) to afford a tan powder (0.472 g, 0.275 mmol, 87% yield) assigned as **Cu-ap crown**. X-ray quality crystals were obtained from a concentrated THF solution stored at -35 °C. Elemental analysis of $C_{92}H_{154}N_2O_{18}K_2Cu_1$: Calculated, C, 64.32; H, 9.04; N, 1.63. Found, C, 64.05; H, 8.89; N, 1.50.

3.3 Copper Iminoquinone Complexes

3.3.1 Synthesis of **Cu-iq**

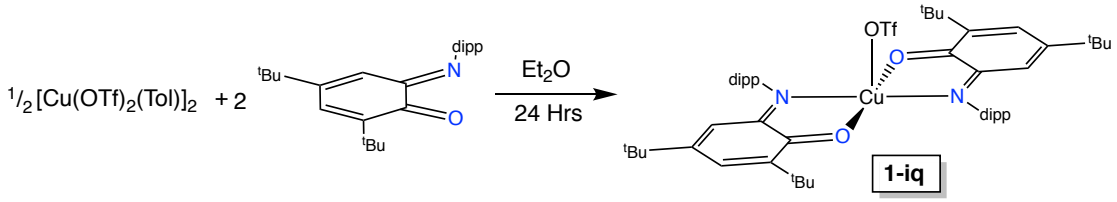

Figure 3.2: Synthesis of the copper iminoquinone complex, **Cu-iq**.

Studies initially targeted a copper iminoquinone complex featuring two neutral ligands. Attempted synthesis with copper monohalides yielded mono-ligand species with dimeric

structures that bridge through halide anions. In order to attain a bis(ligand) complex, a more labile anionic group was employed. Cuprous triflate was treated with two equivalents of ligand, resulting in a darkening of solution to red. After workup, a reddish-black solid was attained in good yield (74%). Proton NMR analysis revealed 8 diamagnetic resonances corresponding to the iminoquinone ligand. Fluorine NMR confirmed the presence of a triflate ion with a single peak at -78 ppm. Crystals suitable for X-ray crystallography were grown from a concentrated toluene solution and confirmed the presence of two ligands in a pseudo-pentagonal bipyramidal orientation.

3.3.2 X-Ray Crystallography of **Cu-iq**

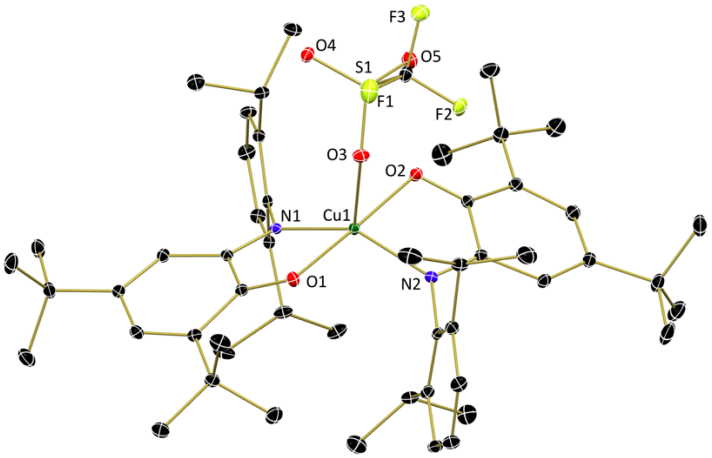

Figure 3.3: Molecular structure of **Cu-iq**.
Structure shown with 30% probability ellipsoids and hydrogen atoms and co-crystallized solvent molecules have been omitted for clarity.

Structure determination is one of the most rewarding techniques for the inorganic chemist, thus all copper iminoquinone complexes were analyzed using single-crystal X-ray diffraction. **Cu-iq** crystallizes from toluene in the monoclinic space group $P2_1/c$, revealing a five-coordinate

copper complex. Two iminoquinone ligands and one triflate ion are bound in a pseudo-trigonal bipyramidal geometry (τ_5=0.61). The interaction of the triflate ion with the copper atom is weak, as demonstrated by the relatively long linkage of 2.1977(13) Å. For comparison, the copper-oxygen bonds of the iminoquinone ligands are shorter, 2.1688(12) and 2.1832(12) Å, despite being dative interactions. Indeed, the nitrogen atoms of the iminoquinone ligands are the shortest bonds to copper at 1.9345(14) and 1.9352(14) Å.

3.4 Copper Iminosemiquinone Complexes

3.4.1 Synthesis of **Cu-isq**

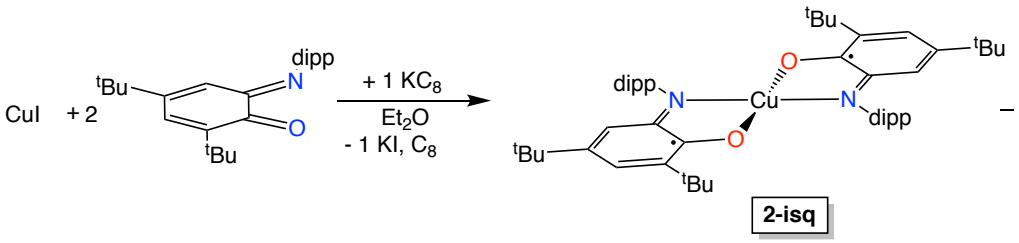

Figure 3.4: Synthesis of the copper iminosemiquinone complex, **Cu-isq**.

The copper bis(iminosemiquinone) complex, **Cu-isq**, was generated via salt metathesis of copper iodide with one equivalent of potassium graphite in the presence of two equivalents of ligand. The solution changes color from brown/red to green with addition of reductant, corresponding to the change in oxidation state of the ligand. The proton NMR spectrum features broad, paramagnetic resonances ranging from -30 to +30 ppm. This paramagnetism is not unusual for the iminosemiquinone ligand, and has been observed with other metals, even diamagnetic ones.

3.4.2 X-Ray Crystallography of **Cu-isq**

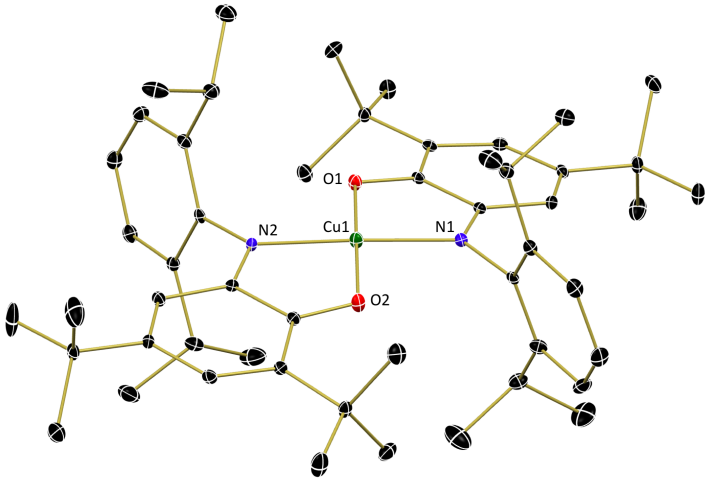

Figure 3.5: Molecular structure of **Cu-isq**.
Structure shown with 30% probability ellipsoids and hydrogen atoms and co-crystallized solvent molecules have been omitted for clarity.

The confirmation of structure was accomplished by analysis of crystals grown from toluene, showing a square planar coordination with nitrogen atoms *trans* from each other, in the sterically favorable conformation.

Crystals of **Cu-isq**, grown from toluene, were analyzed and found to be in the monoclinic space group P_n. This square planar complex (τ_4'=0.04) has two iminoquinone ligands bound to the copper center, with nitrogen atoms *trans* to each other, in sterically favorable positions. The copper-oxygen bond distances are short, at 1.909(3) and 1.905(3) Å, signifying anionic linkages. On the other hand, the copper-nitrogen bond distances of 1.938(3) and 1.933(3) Å are on par with those of **Cu-iq**, suggesting they maintain their dative bonding.

3.4.3 Cyclic Voltammetry of **Cu-isq**

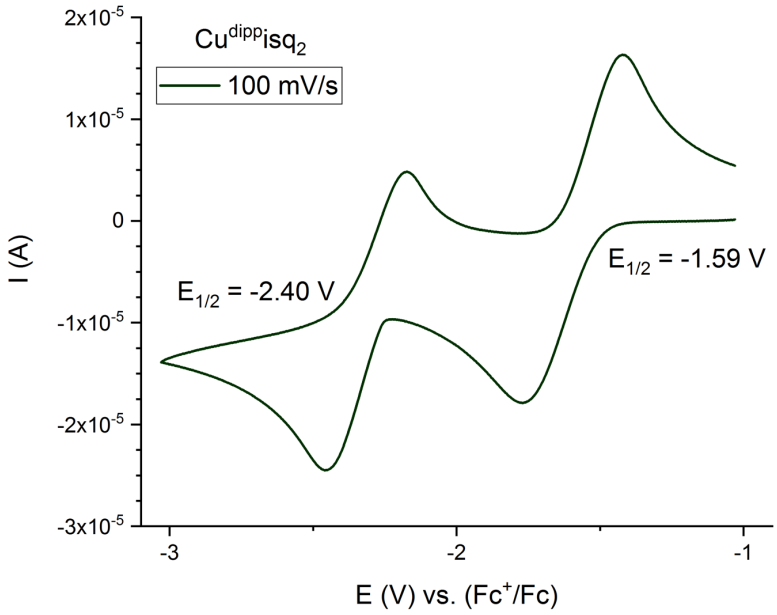

Figure 3.6: Cyclic Voltammetry of **Cu-isq** vs. Fc/Fc^{+}.
Data recorded in 4 mL 1.0 M [(*n*-Bu)$_4$N][PF_6] THF solutions at 25 °C.

Cu-isq was examined using electrochemistry to study the nature of oxidation and reduction of the complex. In a THF solution, analysis of cathodic scans revealed one reversible oxidation at -0.51 V. However, further scanning yielded poor reversibility and rapid decay of signal. The observed phenomenon is likely due to the iminoquinone ligand dissociating from the complex and undergoing deleterious side reactions. This behavior has been noted previously for the ligand, forming unidentifiable polymerization products. Anodic scans proved much more rewarding. Two, quasi-reversible reductions were observed at -1.59 and -2.40 V. These signals correspond to the sequential reduction of each ligand by one electron, forming the bis(amidophenolate) species *in situ*. The quasi-reversible nature, along with crystallographic results suggest that the molecule has

some sort of re-arrangement upon reduction. Based on these reversible, accessible electrochemical reductions, further reduction of the ligands of our copper complexes was explored.

3.5 Copper Amidophenolate Complexes

3.5.1 Synthesis of **Cu-ap** and **Cu-ap crown**

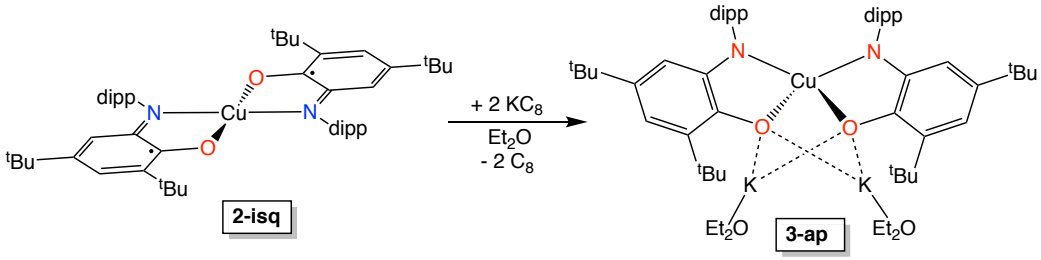

Figure 3.7: Synthesis of the copper amidophenolate (**Cu-ap**) complex by reduction of **Cu-isq**.

Interested in pushing the limits of the iminoquinone ligand, reduction of the copper bis(iminosemiquinone) was accomplished with two equivalents of potassium graphite. The green solution immediately changed color to purple. Upon workup, a purple solid was attained in good yield (78%). The molecular structure was determined using X-ray crystallography, showing potassium coordination to the dianionic ligands, bending them into a pseudo-tetrahedral geometry. This is not unlike the coordination of the potassium ions to the ligands in **Ln-ap**, with two solvent molecules bound.

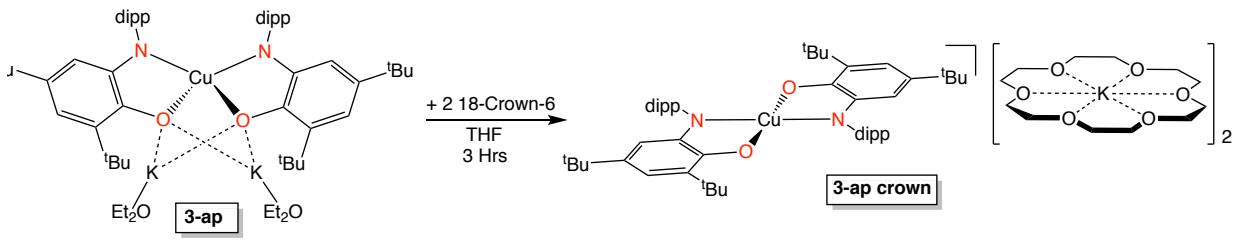

Figure 3.8: Synthesis of the copper bis(amidophenolate) dipotassium crown ether complex (**Cu-ap crown**).

To extract the potassium ions and prevent the conformational bending observed in **Cu-ap**, 18-crown-6 (18-C-6) was employed. Upon adding the crown ether to a light red THF solution of **Cu-ap**, an immediate change in solubility is observed. A shimmering suspension of brown powder forms and does not easily settle. Upon workup, a tan powder is obtained (87% yield) that is poorly soluble in non-polar solvents. Once again, X-ray crystallography was employed to determine the connectivity and identity of the species. Initially, crystals from THF or ACN provided subpar data, with large amounts of disorder. Finally, after several attempts, a suitable sample was found.

3.5.2 X-Ray Crystallography of **Cu-ap** and **Cu-ap crown**

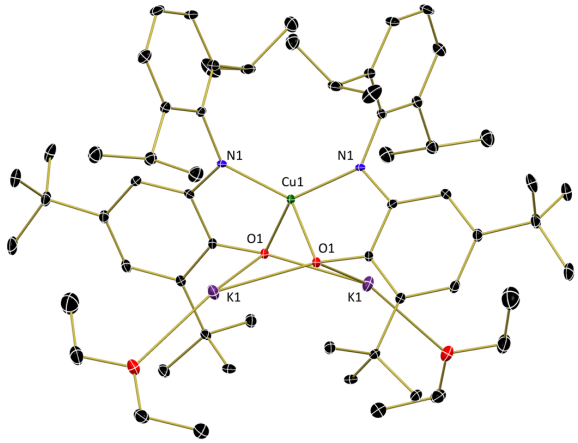

Figure 3.9: Molecular structure of **Cu-ap**.
Structure shown with 30% probability ellipsoids and hydrogen atoms and co-crystallized solvent molecules have been omitted for clarity.

The bis(amidophenolate) complex (**Cu-ap**) crystallized from diethyl ether in the orthorhombic space group P_{bcn}. The copper center is located on a 2-fold rotation center, creating crystallographically symmetric ligands. The diethyl ether-bound potassium ions coordinate to the oxygen atoms of the ligands and appear to bend them into a pseudo-tetrahedral geometry (τ_4=0.67, τ_4'=0.65). The copper-oxygen bond distances of 1.9813(16) Å are quite long, while the copper-nitrogen bond distances of 1.9332(18) Å are similar to those of **Cu-isq**. The observed lengthening of the copper-oxygen bonds can be attributed to the potassium ion "pulling" the oxygen atom away from the copper.

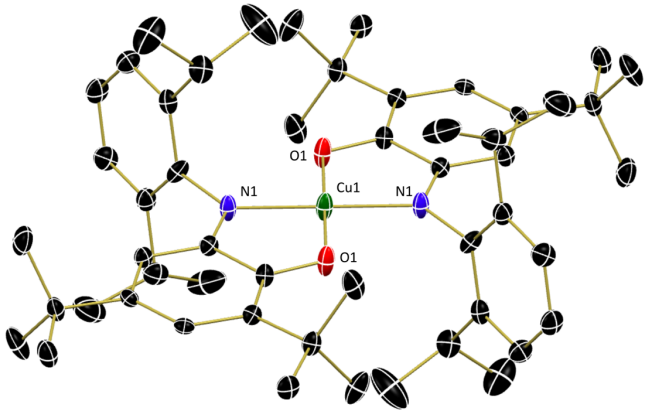

Figure 3.10: Molecular structure of **Cu-ap crown**.
Structure shown with 30% probability ellipsoids and hydrogen atoms, co-crystallized solvent molecules and potassium-bound crown ether molecules have been omitted for clarity.

Cu-ap crown crystallizes from THF in the triclinic space group P-1 as a 1:1 rotational twin. Refinement of the data reveal two potassium ions sequestered by crown ether molecules and with coordinated tetrahydrofuran molecules completing their coordination sphere. The copper center is ligated by two iminoquinone ligands in a square planar geometry (τ_4'=0.00), similar to **Cu-isq**. The copper atom is located on an inversion center, producing crystallographically symmetric ligands, with nitrogen atoms *trans* to each other. The copper oxygen bond distances of 1.940(3) Å are shorter than those of **Cu-ap**, with potassium ions completely removed from the coordination sphere. The copper-nitrogen distances of 1.923(3) Å are only slightly contracted compared to **Cu-isq** and **Cu-ap**.

3.6 UV-Vis/NIR of **Cu-iq**, **Cu-isq**, **Cu-ap** and **Cu-ap crown**

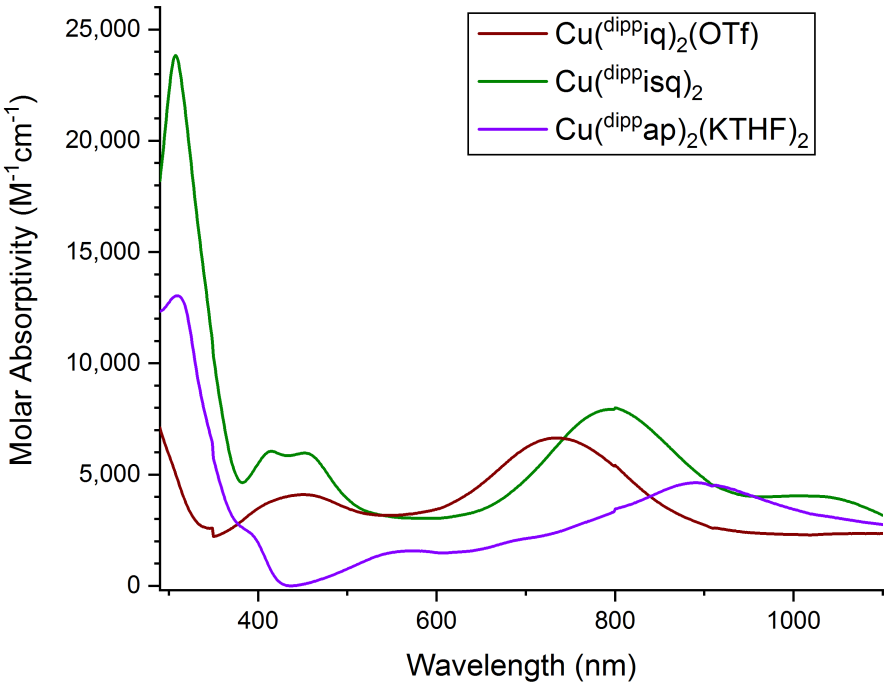

Figure 3.11: Electronic absorption spectra for **Cu-iq**, **Cu-isq** and **Cu-ap**. Data recorded in toluene at 25 °C.

Given the distinctive colors of copper iminoquinone complexes, electronic absorption spectroscopy was employed to examine the effect of reduction on electronic transitions. The spectrum of **Cu-iq** in toluene shows two strong absorptions at 452 (4099 M^{-1} cm^{-1}) and 734 nm (6646 M^{-1} cm^{-1}), responsible for the observed dark green color. Green, **Cu-isq** displays 5 absorbance maxima at 1009 (4,049 M^{-1} cm^{-1}), 796 (7,933 M^{-1} cm^{-1}), 452 (5,969 M^{-1} cm^{-1}), 415 (6,049 M^{-1} cm^{-1}) and 308 (23,838 M^{-1} cm^{-1}) nm. **Cu-ap** displays 3 absorbance at 891 (4,634 M^{-1} cm^{-1}), 569 (1,574 M^{-1} cm^{-1}) and 310 nm (13,036 M^{-1} cm^{-1}), producing a bright purple color.

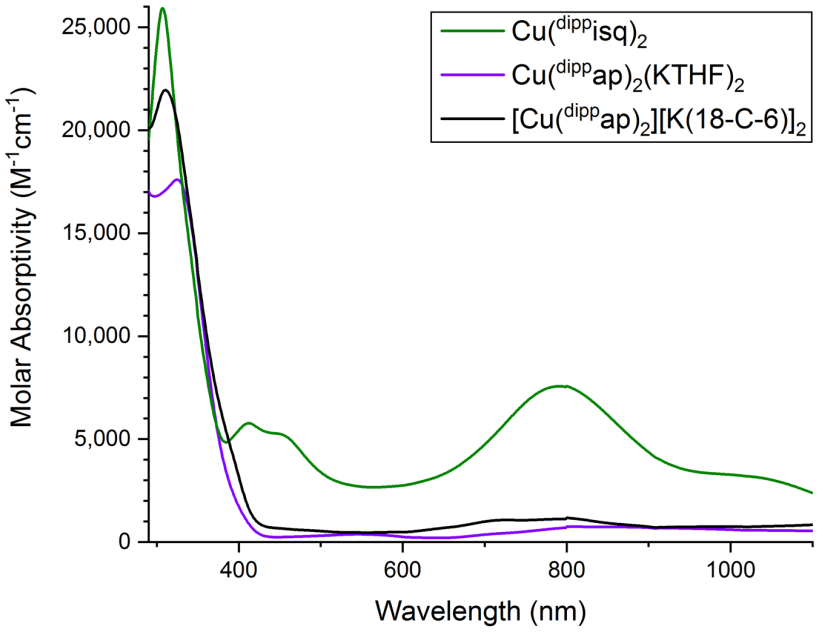

Figure 3.12: Electronic absorption spectra of **Cu-isq**, **Cu-ap** and **Cu-ap crown**. Data recorded in THF at 25 °C.

Cu-ap was noted to change color when dissolved in different solvents. Non-polar solvents such as pentane, toluene and benzene made purple solutions of **Cu-ap**, similar to the color of the powder. When **Cu-ap** was dissolved in THF, a bleaching of solution was noted with only a faint red color was observed. Hypothesizing that this solvatochromism was due to the potassium binding to the copper iminoquinone complex and causing a structural distortion, 18-crown-6 was used to sequester the potassium ions. Upon addition of the crown ether, a tan powder was obtained that is insoluble in non-polar solvents, and faintly red-colored in polar ones. The electronic absorption spectrum of **Cu-ap** and **Cu-ap crown** in THF show almost identical features (or lack of), only one strong absorption at ~375 nm. In contrast, the spectrum of **Cu-isq** collected in THF retains its five, strong absorption features from 308 to 1009 nm. Notably, the spectra of **Cu-ap** in toluene and THF are very different, with toluene solutions featuring many more absorptions, giving rise to its observed purple color.

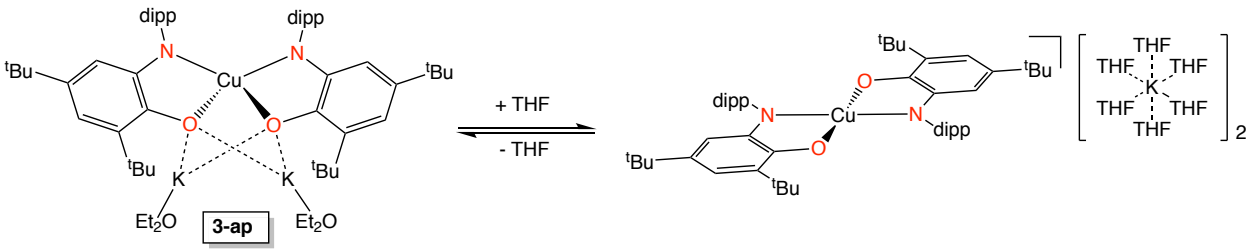

Figure 3.13: Proposed equilibrium responsible for the purple and colorless forms of **Cu-ap**. Coordinating solvents result in a bleaching of the purple **Cu-ap**.

3.7 Intraligand Bond Distance Comparison of **Cu-iq**, **Cu-isq**, **Cu-ap** and **Cu-ap crown**

Intraligand bond distances can aid in oxidation state assignment (ligand and metal) and the iminoquinone has a robust library of organometallic complexes available for comparison. This popular ligand has been studied enough that an equation has been developed to predict the oxidation state of the ligand based on structural changes. The output of the equation (MOS or Metrical Oxidation State) of each of the ligands will be discussed, along with other effects.

Each of the complexes **Cu-iq**, **Cu-isq** and **Cu-ap crown** feature the iminoquinone ligand in different oxidation state and intraligand bond distance vary accordingly. A good indication of reduction can be found in the C-O and C-N bonds of the ligands. When reduced, the bonds begin to lose their double-bond character, converting to a single-bond with occupation of the low-lying π*–orbital. **Cu-iq** features short C-O (1.238(2) and 1.236(2) Å) and C-N (1.238(2) and 1.236(2) Å) bond lengths, which are close to those of the free ligand (C-O = 1.221(2) and C-N = 1.287(2) Å). In **Cu-isq**, single reduction at each ligand lengthens the C-O bonds to 1.294(5) and 1.292(5) Å and C-N bonds to 1.334(5) and 1.342(5) Å, indicating more single bond character. Further reduction of the ligand lengthens the C-O bonds to 1.328 Å and C-N bonds to 1.369(5) Å, as measured in **Cu-ap crown**.

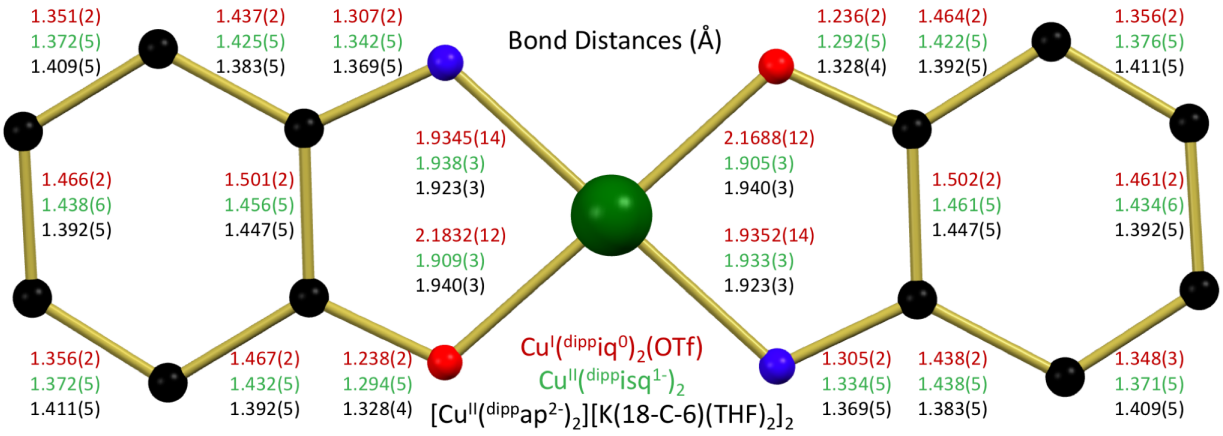

Figure 3.14: Bond distance comparison for **Cu-iq**, **Cu-isq** and **Cu-ap crown**.

Applying these C-O and C-N lengths (and the C-C bond lengths of the ring) to the MOS calculator, we are able to get a number representing the amount of reduction of the ligands. For **Cu-iq**, the MOS values for each ligand are -0.06 and -0.07. These numbers correspond well with our other characterization and assignment as two, neutral ligands. The MOS of **Cu-isq** was calculated to be -0.77 and -0.81. These values are close to -1 and could be slightly too high because the model is based on all iminoquinone complexes, and not just the dipp-substituted ligands. For **Cu-ap crown**, the MOS calculation produces a value of -1.61 for each ligand. While this could suggest that one ligand is -1 and one is -2 (averaging to -1.5), it is more likely the model is slightly off for this specific ligand set (as observed in **Cu-isq**).

3.8 EPR of **Cu-isq** and **Cu-ap**

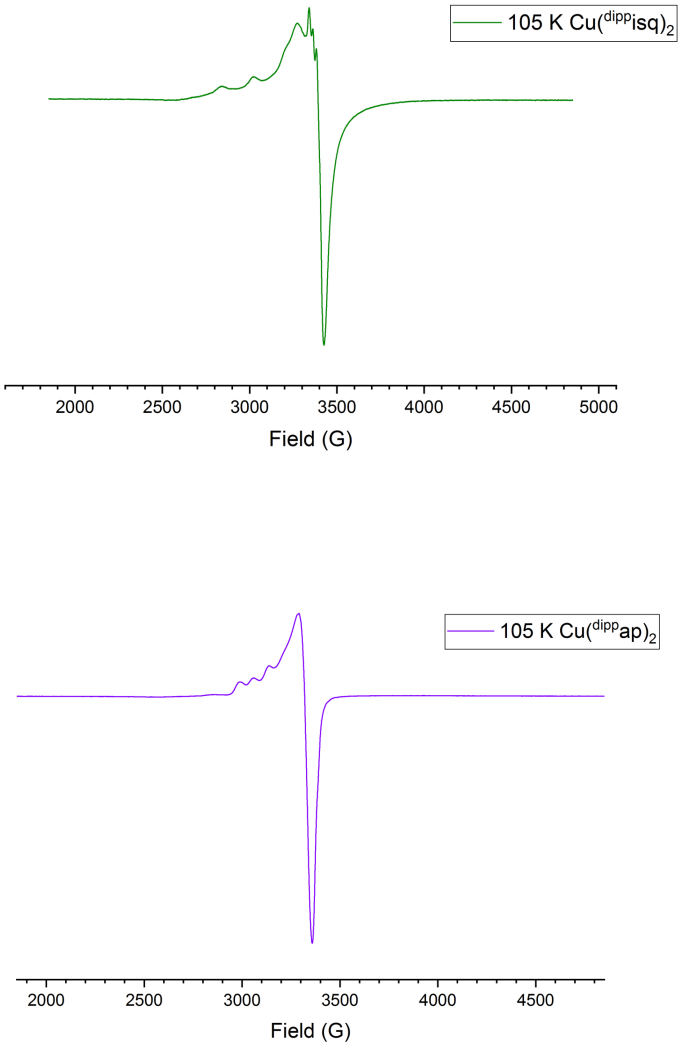

Figure 3.15: EPR spectra of **Cu-isq** and **Cu-ap**.
Data recorded in toluene at -168 °C. Frequency: 9.501 GHz. Power: 100 mW. Modulation: 10 G/100 kHz.

The iminoquinone ligand has been well studied for its ability to stabilize radicals in its monoanionic (iminosemiquinone) form. Additionally, Cu^{2+} is a d^9 species that contains an unpaired d-electron. Interested in studying the nature of these radical species, EPR spectroscopy

was carried out in toluene at 105 K and room temperature for each sample. At low temperature, **Cu-ap** shows an axial signal with hyperfine coupling to the Cu^{2+} nucleus. This is not uncommon for Cu^{2+} species. On the other hand, **Cu-isq** shows additional features at low temperature, located at approximately g = 2, with sharper features. This aides in the assignment of the ligand radical. Both of these spectra are consistent with the assignment of a Cu^{2+}, d^9 species and, in the case of **Cu-isq**, a ligand-based radical.

3.9 Conclusion

The synthesis and characterization of a series of copper complexes bearing the redox-active, iminoquinone ligand has been described. The iminoquinone species (**Cu-iq**) features a five-coordinate copper(I) center ligated by a triflate ion and two iminoquinone ligands. Upon removal of the triflate, the copper is oxidized by one electron to copper(II), forming a complex with two monoanionic, iminosemiquinone ligands (**Cu-isq**). This species features two ligand radicals, as observed by EPR spectroscopy. Further reduction with KC_8 allows access to the bis(amidophenolate) copper(II) complex (**Cu-ap**), with two dianionic ligands. This complex is of note, as previous literature has isolated the neutral and mono-anionic ligand species, but not the dianionic species. This highly reduced complex is stabilized by potassium coordination to the ligands, bending the species into a pseudo-tetrahedral geometry. Extracting the potassium ion (as in **Cu-ap crown**) from the coordination sphere has several effects. It bleaches the color of the complex from purple to tan, decreases its solubility in organic solvents, and returns the ligands to a square planer geometry, as in **Cu-isq**.

The work discussed here provides a study of the iminoquinone ligand, isolated in 3 oxidation states, on a copper metal center. The ability to isolate all three oxidation states allows for comparisons not noted in previous studies. The electronic structure, bonding preferences, and

reactivity was studied using multinuclear NMR, EPR, UV-Vis, and X-ray crystallography. Of particular interest is **Cu-ap crown**, which has four "stored" electrons that can be used to make new bonds with oxidants. Future studies aim to harness these electrons to make new bonding motifs and facilitate difficult reactions.

3.10 References

[1] Speier, G., Csihony, J., Whalen, A. M. & Pierpont, C. G. "Studies on Aerobic Reactions of Ammonia/ 3,5-Di- tert -butylcatechol Schiff-Base Condensation Products with Copper, Copper (I), and Copper (II). Strong Copper (II) - Radical Ferromagnetic Exchange and Observations on a Unique N - N Coupling Reaction." *Inorganic Chemistry.* **1996**, 35, 3519–3524.

[2] Rakshit, R., Ghorai, S., Biswas, S. & Mukherjee, C. Effect of Ligand Substituent Coordination on the Geometry and the Electronic Structure of Cu(II)-Diradical Complexes *Inorganic Chemistry.* **2014**, 53, 3333–3337.

[3] Ye, S., Sarkar, B., Lissner, F., Schleid, T., Slageren, J. V., Fiedler, J., Kaim, W. Three-spin system with a twist: A bis(semiquinonato)copper complex with a nonplanar configuration at the copper(II) center. *Angew. Chemie - Int. Ed.* **2005**, 44, 2103–2106.

[4] Chaudhuri, P. et al. Electronic Structure of Bis(o-iminobenzosemiquinonato) Metal Complexes (Cu, Ni, Pd). The Art of Establishing Physical Oxidation States in Transition-Metal Complexes Containing Radical Ligands. *J. Am. Chem. Soc.* **2001**, 123, 2213–2223.

[5] Zhu, S. X. & Chiba, S. "Copper-catalyzed Oxidative Carbon-Heteroatoms Bond Formation: A Recent Update." *Chem. Soc. Rev.* **2016**, 45, 4504–4523.

[6] Ren, Y., Cheaib, K., Jacquet, J., Vezin, H., Fensterbank, L., Orio, M., Blanchard, S.

D., Murr, M. "Copper-Catalyzed Aziridination with Redox-Active Ligands: Molecular Spin Catalysis." *Chem. - A Eur. J.* **2018**, 24, 5086–5090.

[7] Mukherjee, C., Weyhermüller, T., Bothe, E. & Chaudhuri, P. "Oxidation of an o -Iminobenzosemiquinone Radical Ligand by Molecular Bromine : Structural , Spectroscopic , and Reactivity Studies of a Copper (II) o -Iminobenzoquinone Complex." *Inorganic Chemistry*. **2008** 47, 2740–2746.

[8] Paul, G. C., Das, K., Maity, S., Begum, S., Srivastava, H. K., Mukherjee, C. "Geometry-Driven Iminosemiquinone Radical to Cu(II) Electron Transfer and Stabilization of an Elusive Five-Coordinate Cu(I) Complex: Synthesis, Characterization, and Reactivity with KO_2." *Inorganic Chemistry*. **2019**, 58, 1782-1793.

[9] Balaghi, S. E., Safaei, E., Chiang, L., Wong, E. W. Y., Savard, D., Clarke, R. M. Storr, T. "Synthesis, characterization and catalytic activity of copper(ii) complexes containing a redox-active benzoxazole iminosemiquinone ligand." *Dalt. Trans.* **2013**, 42, 6829–6839.

[10] Mondal, M. K. & Mukherjee, C. An unprecedented one-step synthesis of octahedral Cu(II)-bis(iminoquinone) complexes and their reactivity with $NaBH_4$. *Dalt. Trans.* **2016**, 13532–13540.

[11] Pangborn, A. B.; Giardello, M. A.; Grubbs, R. H.; Rosen, R. K.; Timmers, F. J. "Safe and Convenient Procedure for Solvent Purification" *Organometallics* **1996,** 15, 1518-1520.

[12] Abakumov, G. A.; Cherkasov, V. K.; Piskunov, A. V.; Meshcheryakova, I. N.; Maleeva, A. V.; Poddel'skii, A. I.; Fukin, G. K. "Zinc Molecular Complexes with Sterically Hindered O-Quinone and O-Iminoquinone" *Dokl. Chem.* **2009,** 427, 168-171.

[13] Chakraborty, S.; Chattopadhyay, J.; Guo, W.; Billups, W. E. *Angew. Chem. Int. Ed.* **2007,** 46, 4486-4488

[14] Bruker (2016). Apex3 v2016.9-0, Saint V8.34A,SAINT V8.37A, Bruker AXS Inc.: Madison (WI), USA 2013/2014.

[15] G. M. Sheldrick. "Crystal structure refinement with SHELXL", *Acta Cryst. C*, **2015**, *71*, 3.

[16] C. B. Hübschle, G. M. Sheldrick, B. Dittrich, *J. Appl. Cryst.*, **2011**, *44*, 1281.

VITA

Ezra J. Coughlin received his Bachelor of Arts from St. Olaf College in Northfield, Minnesota as a Chemistry and Math major in the spring of 2015. He excelled in his organometallic and inorganic courses as an undergraduate and proceeded to pursue research in the laboratory of Gary Miessler. His research focused on the synthesis and characterization of first row transition metal cluster complexes as enzyme mimics. He learned a variety of air- and moisture-free analytical techniques including IR, UV-Vis, NMR and MALDI mass spectrometry. This experience, coupled with an industrial internship at a medical device company, motivated Ezra to continue on to graduate school.

Upon arriving in West Lafayette in 2015, Ezra joined the organometallic synthesis lab of Professor Suzanne C. Bart. His projects at Purdue focused on installing the iminoquinone ligand on *f*-block elements and isolating complexes with the ligands in different oxidation states. With rigorous characterization and reactivity studies, this work was published in *Angew. Int. Ed.* and *J. Am. Chem. Soc.* Ezra presented his work at multiple conferences, as well as at St. Olaf. His work was awarded 1st place in the Innovations in Nuclear Technology Awards administered by the U.S. Department of Energy and has been highlighted in the magazines *Nachrichten aus der Chemie* and *Chemical & Engineering News*.

With this experience at Purdue, Ezra has learned extensive characterization techniques including multi-nuclear NMR, IR, EPR, and electronic absorption spectroscopies. Adding to his experience, Ezra was selected to be the lab assistant for the X-ray diffraction facility at Purdue and worked with Dr. Matthias Zeller to install, maintain, operate and troubleshoot XRD instruments for three years.

PUBLICATIONS

GDCh Communications Angewandte International Edition Chemie

Redoxactive Ligands

International Edition: DOI: 10.1002/anie.201705423
German Edition: DOI: 10.1002/ange.201705423

Neodymium(III) Complexes Capable of Multi-Electron Redox Chemistry

*Ezra J. Coughlin, Matthias Zeller, and Suzanne C. Bart**

Abstract: *A family of neodymium complexes featuring a redox-active ligand in three different oxidation states has been synthesized, including the iminoquinone (L^0) derivative, (^{dipp}iq)$_2$NdI$_3$ (**1-iq**), the iminosemiquinone (L^{1-}) compound, (^{dipp}isq)$_2$NdI(THF) (**1-isq**), and the amidophenolate (L^{2-}) [K(THF)$_2$][(^{dipp}ap)$_2$Nd(THF)$_2$] (**1-ap**) and [K(18-crown-6)][(^{dipp}ap)$_2$Nd(THF)$_2$] (**1-ap crown**) species. Full spectroscopic and structural characterization of each derivative established the +3 neodymium oxidation state with redox chemistry occurring at the ligand rather than the neodymium center. Oxidation with elemental chalcogens showed the reversible nature of the ligand-mediated reduction process, forming the iminosemiquinone metallocycles, [K(18-crown-6)][(^{dipp}isq)$_2$Nd(S$_5$)] (**2-isq crown**) and [K(18-crown-6)(THF)][(^{dipp}isq)$_2$Nd(Se$_5$)] (**3-isq crown**), which are characterized to contain a 6-membered twist-boat ring.*

The rare earth elements are well known for their characteristic magnetic, luminescent, and Lewis acidic properties, giving rise to their essential roles in medicine, energy, and technology.[1] Their redox chemistry, especially when considering organometallic transformations, is known to a lesser extent because the thermodynamically stable +3 oxidation state is generally redox-restricted (except Ce, Nd, Sm, Eu, Dy, Yb).[2] An effective strategy to circumvent the redox-inactivity of lanthanides is the use of redox-active ligands, which have been established to facilitate multi-electron transfer with metals of the p,[3,4] d,[5] and f[6,7] blocks of the periodic table.

While redox-active ligands have been proven to impart interesting magnetic[8,9] or electrochemical[10–12] properties to the rare earth elements due to their ability to stabilize ligand radicals,[13,14] fewer examples exist that demonstrate productive electron movement for new bond formation. Mazzanti et al. reported tetradentate Schiff base complexes of Nd, Eu, Tb, Yb that, upon reduction, store two electrons in a new C–C σ bond.[15] These species can be oxidized using AgOTf or I_2, highlighting the reversibility of this redox process as seen by C–C bond cleavage. Reactivity with 9,10-phenanthrenequinone shows reduction to the corresponding potassium catecholate, thus this approach is effective for small molecule activation. Application of redox-active ferrocene diamide ligands has also led to productive polymerization chemistry as demonstrated by Diaconescu and co-workers with their redox switchable rare earth catalysts.[16]

Based on these exciting examples of ligand mediated redox chemistry for bond formation reactions, we sought to apply this methodology to redox-active ligands that store reducing equivalents in conjugated π systems (Figure 1). We have recently demonstrated this principle with the synthesis, characterization, and reactivity of uranium(IV) complexes, (^{R}ap)$_2$U(THF)$_2$ [R = *t*-Bu, Ad, dipp (dipp = 2,6-diisopropylphenyl)], supported by two redox-active 4,6-di-*tert*-butyl-2-(*R*)-amidophenolate ([ap]$^{2-}$) ligands.[17] These species readily undergo oxidative addition with $PhICl_2$, forming the bis-(4,6-di-*tert*-butyl-2-(R)iminosemiquinone) ([^{R}isq]$^{1-}$) uranium(IV) dichloride dimer, [(^{R}isq)$_2$UCl]$_2$(μ^2-Cl)$_2$. In these cases, the redox chemistry is relegated to the ligand, which acts as an electron source, converting the amidophenolates to iminosemiquinones. This exciting multi-electron reactivity prompted investigation of these ligands for supporting rare earth complexes. Herein, we present the synthesis and characterization of a family of neodymium complexes where the redox active ligand is featured in multiple oxidation states. Reversible multi-electron redox chemistry is demonstrated with oxidation of the electron-rich bis(amidophenolate) neodymium derivative by elemental chalcogens.

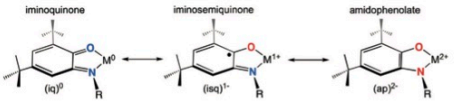

Figure 1. Redox chemistry for the iminoquinone ligand. Blue atoms indicate dative bonding to M, red atoms indicate anionic bonding to M.

The first entry in the family was generated by stirring two equivalents of the dipp-substituted iminoquinone (^{dipp}iq) with $NdI_3(THF)_{3.5}$, which afforded the metallated product, (^{dipp}iq)$_2$NdI$_3$ (**1-iq**) as a red powder in moderate yield after workup (Figure 2). Reduction of **1-iq** was performed to engage the redox activity of the iminoquinone using two equiv of KC_8. Workup and isolation of the product resulted in the reduced species, (^{dipp}isq)$_2$NdI(THF) (**1-isq**), as a dark green powder. The final entry in the series, [K(THF)$_2$][(^{dipp}ap)$_2$Nd(THF)$_2$] (**1-ap**) was accessed by further reduction of **1-isq** using two more equiv of KC_8. In this case, filtration and washing of the product resulted in isolation of a pale blue solid. To ensure removal of the potassium from the coordination sphere, **1-ap** was treated with 18-crown-6 (18-c-6),

[*] E. J. Coughlin, Dr. M. Zeller, Prof. S. C. Bart
H.C. Brown Laboratory, Department of Chemistry, Purdue University
West Lafayette, IN 47907 (USA)
E-mail: sbart@purdue.edu

Supporting information and the ORCID identification number(s) for the author(s) of this article can be found under: https://doi.org/10.1002/anie.201705423.

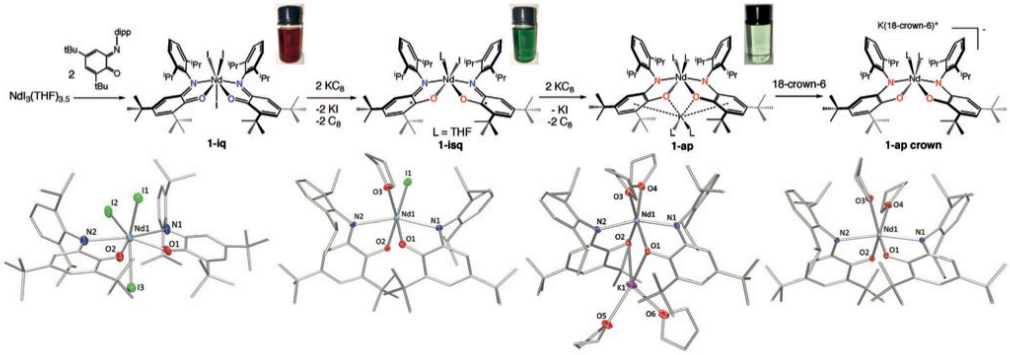

Figure 2. Synthesis and molecular structures of **1-iq**, **1-isq**, and **1-ap crown**. Molecular structures are shown at 30% probability ellipsoids with hydrogen atoms, co-crystallized solvent molecules, and the potassium cation with coordinated (18-c-6) removed for clarity. Insets show solutions of each compound in THF at ambient temperature.

yielding [K(18-c-6)][(^{dipp}ap)$_2$Nd(THF)$_2$] (**1-ap crown**). Given that the solution ^{1}H NMR spectra of **1-ap** and **1-ap crown** are distinct (Figures S3 and S4 in the Supporting Information), the potassium likely retains its coordination to the ligands in the absence of the crown ether. In each case, the +3 oxidation state of the neodymium is maintained, as reduction events are restricted to the ligands; thus, paramagnetically broadened and shifted ^{1}H NMR spectra are noted for the Nd^{III}, f^3 systems (see the Supporting Information).

Structural characterization was performed, as metrical parameters can be an indicator of ligand oxidation state.[18] A discussion of representative distances from **1-iq**, **1-isq**, and **1-ap crown** are presented (Figure 3), whereas data for **1-ap** appears in the Supporting Information.

Compound **1-iq** features a 7-coordinate, distorted pentagonal bipyramidal neodymium center. The respective Nd–O and Nd–N of 2.479(3) and 2.702(4) Å are consistent with dative interactions between neodymium and iminoquinone ligand, as expected from the oxidized form. This is corroborated by the C–N (1.300(6) Å) and C–O (1.238(6) Å) bond distances that are on the order of double bonds. Reduction of the ligand in octahedral **1-isq** is supported by contraction of the Nd–O bond to 2.317(9) Å as compared to **1-iq**, as would

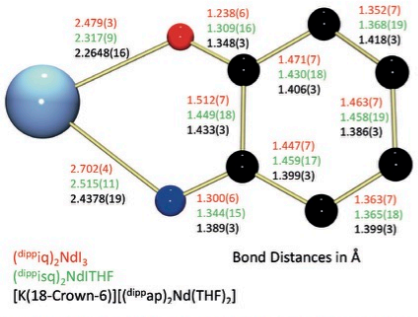

Figure 3. Bond distance [Å] comparison for **1-iq**, **1-isq**, and **1-ap crown**.

be expected from changing a dative bond to an anionic one, and by an elongation of the C–O bond. The Nd–N and C–N bond lengths change very little as compared to **1-iq**, since both maintain dative linkages with imine functionalities. The most reduced species, **1-ap crown**, maintains the short Nd–O bond of 2.2648(16) Å, but now displays a short Nd–N bond (2.4378(19) Å) as well, expected for anionic bonds to the distorted octahedral neodymium. Examination of the intra-ligand distances shows an aromatic ring, with similar distances throughout, and C–O and C–N bond distances that signify single bonds. In **1-ap**, where the crown is absent, the ligand distances are similar, but the potassium is bound to the oxygen atoms of the ap ligand blocking access to the Nd atom.

The ligand radical in **1-isq** was further confirmed by EPR spectroscopy (Figure S8), which showed a g-value of 2.0026 at 25 °C in toluene solution (2.04 mM). This spectrum is reminiscent of that previously observed for iminosemiquinone radicals reported by Heyduk,[19] which featured a g-value of 2.0061 (DMSO, 25 °C).

The energies associated with the electronic transitions for the intensely colored family of reduced species were quantified using electronic absorption spectroscopy. Data were collected from 300 to 900 nm in toluene at 25 °C. Both **1-iq** and **1-isq** absorb strongly in the visible region, while colorless **1-ap crown** does not. Compound **1-iq** shows an intense absorption at 484 nm (6000 M^{-1} cm^{-1}), giving rise to the observed deep red color, whereas **1-isq** shows a color-producing band at 779 nm (2000 M^{-1} cm^{-1}), responsible for the dark green hue. Based on the lack of d electrons and the constant f^3 ground state in this neodymium series, the ligand oxidation state dictates the appearance, making color a useful metric for ligand oxidation state identification.

Synthesis and characterization of **1-iq**, **1-isq**, **1-ap,** and **1-ap crown** demonstrate that lanthanide-containing small molecules can undergo multi-electron reduction chemistry in the appropriate ligand environments, since ultimately the π* orbitals of the ligands are where the electrons reside. To determine the lability of the ligand and f electrons for the most reduced species, **1-ap crown**, the reverse multi-electron

oxidation was tested. Elemental chalcogens were chosen due to their strongly oxidizing nature and the utility of Ln-chalcogen bonds in Ln/An separations.

Exposure of **1-ap crown** to 5/8 equiv of S_8 or 5 equiv of Se powder immediately turned the colorless solution to dark blue-green, consistent with formation of iminosemiquinone-containing products [Eq. (1)]. Following workup, the products, identified as $[K(18\text{-c-}6)][(^{dipp}isq)_2Nd(S_5)]$ (**2-isq crown**) and $[K(18\text{-c-}6)(THF)][(^{dipp}isq)_2Nd(Se_5)]$ (**3-isq crown**), respectively, were isolated in high yields. Once again, paramagnetically broadened and shifted ^1H NMR spectra were observed in the range of -100 to $+40$ ppm (C_6D_6, 25 °C); this range is most similar to that observed for **1-isq**, indicating that two ligand-based one-electron oxidations had occurred during the reaction. This formulation is corroborated by EPR spectroscopy, which showed g-values of 2.0026 in the spectra of **2-isq crown** and **3-isq crown**, consistent with the presence of organic radicals.

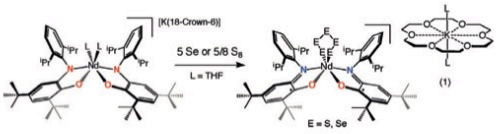

Structural support of the iminosemiquinone ligands in **2-isq crown** and **3-isq crown** was obtained using X-ray crystallography (Figure 4). Analysis and refinement of the data showed analogous structures, with the S_5 and Se_5 fragments forming 6-membered twist-boat metallocycles with the neodymium ion. Examination of the ligand distances (see Table S7) show average Nd–O bonds of 2.359 Å (**2-isq crown**) and 2.348 Å (**3-isq crown**) as well as average Nd–N bonds of 2.529 Å (**2-isq crown**) and 2.537 Å (**3-isq crown**), all confirming the assignment as iminosemiquinone ligands. The C–N and C–O bond distances track accordingly. Thus, **2-isq crown** and **3-isq crown** are formed from two-electron oxidation of the ligands in **1-ap crown**.

Elemental chalcogen activation has been previously noted with uranium, but generally persulfide (S_2^{2-}) compounds result.[20,21] Furthermore, the unusual twist-boat metallacycle noted here for Nd is unique to the bottom of the Periodic Table; transition metal counterparts do not display this conformer. Previously, Ryan and co-workers reported formation of twist-boat $Cp^*_2Th(S_5)$ by treating $Cp^*_2ThCl_2$ with Li_2S_5.[22] An analogous Sm^{III} derivative, $Tp^{iPr2}Sm(\kappa^1\text{-}3,5\text{-}^{iPr2}Hpz)(S_5)$ (Tp^{iPr2} = hydrotris(3,5-di-isopropylpyrazolyl)borate), was identified by Takats and Edelmann as one of the oxidation products from exposing divalent $(Tp^{iPr2})_2Sm$ to one equiv of S_8.[23] Surprisingly, the selenium metallacycle reported here is the first for an f-element, despite being previously known for the d-block.[24,25]

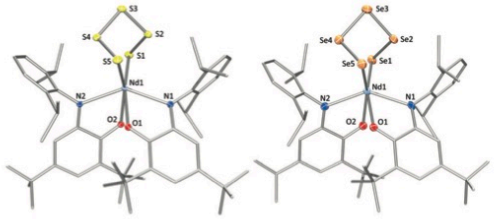

Figure 4. Molecular structures of **2-isq crown** and **3-isq crown** shown at 30% probability ellipsoids. Hydrogen atoms, co-crystallized solvent molecules, and potassium cations with coordinated 18-c-6 have been omitted for clarity.

Interestingly, reactivity of the neodymium amidophenolate derivatives with Se is only observed in the presence of the crown ether, although both **1-ap** and **1-ap crown** react with sulfur. Performing the analogous experiment with **1-ap** results in no reaction; however, upon addition of the crown ether to the mixture, immediate procession of the reaction is noted. We hypothesized that this is either due to 1) blocking of the neodymium center by the potassium ion that is held in place by interaction with the ligand, or 2) that the oxidation potential of **1-ap** is sufficiently higher such that elemental selenium is not a strong enough oxidant to remove an electron from the ligand π^* orbitals. To test the latter idea, electrochemical measurements of **1-ap** and **1-ap crown** were performed in THF solutions with a supporting electrolyte ($[NBu_4][PF_6]$). Cyclic voltammetric data for **1-ap** showed a quasi-reversible oxidation, $E_{1/2} = -0.864$ V (vs. Fc/Fc^+), corresponding to formation of **1-isq** in solution. Further oxidation showed an irreversible wave, consistent with oxidation of the ligand to iminoquinone. The loss of anionic linkages between the ligand and Nd facilitates ligand substitution with THF, explaining the irreversible nature of this wave. Cyclic voltammetric data for **1-ap crown** displayed very similar oxidations with the first quasi-reversible oxidation, $E_{1/2} = -0.772$ V. These data suggest that **1-ap crown** is more difficult to oxidize, thus the lack of reactivity is likely due to blocking of the neodymium by the potassium; thus, sequestration of the potassium ion is necessary for the reaction to proceed.

In summary, a series of bis(ligand) neodymium complexes was synthesized featuring ligands in three different oxidation states. These species were fully characterized and the most electron-rich derivative, **1-ap crown**, was used as a potent reductant towards elemental chalcogens. Produced are complexes that feature rare 6-membered metallacycles (**2-isq crown** and **3-isq crown**) in a twist-boat conformation. The redox chemistry noted here is significant, as rare earth element complexes are not commonly known to participate in multi-electron processes. Such cooperative electron movement has been exploited to facilitate organometallic processes and metal–element multiple bond formation in the d-block and actinide series. Future studies will focus on extending this principle to other rare earths, helping to expand the utility of these elements past their typical Lewis acidic, magnetic, and luminescent properties.

Acknowledgements

This material is based upon work supported by the U.S. Department of Energy, Office of Science, Office of Basic

Energy Sciences under Award Number DE-SC0008479. The X-ray crystallographic data in this work was obtained on instruments funded by the National Science Foundation through the Major Research Instrumentation Program under Grant No. CHE 1625543.

Conflict of interest

The authors declare no conflict of interest.

Keywords: lanthanide · neodymium · oxidation · redox-active ligand · reduction

How to cite: *Angew. Chem. Int. Ed.* **2017**, *56*, 12142–12145
Angew. Chem. **2017**, *129*, 12310–12313

[1] M. Murugesu, E. J. Schelter, *Inorg. Chem.* **2016**, *55*, 9951–9953.
[2] N. N. Greenwood, A. Earnshaw, *Chemistry of the Elements*, 2nd ed., Butterworth Heinemann, Oxford, **1998**.
[3] T. W. Myers, A. L. Holmes, L. A. Berben, *Inorg. Chem.* **2012**, *51*, 8997–9004.
[4] B. E. Cole, J. P. Wolbach, W. G. Dougherty, N. A. Piro, W. S. Kassel, C. R. Graves, *Inorg. Chem.* **2014**, *53*, 3899–3906.
[5] P. J. Chirik, *Acc. Chem. Res.* **2015**, *48*, 1687–1695.
[6] N. H. Anderson, S. O. Odoh, Y. Yao, U. J. Williams, B. A. Schaefer, J. J. Kiernicki, A. J. Lewis, M. D. Goshert, P. E. Fanwick, E. J. Schelter, J. R. Walensky, L. Gagliardi, S. C. Bart, *Nat. Chem.* **2014**, *6*, 919–926.
[7] E. Lu, S. T. Liddle, *Dalton Trans.* **2015**, *44*, 12924–12941.
[8] S. Demir, M. Nippe, M. I. Gonzalez, J. R. Long, *Chem. Sci.* **2014**, *5*, 4701–4711.
[9] H. Sugiyama, I. Korobkov, S. Gambarotta, A. Möller, P. H. M. Budzelaar, *Inorg. Chem.* **2004**, *43*, 5771–5779.
[10] E. J. Schelter, R. Wu, J. M. Veauthier, E. D. Bauer, C. H. Booth, R. K. Thomson, C. R. Graves, K. D. John, B. L. Scott, J. D. Thompson, D. E. Morris, J. L. Kiplinger, *Inorg. Chem.* **2010**, *49*, 1995–2007.
[11] J. A. Bogart, A. J. Lewis, S. A. Medling, N. A. Piro, P. J. Carroll, C. H. Booth, E. J. Schelter, *Inorg. Chem.* **2013**, *52*, 11600–11607.
[12] J. E. Kim, J. A. Bogart, P. J. Carroll, E. J. Schelter, *Inorg. Chem.* **2016**, *55*, 775–784.
[13] I. L. Fedushkin, O. V. Maslova, A. G. Morozov, S. Dechert, S. Demeshko, F. Meyer, *Angew. Chem. Int. Ed.* **2012**, *51*, 10584–10587; *Angew. Chem.* **2012**, *124*, 10736–10739.
[14] I. L. Fedushkin, O. V. Maslova, E. V. Baranov, A. S. Shavyrin, *Inorg. Chem.* **2009**, *48*, 2355–2357.
[15] C. Camp, V. Guidal, B. Biswas, J. Pecaut, L. Dubois, M. Mazzanti, *Chem. Sci.* **2012**, *3*, 2433–2448.
[16] W. Huang, P. L. Diaconescu, *Inorg. Chem.* **2016**, *55*, 10013–10023.
[17] E. M. Matson, S. R. Opperwall, P. E. Fanwick, S. C. Bart, *Inorg. Chem.* **2013**, *52*, 7295–7304.
[18] S. C. Bart, K. Chlopek, E. Bill, M. W. Bouwkamp, E. Lobkovsky, F. Neese, K. Wieghardt, P. J. Chirik, *J. Am. Chem. Soc.* **2006**, *128*, 13901–13912.
[19] S. M. Carter, A. Sia, M. J. Shaw, A. F. Heyduk, *J. Am. Chem. Soc.* **2008**, *130*, 5838–5839.
[20] C. Camp, M. A. Antunes, G. Garcia, I. Ciofini, I. C. Santos, J. Pecaut, M. Almeida, J. Marcalo, M. Mazzanti, *Chem. Sci.* **2014**, *5*, 841–846.
[21] S. M. Franke, F. W. Heinemann, K. Meyer, *Chem. Sci.* **2014**, *5*, 942–950.
[22] D. A. Wrobleski, D. T. Cromer, J. V. Ortiz, T. B. Rauchfuss, R. R. Ryan, A. P. Sattelberger, *J. Am. Chem. Soc.* **1986**, *108*, 174–175.
[23] M. Kühling, R. McDonald, P. Liebing, L. Hilfert, M. J. Ferguson, J. Takats, F. T. Edelmann, *Dalton Trans.* **2016**, *45*, 10118–10121.
[24] N. Tzavellas, N. Klouras, C. P. Raptopoulou, *Z. Anorg. Allg. Chem.* **1997**, *623*, 384–388.
[25] A. Kromm, Y. Geldmacher, W. S. Sheldrick, *Z. Anorg. Allg. Chem.* **2008**, *634*, 2191–2198.

Manuscript received: May 26, 2017
Accepted manuscript online: August 1, 2017
Version of record online: August 30, 2017

JACS JOURNAL OF THE AMERICAN CHEMICAL SOCIETY
Cite This: J. Am. Chem. Soc. 2019, 141, 1016−1026
Article
pubs.acs.org/JACS

Uranyl Functionalization Mediated by Redox-Active Ligands: Generation of O−C Bonds via Acylation

Ezra J. Coughlin,[†] Yusen Qiao,[‡] Ekaterina Lapsheva,[‡] Matthias Zeller,[†] Eric J. Schelter,[‡] and Suzanne C. Bart*,[†]

[†]H.C. Brown Laboratory, Department of Chemistry, Purdue University, West Lafayette, Indiana 47907, United States
[‡]P. Roy and Diana T. Vagelos Laboratories, Department of Chemistry, University of Pennsylvania, 231 South 34th Street, Philadelphia, Pennsylvania 19104, United States

Supporting Information

ABSTRACT: A series of uranyl compounds with the redox-active iminoquinone ligand have been synthesized, and their electronic structures elucidated using multinuclear NMR, EPR, electronic absorption spectroscopies, SQUID magnetometry, and X-ray crystallography. Characterization and analysis of the iminoquinone (iq^0) complex, (^{dipp}iq)$UO_2(OTf)_2$THF (**1-iq**), the iminosemiquinone (isq^{1-}) complex, (^{dipp}isq)$_2UO_2$THF (**2-isq**), and the amidophenolate (ap^{2-}) complex, [(^{dipp}ap)$_2UO_2$THF][K(18-crown-6)(THF)$_2$]$_2$(**3-ap crown**) show that reduction events are ligand-based, with the uranium center remaining in the hexavalent state. Reactivity of **2-isq** with B-chlorocatecholborane or pivaloyl chloride leads to U−O_{uranyl} bond scission and reduction of U(VI) to U(IV) concomitant with ligand oxidation along with organic byproducts. ^{18}O isotopic labeling experiments along with IR spectroscopy, mass spectrometry, and multinuclear NMR spectroscopy confirm that the organic byproducts contain oxygen atoms which originate from U−O_{uranyl} bond activation.

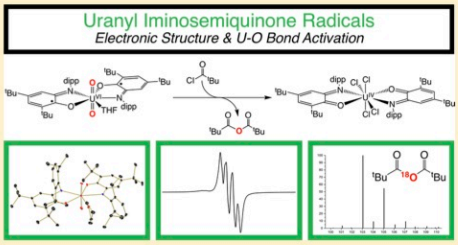

INTRODUCTION

The uranyl ion, $[UO_2]^{2+}$, is the most recognizable-actinide containing species due to its prevalence in aqueous environments and in the solid state.[1] Characterized by its robust *trans*-oxo ligands and +6 oxidation state, derivatives of this ion form naturally from interactions of water with uranium ore deposits, as well as anthropogenically from depleted uranium targets,[2] nuclear waste streams,[3] and uranium mining.[4] The high solubility of this ion in water is problematic as its increased mobility in this form causes environmental contamination. In anaerobic environments, uranyl can be reduced to its +5 (unstable) and +4 (stable) forms, greatly reducing its water solubility and facilitating removal from the environment.[5]

The persistence of uranyl is attributed to its strong uranium−oxygen bonds, which are not easily functionalized or cleaved. Taking inspiration from nature, recent work in nonaqueous uranyl chemistry has demonstrated that transformation of U−O_{uranyl} bonds may be facilitated by reduction events to generate U(IV) ions, in which pentavalent intermediates are likely involved. One strategy, demonstrated by Duval and co-workers, involves the photochemical reduction of hexavalent $[UO_2(dppmo)_2(OPPh_3)][OTf]_2$ (dppmo = $Ph_2P(O)CH_2P(O)Ph_2$) in the presence of BF_4^- anions, producing the corresponding uranium(IV) difluoride species.[6] Reductive silylation of the uranyl ion has also been studied[7−13] and optimized,[7] while strongly Lewis acidic titanium[14] and borane[15] compounds have also proven to be potent reductants for the generation of uranium(IV) via U−O_{uranyl} bond activation. P. L. Arnold and co-workers have pioneered the use of a specialized dipyrrin ligand and strongly Lewis acidic atoms to facilitate uranyl functionalization by shifting the U(V) − U(IV) reduction into an accessible redox range. More recently, work from their lab has also demonstrated reduction of the terminal oxos in uranyl using silanes or boranes.[16] In each case, the corresponding silyl and boryl ethers are released, showing full U−O_{uranyl} bond scission.

Our group has reported the utility of redox-active ligands in uranyl functionalization and U−O_{uranyl} bond scission as well. Treating Cp*UO_2(^{Mes}PDI^{Me}) (Cp* = 1,2,3,4,5-pentamethylcyclopentadienide; ^{Mes}PDI^{Me} = 2,6-((Mes)N = CMe)$_2$-C_5H_3N; Mes = 2,4,6-trimethylphenyl), which contains a singly reduced pyridine(diimine) ligand and a hexavalent uranyl ion, with stoichiometric equivalents of Me_3SiI results in stepwise oxo silylation to form tetravalent $(Me_3SiO)_2UI_2$(^{Mes}PDI^{Me}).[17] Additional equivalents of Me_3SiI results in full uranium-oxo bond cleavage and the formation of UI_4(1,4-dioxane)$_2$ with extrusion of hexamethyldisiloxane. The necessary electron equivalents derive from the reduced pyridine(diimine) ligand and loss of the Cp* ring in this example.

Much of the work in uranyl functionalization is based on silylation and borylation of U−O_{uranyl} bonds, with formation of

Received: October 19, 2018
Published: December 11, 2018

DOI: 10.1021/jacs.8b11302
J. Am. Chem. Soc. 2019, 141, 1016−1026

O−Si and O−B bonds acting as a strong thermodynamic driving force. Currently, there are no examples of transformations of U−O_{uranyl} bonds where O−C bonds are formed. We hypothesized that U−O_{uranyl} bonds could undergo such a conversion with electrophilic carbon-containing substrates when mediated by reduced redox-active ligands. The iminoquinone family would be effective for such a task, as this ligand set has mediated multielectron reactions with low-valent metals[18−23] and would obviate the need for an external reductant by its ability to exist in a reduced state (Figure 1).

Figure 1. Redox chemistry demonstrated by the iminoquinone/amidophenolate ligand. Red atoms denote anionic bonds, while blue atoms engage in dative (neutral) bonding.

The most oxidized form of this ligand, the iminoquinone (iq^0), can be reduced to the iminosemiquinone (isq^{1-}), which is characterized by a ligand radical. Further reduction results in the formation of the amidophenolate ligand (ap^{2-}), which stores two electrons in its π^* orbitals.[24]

Herein, we report a new series of uranyl derivatives containing redox-active iminoquinone/amidophenolate ligands. Storing electrons in this ligand framework generates uranyl complexes with unprecedented electronic structures, including an unusual diradical species. These ligands facilitate multielectron chemistry at uranyl centers, allowing the complete functionalization and removal of the robust *trans*-oxo ligands through borylation and acylation reactions. Full spectroscopic, structural, and magnetic characterization is provided, as well as isotopic labeling experiments to highlight the transformation of the uranyl moiety.

■ EXPERIMENTAL SECTION

General Considerations. All air- and moisture-sensitive manipulations were performed using standard Schlenk techniques or in an MBraun inert atmosphere drybox with an atmosphere of purified nitrogen. The MBraun drybox was equipped with a cold well used for freezing samples in liquid nitrogen as well as two −35 °C freezers for cooling samples and crystallizations. Solvents for sensitive manipulations were dried and deoxygenated using literature procedures with a Seca solvent purification system.[25] Water (^{18}O, 97%) was purchased from Cambridge Isotope Laboratories and used as received. Benzene-d_6 was purchased from Cambridge Isotope Laboratories, dried with molecular sieves and sodium, and degassed by three freeze−pump−thaw cycles. Chloroform-*d* and pyridine-d_5 were purchased from Cambridge Isotope Laboratories, dried with molecular sieves, and degassed by three freeze−pump−thaw cycles. 4,6-Di-*tert*-butyl-2-[(2,6-diisopropylphenyl)imino]quinone (^{dipp}iq),[23] potassium graphite (KC_8),[26] uranyl dichloride ($[UO_2Cl_2(THF)_2]_2$),[27] uranyl triflate $UO_2(OTf)_2(THF)_3$,[28] and uranium tetrachloride (UCl_4)[29] were prepared according to literature procedures. 18-Crown-6 (18-C-6) and B-chlorocatecholborane (Cl-BCat) were purchased from Sigma-Aldrich and dried under vacuum on a Schlenk line overnight prior to use. Pivaloyl chloride (Piv-Cl) was purchased from Sigma-Aldrich, degassed by three freeze−pump−thaw cycles, and dried with molecular sieves prior to use.

^1H NMR spectra were recorded on a Varian Inova 300 or Bruker AV-III-400-HD spectrometer operating at 299.99 and 400.13 MHz, respectively. All chemical shifts are reported relative to the peak for $SiMe_4$, using ^1H (residual) chemical shifts of the solvent as a secondary standard. $^{13}C\{^1H\}$ NMR spectra were recorded on a Bruker AV-III-HD spectrometer operating at 100.61 MHz. ^{19}F NMR spectra were recorded on a Bruker AV-III-HD spectrometer operating at 376.50 MHz. ^{11}B NMR spectra were recorded on a Varian Inova 300 spectrometer operating at a frequency of 96.24 MHz. ^{11}B chemical shifts are reported relative to the peak for $BF_3{\cdot}Et_2O$ (0.0 ppm). The spectra for all paramagnetic molecules were obtained by using an acquisition time of 0.5 s, thus, the peak widths reported have an error of ±2 Hz. For all paramagnetic molecules, the ^1H NMR data are reported with the chemical shift, followed by the peak width at half height in Hz, the integration value, and, where possible, the peak assignment. All voltammetric data were obtained under inert atmosphere conditions using external electrical ports of the MBraun inert drybox. All data were obtained using a Gamry Instruments Interface 1000 model potentiostat using the Gamry Instruments Laboratory software. All data were collected on samples in THF with 0.1 M $[Bu_4N][PF_6]$ supporting electrolyte concentration and using an internal resistance compensation of approximately 2000 ohms. Solutions were analyzed in 10 mL beakers, with a 3 mm glassy carbon working electrode, a Pt wire counter electrode, and an Ag wire quasi-reference electrode. Potential corrections were performed at the end of the experiment using the Fc/Fc^+ couple as an internal standard. X-Band EPR spectra were recorded on a Bruker EMX EPR spectrometer and simulated using the EasySpin toolbox in MATLAB. Electronic absorption measurements were recorded at 294 K in THF in sealed, 1 cm quartz cuvettes with a Cary 6000i UV−vis/NIR spectrophotometer. Elemental analyses were performed by Midwest Microlab (Indianapolis, IN). Solid state infrared spectra were recorded using a Thermo Nicolet 6700 spectrophotometer.

Synthesis of (^{dipp}**iq**)$UO_2(OTf)_2THF$ (**1-iq**). A 20 mL scintillation vial was charged with $UO_2(OTf)_2(THF)_3$ (0.100 g, 0.176 mmol) and 5 mL diethyl ether. A separate 20 mL scintillation vial was charged with ^{dipp}iq (0.067 g, 0.176 mmol), dissolved in 5 mL diethyl ether, and added dropwise to the stirring $UO_2(OTf)_2(THF)_3$ slurry. A reddish-brown solution was observed. After 6 h, the volatiles were removed in vacuo. The resulting reddish-purple solid was washed with cold diethyl ether (3 × 10 mL) to afford a red powder (0.106 g, 0.132 mmol, 75% yield), assigned as **1-iq**. X-ray quality crystals were obtained from a concentrated toluene solution stored at −35 °C. Elemental analysis of $C_{32}H_{45}NO_{10}F_6S_2U$: calculated, C, 37.69; H, 4.45; N, 1.37. Found, C, 38.07; H, 4.80; N, 1.29. ^1H NMR (C_6D_6, 300 MHz, 25 °C): δ = 0.64 (s, 9H, $C(CH_3)_3$), 0.84 (d, 7, 6H, $CH(CH_3)_2$), 1.21 (d, 7, 6H, $CH(CH_3)_2$), 1.44 (s, 9H, $C(CH_3)_3$), 1.93 (br s, 4H, THF), 2.70 (sept, 7, 2H, $CH(CH_3)_2$), 5.26 (br s, 4H, THF), 6.17 (d, 2, 1H, *CH*), 7.28 (d, 2, 1H, *CH*), 7.31 (s, 2H, *CH*), 7.28 (s, 1H, *CH*). ^1H NMR ($CDCl_3$, 400 MHz, 25 °C): δ = 1.03 (d, 6.8, 6H, $CH(CH_3)_2$), 1.04 (d, 6.8, 6H, $CH(CH_3)_2$), 1.19 (s, 9H, $C(CH_3)_3$), 1.72 (s, 9H, $C(CH_3)_3$), 2.46 (br s, 4H, THF), 2.53 (sept, 6.8, 2H, $CH(CH_3)_2$), 5.21 (br s, 4H, THF), 6.21 (s, 1H, *CH*), 7.45 (d, 7.7, 2H, *CH*), 7.53 (t, 7.7, 2H, *CH*), 7.28 (s, 1H, *CH*). $^{13}C\{^1H\}$ NMR ($CDCl_3$, 100 MHz, 25 °C): δ = 22.66, 24.99, 26.35, 27.89, 29.10, 36.16, 36.50, 116.36, 124.85, 129.64, 138.11, 143.90, 145.39, 150.40, 160.90, 169.15, 195.99. ^{19}F NMR ($CDCl_3$, 376.5 MHz, 25 °C): δ = −78.10.

Synthesis of (^{dipp}**isq**)$_2UO_2THF$ (**2-isq**). A 20 mL scintillation vial was charged with $[UO_2Cl_2(THF)_2]_2$ (0.100 g, 0.103 mmol) and 5 mL THF. A separate 20 mL scintillation vial was charged with ^{dipp}iq (0.156 g, 0.412 mmol), dissolved in 5 mL THF, and added dropwise to the stirring $[UO_2Cl_2(THF)_2]_2$ slurry. After stirring for 15 min, KC_8 (0.056 g, 0.412 mmol) was weighed by difference and added over 5 min, resulting in a rapid color change from red to dark green. After 2 h, the slurry was filtered through Celite and volatiles were removed in vacuo. The remaining mixture was recrystallized from *n*-pentane to afford a green powder (0.152 g, 0.138 mmol, 67% yield) assigned as **2-isq**. Single, X-ray quality crystals were obtained from a concentrated diethyl ether solution at −35 °C. Elemental analysis of $C_{56}H_{82}N_2O_5U$: calculated, C, 61.07; H, 7.51; N, 2.54. Found, C, 60.94; H, 7.70; N, 2.22. ^1H NMR (C_6D_6, 300 MHz, 25 °C): δ = 0.05 (br s), 1.50 (br s), 2.47 (br s), 3.68 (br s), 3.89 (br s), 6.86 (br s), 7.70 (br s), 16.47 (br s), 53.64 (br s).

DOI: 10.1021/jacs.8b11302
J. Am. Chem. Soc. 2019, 141, 1016−1026

Synthesis of $[[(^{dipp}\mathbf{ap})_2\mathbf{U}][\mathbf{K(THF)_2}]_2]_2$ (**3-ap**) from **2-isq**. A 20 mL scintillation vial was charged with **2-isq** (0.100 g, 0.091 mmol) and 10 mL THF. While stirring, KC_8 (0.025 g, 0.181 mmol) was weighed by difference and added over 5 min, resulting in a rapid color change from dark green to black. After 1 h, the solution was filtered through Celite and volatiles were removed in vacuo. The crude mixture was washed with 10 mL cold *n*-pentane to afford a tan powder (0.140 g, 0.056 mmol, 62% yield) assigned as **3-ap**. Single, X-ray quality crystals were obtained from a concentrated diethyl ether solution at −35 °C. Elemental analysis of $C_{120}H_{180}N_4O_{12}K_4U_2$: calculated, C, 57.58; H, 7.25; N, 2.24. Found, C, 57.84; H, 7.34; N, 2.34. ^{1}H NMR (NC_5D_5, 300 MHz, 25 °C): δ = 0.82 (d, 7, 12H, $CH(CH_3)_2$), 1.29 (d, 7, 12H, $CH(CH_3)_2$), 1.40 (s, 18H, $C(CH_3)_3$), 1.83 (s, 18H, $C(CH_3)_3$), 4.37 (sept, 7, 4H, $CH(CH_3)_2$), 5.73 (s, 2H, *CH*), 6.49 (s, 2H, *CH*), 6.80 (t, 8, 2H, *CH*), 7.02 (d, 8, 4H, *CH*). ^{13}C{^{1}H} NMR (NC_5D_5, 100 MHz, 25 °C): δ = 23.28, 25.48, 26.20, 26.95, 30.80, 32.39, 34.26, 34.81, 67.50, 107.69, 110.48, 122.19, 122.78, 130.77, 137.50, 148.31, 154.09, 156.96.

Synthesis of $[(^{dipp}\mathbf{ap})_2\mathbf{UO_2THF}][\mathbf{K(18\text{-}crown\text{-}6)(THF)_2}]_2$ (**3-ap crown**) from **3-ap**. A 20 mL scintillation vial was charged with **3-ap** (0.100 g, 0.040 mmol) and 5 mL THF. While stirring, 18-crown-6 (0.042 g, 0.160 mmol) was weighed by difference and added. After 1 h, volatiles were removed in vacuo. The crude mixture was washed with 10 mL cold diethyl ether to afford a white powder (0.121 g, 0.061 mmol, 76% yield) assigned as **3-ap crown**. Single, X-ray quality crystals were obtained from a concentrated THF/toluene (1:1) solution stored at −35 °C. Elemental analysis of $C_{96}H_{162}N_2O_{21}K_2U$: calculated, C, 57.75; H, 8.18; N, 1.40. Found, C, 57.27; H, 8.07; N, 2.14. The EA values for C and N are off by more than 0.4%, which may be an indication of decomposition as a result of the reactive nature of this complex. ^{1}H NMR (NC_5D_5, 300 MHz, 25 °C): δ = 1.24 (d, 7, 12H, $CH(CH_3)_2$), 1.37 (d, 7, 12H, $CH(CH_3)_2$), 1.44 (s, 18H, $C(CH_3)_3$), 1.55 (s, 18H, $C(CH_3)_3$), 3.43 (s, 24H, CH_2), 4.87 (sept, 7, 4H, $CH(CH_3)_2$), 5.90 (d, 2, 2H, *CH*), 6.56 (d, 3, 2H, *CH*), 7.06 (t, 8, 2H, *CH*), 7.38 (d, 8, 4H, *CH*). ^{13}C{^{1}H} NMR (NC_5D_5, 100 MHz, 25 °C): δ = 23.74, 24.67, 25.49, 26.53, 26.90, 30.92, 31.33, 32.63, 33.94, 34.27, 34.96, 67.50, 70.08, 106.69, 108.35, 121.58, 122.64, 130.49, 135.82, 148.59, 153.97, 156.48, 159.31.

Synthesis of $(^{dipp}\mathbf{iq})(^{dipp}\mathbf{isq})\mathbf{UO_2Cl}$ (**4-iq/isq**). A 20 mL scintillation vial was charged with $[UO_2Cl_2(THF)_2]_2$ (0.275 g, 0.283 mmol) and 8 mL THF. A separate 20 mL scintillation vial was charged with ^{dipp}iq (0.430 g, 1.133 mmol), dissolved in 10 mL THF, and added dropwise to the stirring $[UO_2Cl_2(THF)_2]_2$ slurry. After stirring for 15 min, KC_8 (0.077 g, 0.567 mmol) was weighed by difference and added over 5 min, resulting in a rapid color change from red to brown. After 2 h, the slurry was filtered through Celite, and volatiles were removed in vacuo. The brown solid was triturated with diethyl ether (2 × 10 mL) and *n*-pentane (2 × 10 mL) then dried in vacuo. The resulting black powder was washed with cold *n*-pentane (3 × 10 mL) to afford a greenish brown powder (0.400 g, 0.376 mmol, 66% yield) assigned as **4-iq/isq**. Single, X-ray quality crystals were obtained from a concentrated diethyl ether solution at −35 °C. Elemental analysis of $C_{52}H_{74}N_2O_4ClU$: calculated, C, 58.66; H, 7.01; N, 2.63. Found, C, 58.91; H, 7.13; N, 2.53. ^{1}H NMR (C_6D_6, 300 MHz, 25 °C): δ = 2.09 (br s), 3.10 (br s), 4.90 (br s).

Reaction of **2-isq** with 4 eq. **Cl-BCat**. A 20 mL scintillation vial was charged with **2-isq** (0.100 g, 0.091 mmol) and 10 mL of THF. The vial was placed in the coldwell, and the solution was frozen. Upon thawing, Cl-BCat (0.056 g, 0.363 mmol) was weighed by difference and added to the stirring solution. After warming to room temperature for 1 h, volatiles were removed in vacuo. The products of the reaction were identified to be $UCl_4(^{dipp}iq)_2(THF)_2$ and $BOBCat_2$ by ^{1}H and ^{11}B NMR. The reaction mixture was washed with cold *n*-pentane (2 × 5 mL) to separate organics from the uranium product, producing a black powder (0.057 g, 0.063 mmol, 69% yield).

Independent synthesis of $^{dipp}\mathbf{iqUCl_4(THF)_2}$ (**5-iq**). A 20 mL scintillation vial was charged with UCl_4 (0.100 g, 0.263 mmol) and 10 mL THF. In a separate vial, ^{dipp}iq (0.100 g, 0.263 mmol) was dissolved in 5 mL of THF and added dropwise to the stirring UCl_4 solution. The solution immediately changed color from green to black. After 8 h, the solvent was removed in vacuo and washed with *n*-pentane (2 × 5 mL) to yield a black powder (0.184 g, 242 mmol, 92% yield). This sample was submitted for elemental analysis. Single, X-ray quality crystals were obtained from a concentrated THF solution at −35 °C. Elemental analysis of $C_{26}H_{37}N_1O_1Cl_4U$ (solvent free): calculated, C, 41.12; H, 4.91; N, 1.84. Found, C, 40.83; H, 5.02; N, 1.64. ^{1}H NMR (C_6D_6, 300 MHz, 25 °C): δ = −14.89 (4, 1H, *CH*), −6.49 (3, 9H, $C(CH_3)_3$), −5.16 (103, 3H, $CH(CH_3)$), −5.07 (35, 4H, THF), −3.79 (106, 3H, $CH(CH_3)$), −3.61 (35, 4H, THF), −1.07 (4, 9H, $C(CH_3)_3$), −0.54 (4, 1H, *CH*), 1.98 (32, 2H, *CH*), 9.11 (t, *J* = 7 Hz, 1H, *CH*), 10.87 (37, 4H, THF), 11.65 (36, 4H, THF), 12.29 (115, 3H, $CH(CH_3)$), 13.99 (118, 3H, $CH(CH_3)$), 19.44 (10, 2H, *CH*).

Reaction of **2-isq** with 4 eq. **Piv-Cl**. A 20 mL scintillation vial was charged with **2-isq** (0.080 g, 0.073 mmol), dissolved in 10 mL benzene, and transferred to a 25 mL receiving flask. Pivaloyl chloride (0.035 g, 0.290 mmol) was weighed by difference and added to the green, stirring solution. The flask was sealed and then heated to 50 °C for 8 h, producing a red solution. After cooling to room temperature for 1 h, volatiles were removed in vacuo. The products of the reaction were identified by ^{1}H NMR to be pivaloyl anhydride and **6-iq**. The reaction mixture was washed with cold *n*-pentane (2 × 5 mL) to separate organics from the uranium product, producing a brown powder (0.061 g, 0.053 mmol, 73% yield).

Independent synthesis of $^{dipp}\mathbf{iq_2UCl_4}$ (**6-iq**). A 20 mL vial was charged with UCl_4 (0.056 g, 0.142 mmol) and 8 mL benzene. In a separate vial, ^{dipp}iq (0.119 g, 0.312 mmol) was dissolved in benzene (8 mL) and added dropwise to the stirring UCl_4 slurry. The reddish-brown mixture was then transferred to a receiving flask, sealed, and heated to 50 °C for 16 h. The solvent was removed in vacuo and the resulting brown powder washed with *n*-pentane (2 × 10 mL), leaving **6-iq** (0.144 g, 0.126 mmol, 89% yield). Elemental analysis of $C_{52}H_{74}N_2O_2Cl_4U$: calculated, C, 54.83; H, 6.55; N, 2.46. Found, C, 55.64; H, 6.37; N, 2.59. ^{1}H NMR (C_6D_6, 300 MHz, 25 °C): δ = −75.30 (19, 2H, *CH*), −5.66 (t, *J* = 7 Hz, 2H, *CH*), −2.36 (12, 18H, $C(CH_3)_3$), 7.03 (8, 12H, $CH(CH_3)_2$), 7.25 (8, 2H, *CH*), 8.81 (10, 12H, $CH(CH_3)_2$), 19.07 (7, 18H, $C(CH_3)_3$), 28.96 (27, 4H, $CH(CH_3)_2$), 56.68 (d, *J* = 7 Hz, 4H, *CH*).

Synthesis of ^{18}O-labeled $[\mathbf{UO_2Cl_2(THF)_2}]_2$. This procedure was developed by adapting literature procedures.[27,30] A 25 mL, borosilicate glass Schlenk flask was charged with approximately 1 g of $UO_2Cl_2(H_2O)_x$ (x = 1−3) and purged with argon. Against a flow of argon, 1 mL of $H_2{}^{18}O$ was added *via* pipet. After 1 min of purging with argon, the flask was sealed. The yellow solution was gently stirred in front of a UV lamp (365 nm). Note, using $[UO_2Cl_2(THF)_2]_2$ as the uranium source leads to decomposition of the material, as evidenced by color change from yellow to green and precipitation. After 12 days, the water was removed from the yellow slurry in vacuo, yielding a yellow powder. From this material, anhydrous ^{18}O-labeled $[UO_2Cl_2(THF)_2]_2$ was obtained via a previously published procedure.[27] IR spectroscopy was employed to confirm the incorporation of ^{18}O into the U−O_{uranyl} (Figure S20).

RESULTS AND DISCUSSION

Synthesis and Characterization of Reduction Series. Initially, a neutral ^{dipp}iq U(VI) complex was synthesized to provide a baseline for studies of more reduced species and allow comparison of spectroscopic data. Ligation of uranyl triflate, $UO_2(OTf)_2(THF)_3$, was accomplished by stirring with an equimolar amount of ^{dipp}iq in diethyl ether (eq 1). Upon

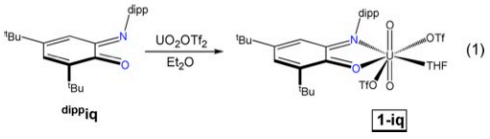

dippiq 1-iq (1)

DOI: 10.1021/jacs.8b11302
J. Am. Chem. Soc. 2019, 141, 1016−1026

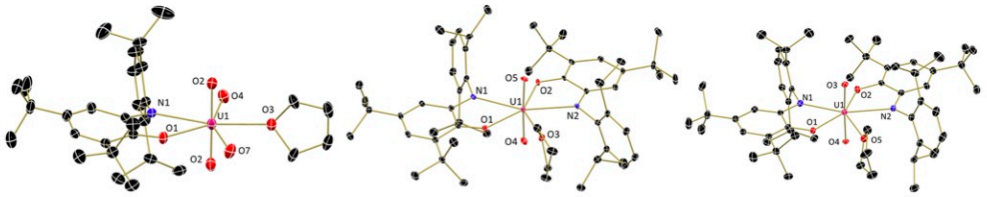

Figure 2. Molecular structure of **1-iq** (left), **2-isq** (middle), and **3-ap crown** (right) shown with 30% probability ellipsoids. Hydrogen atoms, cocrystallized solvent molecules, potassium ions, crown ether molecules, and bound triflate ions (except coordinated oxygen atoms) are omitted for clarity.

Table 1. Selected Uranyl Bond Distances (Å) and Angles (°) for 1-iq, 2-isq, 3-ap, 3-ap crown, and 4-iq/isq

	1-iq	2-isq	3-ap	3-ap crown	4-iq/isq
$U-O_{Uranyl}$	1.745(5)	1.762(4)	1.824(3)	1.812(2)	1.757(3)
$U-O_{Uranyl}$	1.745(5)	1.786(3)	1.834(3)	1.814(2)	1.758(3)
$O_{Uranyl}-U-O_{Uranyl}$	179.1(2)	175.42(17)	172.22(12)	174.54(10)	175.09(13)

Scheme 1. Synthesis of Complexes 2-isq, 3-ap, and 3-ap crown

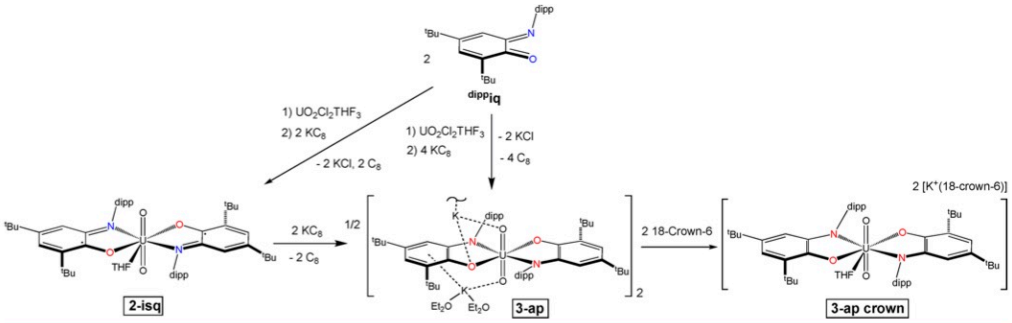

workup, a red-purple powder was obtained in good yield (76%). The ^{1}H NMR spectrum (Figure S1) displayed 9 resonances slightly shifted from those observed for the free ligand, indicative of binding to the diamagnetic, U(VI), f^0 ion. Two additional, broad resonances, assignable as one bound THF molecule, were also observed at 1.93 and 5.26 ppm.

To unequivocally determine the number of coordinated ligands and examine the structural parameters of the complex, single crystals of **1-iq**, grown from toluene, were analyzed using X-ray diffraction. Refinement of the data revealed a seven-coordinate pentagonal bipyramidal uranyl coordination complex with one ^{dipp}iq ligand, one THF molecule, and two bound triflate anions in the equatorial plane along with the oxo ligands in axial positions (Figure 2, left; Table 1). The $U-O_{uranyl}$ distance of 1.745(5) Å and $O_{uranyl}-U-O_{uranyl}$ angle of 179.1(2)° are as expected based on similar uranyl compounds.[31] If the reaction is performed with excess ^{dipp}iq ligand, formation of **1-iq** is still observed, suggesting the triflate anions are not subject to substitution by neutral ^{dipp}iq despite the chelation effect of the bidentate ligand.

After successful metalation of the neutral ^{dipp}iq ligand, the redox-active nature of the ligand was engaged by stirring two equivalents of ^{dipp}iq with one equivalent of $UO_2Cl_2(THF)_3$ followed by slow addition of two equivalents of KC_8 (Scheme 1), causing a color change from red/brown to dark green. After workup, a green powder was isolated in moderate yield (67%). The ^{1}H NMR spectrum (Figure S5) displays broad, paramagnetically shifted signals ranging from 0−55 ppm. In this case, the paramagnetism can arise either from (1) reduction of the uranium(VI) (f^0) center to uranium(V) (f^1) while maintaining a neutral iminoquinone ligand or (2) from ligand reduction to generate two radical-containing iminosemiquinone ligands.

To further elucidate the electronic structure of **2-isq**,[17,32,33] X-ray crystallography was employed, as structural parameters, including intraligand bond distances, can often aid in ligand oxidation state assignment.[34] Crystals of **2-isq** grown from diethyl ether at −35 °C were analyzed. Refinement of the data revealed a seven coordinate uranyl species, with two ^{dipp}iq ligands and a THF molecule coordinated in the equatorial plane (Figure 2, middle). As with **1-iq**, a pentagonal bipyramidal geometry with the uranyl oxygen atoms in axial positions was observed. Additionally, the $U-O_{uranyl}$ bond distances of 1.762(4) and 1.786(3) Å (Table 1) are within the range of 1.76−1.79 Å observed for U(VI) uranyl molecules.[31,32,35] These $U-O_{uranyl}$ distances suggest the reduction is ligand-based rather than occurring at the uranium.

To further confirm the presence of ligand radicals, EPR spectroscopy was performed. The EPR spectrum of **2-isq** (Figure 3) displays an isotropic signal at g = 1.993, which is shifted from that of 2.0061 observed for 4,6-di-*tert*-butyl-2-*tert*-butyl-iminosemiquinone (H^{tBu} isq•).[36] This value agrees well

DOI: 10.1021/jacs.8b11302
J. Am. Chem. Soc. 2019, 141, 1016−1026

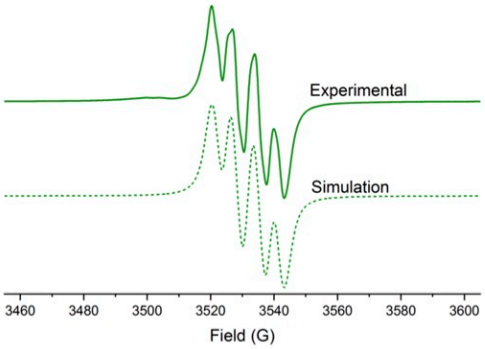

Figure 3. EPR spectrum of **2-isq** (*n*-pentane, 5.8 mM) recorded at 25 °C. g_{iso} = 1.993. Frequency: 9.852 GHz. Power: 10 mW. Modulation: 0.5 G/100 kHz.

with the g-value previously observed for hexavalent uranyl species featuring redox-active ligands, such as $Cp^*UO_2(^{Mes}PDI^{Me})$ (g_{iso} = 1.974), $Cp^*UO_2(^{t}Bu\text{-}^{Mes}PDI^{Me})$ (g_{iso} = 1.936), and $[UO_2(salophen)^{fBu}(H_2O)]^+$ (g_{av} = 1.997) ($^{t}Bu\text{-}^{Mes}PDI^{Me}$ = 2,6-((Mes)-N = CMe)$_2$-*p*-C$(CH_3)_3C_5H_2N$; salophen = *N*,*N*′-bis(3-^{t}Bu-(5-^{t}Bu)-salicylidene)-1,2-phenylenediamine).[17] Spin−orbit coupling of the ligand-based radical with the empty *f*-orbitals of the uranium center is likely the cause of the high-field shift from the *g*-value observed for H^{tBu}isq•. Simulation of the spectrum was accomplished with one nitrogen (I = 1) and one hydrogen atom (I = 1/2) of the ligand, yielding hyperfine coupling constants of A_N = 19.48 and A_H = 13.97 MHz. These values suggest a stronger interaction with the nitrogen atom than the hydrogen atom of the ligand. This hyperfine pattern agrees with previously noted results.[18,36] Thus, these measurements support the presence of an iminosemiquinone ligand radical with only a weak interaction with uranium.

Variable-temperature and field-dependent magnetic measurements were performed to elucidate the uranium and ligand oxidation states in **2-isq** (Figure 4). At room temperature, the μ_{eff} value (2.45 μ_B) was consistent with that expected for two isolated, unpaired electrons with g = 2.0 (theoretical μ_{eff} value = 2.45 μ_B).[37] Upon cooling, the μ_{eff} value slightly increased to

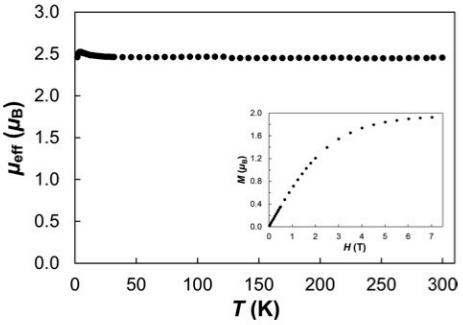

Figure 4. Variable temperature molar magnetic data (μ_{eff}) for **2-isq** and variable field data collected at 2 K (inset).

2.52 μ_B at 4 K. The increase in moment resulted from the ferromagnetic coupling of the two unpaired electrons. The data were fitted by the Bleaney−Bowers equation[38] with g = 2.00 and exchange coupling constant J = 0.4 cm^{-1} (see the Supporting Information for details). The magnetization in the field-dependent measurement saturated at 1.94 μ_B at 2 K was also characteristic of two isolated S = 1/2 spins.[37] Overall, these magnetic data indicated the presence of one U(VI) cation and two ligand-centered radicals with negligible ferromagnetic coupling in **2-isq**. The data supported the presence of two noncommunicating ligand radicals that were measured by EPR and predicted with the metrical parameters deduced by X-ray crystallography (*vide infra*). The radicals in **2-isq** were relegated to the ligand at all temperatures, with little interaction with the uranium. This ruled out alternate potential electronic structures for **2-isq** (Figure 5). These magnetic data also eliminated formation of pentavalent $(isq^{1-})(iq^0)U^VO_2$, which would have both uranium-based and ligand-based radicals, as well as $(iq^0)_2U^{IV}O_2$, which would have closed-shell ligands with only uranium-based electrons unpaired.

To probe the ability of our system to accommodate additional electrons beyond monoreduction of both ligands, electrochemical measurements of **2-isq** were performed in THF (Figure S19). The cyclic voltammetric data for **2-isq** showed a quasi-reversible reduction at −1.58 V, which could be attributed to the reduction of the two ligands from isq^{1-} to ap^{2-} or reduction of uranium from +6 to +5. Encouraged by the electrochemical results, **2-isq** was reduced chemically by stirring with two equivalents of KC_8 in THF. Following workup, a tan powder that is poorly soluble in hydrocarbon solvents was isolated. ^{1}H NMR spectroscopic analysis (pyridine-d_5) showed a spectrum (Figure S6) with 11 resonances. Of these, nine signals were assigned to the ligand and two signals as bound THF, none of which were drastically shifted from the diamagnetic region. These data suggest a closed-shell U(VI), f^0 ion with ^{dipp}ap ligands bound to uranium.

Because solution behavior can be complicated by dynamic inner-sphere and outer-sphere cation exchange, a crown ether was employed to encapsulate the potassium ion for further studies.[18,39,40] To achieve this, two equivalents of 18-crown-6 were added to a stirring solution of **3-ap** in THF. After workup, a white powder was isolated in good yield (76%). The ^{1}H NMR spectrum (Figure S8) is quite similar to that of **3-ap**, with minor differences, including an additional resonance at 3.43 ppm corresponding to the 24 protons associated with 18-crown-6.

Comparison of the structural changes that accompany reduction and examination of the effect of potassium ion sequestration in **3-ap** (Figure 6) and **3-ap crown** (Figure 2, right) were examined using X-ray crystallography. Compound **3-ap** crystallizes as a dimer from diethyl ether or toluene at −35 °C with the oxygen atom and aromatic ring of the ^{dipp}iq ligand and uranyl oxygen atoms interacting with the potassium ions. This dimerization causes out of plane bending of the ligand with the N and O atoms appearing to be sp^3 hybridized to allow for lone pair interaction with the nearby potassium ions. Additionally, the uranyl bond distances of 1.824(3) and 1.834(3) Å (Table 1) are quite long,[31] appearing to result from the potassium binding to the O_{uranyl}. This cation-capping effect has been thoroughly studied by P. L. Arnold and co-workers who employed a large, compartmental, N_8-macrocyclic ligand.[41] In these studies, reduction of uranyl was facilitated

DOI: 10.1021/jacs.8b11302
J. Am. Chem. Soc. 2019, 141, 1016−1026

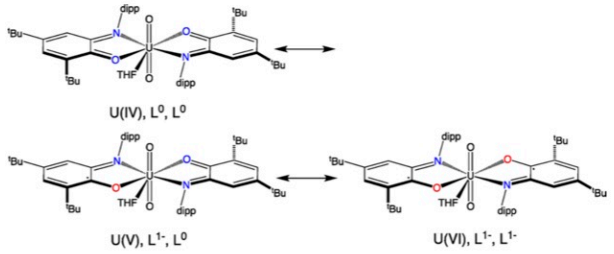

Figure 5. Possible electronic structures of **2-isq**.

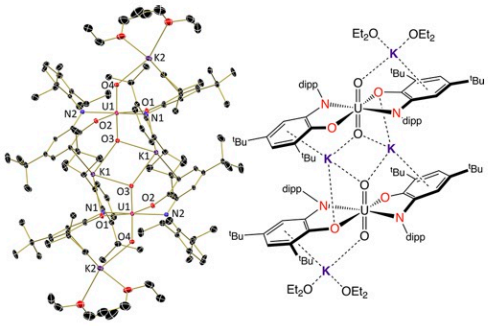

Figure 6. Molecular structure of **3-ap** (left) shown with 30% probability ellipsoids. Co-crystallized solvent molecules and H atoms are omitted for clarity. Schematic representation of **3-ap** (right), with interactions between potassium ions and various parts of the molecule shown as dashed lines.

by coordination of a cation, held in place by the specialized "Pacman" type ligand, to the O_{uranyl}.

The structure of **3-ap crown** shows that sequestering the potassium ions with crown ethers permits the amidophenolate ligands to return to their planar geometry, isostructural to **2-isq**. Interestingly, despite the absence of the interaction of potassium atoms with the uranyl moiety in **3-ap crown**, the $U-O_{uranyl}$ bond distances remain long (1.814(2) and 1.812(2) Å), suggesting ligand reduction plays a role in the elongation of the $U-O_{uranyl}$ bond. This implies that cation coordination is not the only contributing factor in the $U-O_{uranyl}$ bond elongation observed in **3-ap**. $U-O_{uranyl}$ bond lengthening has been previously observed by Hayton and co-workers when they described tris- and tetrakis-ketimide complexes $[Li(THF)(TMEDA)][UO_2(N = C^tBuPh)_3]$ and $[Li(THF)(Et_2O)]_2[UO_2(N = C^tBuPh)_4]$.[42] These ketimide uranyl molecules display $U-O_{uranyl}$ bond lengths of 1.830(5) and 1.804(5) Å (tris-ketimide) and 1.838(4) Å (tetrakis-ketimide). The authors attribute this elongation to the presence of four strong donors in the equatorial plane, which act to weaken the $U-O_{uranyl}$ bonds via electrostatic repulsion and π-donation to the uranium center. Further evidence of this elongation can be found in the imido family of uranyl analogues. Studies of uranium tris-[43] and tetrakis(imidos),[44] featuring strong π-donating imido groups in the equatorial plane, have shown that imido bonds lengthen and weaken with each additional π-donor. The $^{dipp}ap^{2-}$ ligand has been studied as a π-donating ligand for high valent metals previously.[24] As its high-lying π orbitals have the appropriate symmetry to donate electron density to the uranium (VI) center, this is likely a factor in $U-O_{uranyl}$ bond elongation and activation in **3-ap crown**.

The bond metrics vary based on the ligand oxidation state and can therefore provide insight into the electronic structure of **1-iq**, **2-isq**, and **3-ap crown** (Figure 7). The neutral ^{dipp}iq

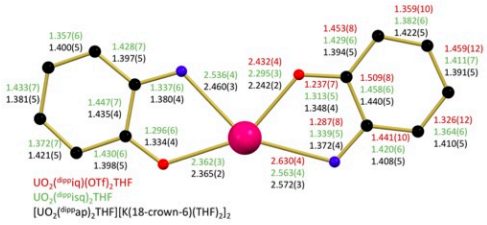

Figure 7. Bond distance comparison (Å) for **1-iq**, **2-isq**, and **3-ap crown**. Carbon atoms shown in black, nitrogen atoms shown in blue, oxygen atoms shown in red, and uranium atom shown in magenta.

ligand of **1-iq** displays relatively long uranium−oxygen (2.432(4) Å) and uranium−nitrogen (2.630(4) Å) bonds that are indicative of a datively bound ligand. Furthermore, the short C−O (1.237(7) Å) and C−N (1.287(8) Å) bonds suggest that the ligand retains double bond character. In contrast, the iminosemiquinone ligands of **2-isq** feature shortened U−O bonds (2.295(3) and 2.362(3) Å) and U−N bonds (2.563(4) and 2.536(4) Å) accompanied by longer C−O (1.313(5) and 1.296(6) Å) and C−N bonds (1.339(5) and 1.337(6) Å), indicating reduction of the ligand.

The bond distances of **3-ap crown** are not as simple to analyze as those of the other compounds of the series. While the expected shortening trend of the U−E (E = O, N) bond is observed for one "E" atom of each ligand, the other "E" atom bond distance is nearly identical to that of **2-isq**. This could be attributed to steric hindrance with the bulky dipp or ^{t}Bu groups that prevent the U−E bonds from contracting toward the metal center upon reduction. In this case, a stronger indication of reduction can be found in the intraligand bond distances (Figure 7). The C−O and C−N bonds in each ligand lengthen, signifying the conversion from a double bond to a single bond. Corroborating evidence can also be found in the C−C bond distances of the rings in the ligands. As the ligand is reduced, the distances throughout the ring become more similar, suggesting aromaticity is present.

As the bond distances in molecules **1-iq**, **2-isq**, and **3-ap crown** change with ligand oxidation state, the bond angles also

DOI: 10.1021/jacs.8b11302
J. Am. Chem. Soc. 2019, 141, 1016−1026

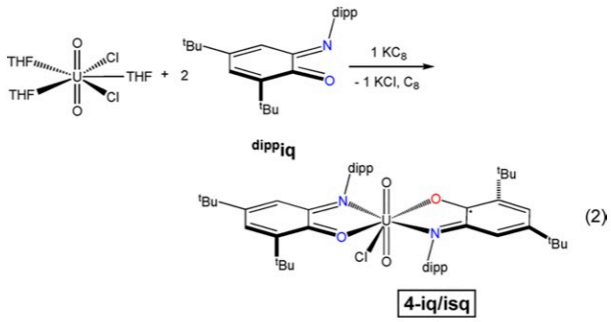

indicate ligand reduction. In particular, this effect is noticeable in the N_{iq}–U–O_{iq} angles of the iminoquinone ligand. As the ligand becomes more reduced, the shortening of the U–O_{iq} and U–N_{iq} bonds causes the N_{iq}–U–O_{iq} bite angle of the ligand to increase from 61.83° (**1-iq**) to 64.44° (**2-isq**) and finally to 65.26° (**3-ap crown**).

Another useful technique for examining the ligand and metal oxidation states in uranium/uranyl systems is electronic absorption spectroscopy. For the current study, this technique is particularly advantageous as **1-iq**, **2-isq**, and **3-ap** all exhibit distinctly different colors (Figure S16 and S17). Spectra were recorded in THF at 25 °C from 375–1800 nm. The spectrum of **1-iq** displays an intense absorption at 385 nm (41,711 M^{-1} cm^{-1}) with a weaker absorption at 511 nm (4,075 M^{-1} cm^{-1}), giving rise to the observed red-purple color. Compound **2-isq** shows an intense absorption at 310 nm (26,600 M^{-1} cm^{-1}) and a much less intense, broad absorption at 747 nm (2,130 M^{-1} cm^{-1}), responsible for the observed green color. Finally, **3-ap** shows only one absorption at 313 nm (15,313 M^{-1} cm^{-1}) and does not absorb significantly in the visible region, consistent with its pale color. Interpretation of these data suggests that the major, color-producing peaks of the spectra can be attributed to the ligand oxidation state, as similar colors have been observed for complexes of early transition metals,[20] lanthanides,[18] and low valent uranium.[21]

Synthesis and Characterization of a Mixed Ligand Species. The extent of radical delocalization in the uranyl iminoquinone complexes was tested by synthesizing a mixed iminoquinone/iminosemiquinone ligand species. We hypothesized that rather than full delocalization of the radical across both ligands, the radical would remain localized on one of the iminosemiquinone ligands and not the other. Preparation of (^{dipp}iq)(^{dipp}isq)UO_2Cl (**4-iq/isq**) was achieved by stirring two equivalents of the iminoquinone ligand with one equivalent of uranyl chloride in the presence of one equivalent of potassium graphite (eq 2). Upon workup, a greenish-brown powder was isolated in moderate yield (66%).

X-ray crystallographic analysis of green-brown crystals grown from diethyl ether show a pentagonal bipyramidal uranium center similar to that of **2-isq** but with a chloride atom instead of a THF molecule (Figure 8, Table 1). Compound **4-iq/isq** shows asymmetric ligands in the solid state, with each ligand's oxidation state undoubtedly assignable based on bond distances (Figure 9). The U–O distances of 2.493(3) and 2.312(3) Å and U–N distances of 2.670(3) and 2.498(3) Å highlight the asymmetric nature of the two ligands, with the shorter contact belonging to the isq ligand and the longer to

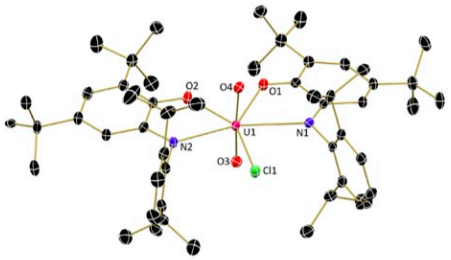

Figure 8. Molecular structure of **4-iq/isq** shown with 30% probability ellipsoids. Co-crystallized solvent molecules and H atoms are omitted for clarity.

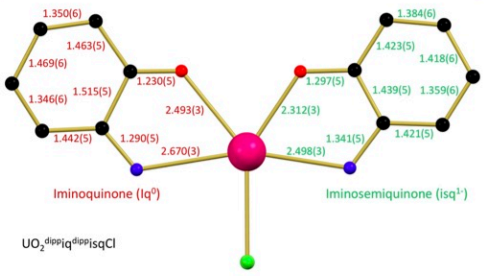

Figure 9. Bond distance comparison (Å) for **4-iq/isq**. Carbon atoms shown in black, nitrogen atoms shown in blue, oxygen atoms shown in red, chloride atoms shown in green, and uranium atom shown in magenta.

the iq ligand. Further evidence can be found in the C–O and C–N distances, as well as the intraligand C–C distances. For the iminoquinone ligand, C–O and C–N bonds of 1.230(5) and 1.290(5) Å are indicative of double bond character, as observed for **1-iq**. However, the C–O and C–N bonds of the other ligand are significantly longer at 1.297(5) and 1.341(5) Å, agreeing well with the ligands of **2-isq**. Additional evidence can be found in the C–C bonds of each ring, with the iminoquinone ligand featuring two short bonds and three long ones, whereas the iminosemiquinone ligand has bonds more similar in length. Both of these trends match well with the ligands of compounds **1-iq** and **2-isq**, respectively.

The presence of a ligand radical in **4-iq/isq** was confirmed using EPR spectroscopy (Figure S18). In a toluene solution, an

DOI: 10.1021/jacs.8b11302
J. Am. Chem. Soc. 2019, 141, 1016–1026

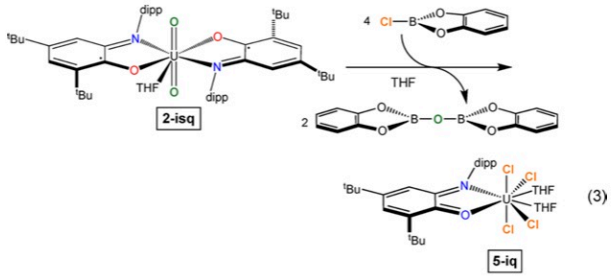

isotropic signal is observed at $g = 1.989$. This is comparable to the g-value of **2-isq** (1.993). Variable temperature SQUID magnetometry provides additional evidence of the ligand radical (Figure S25), which establishes a room temperature μ_{eff} value of 1.86 μ_B. The UV−vis/NIR spectrum of **4-iq/isq** displays absorbance in multiple regions (Figure S16 and S17), which explains the observed brown color. Intense absorbances are noted at 307 nm (15,188 M^{-1} cm^{-1}) and 388 nm (5759 M^{-1} cm^{-1}), while signals at 528 nm (259 M^{-1} cm^{-1}) and 800 nm (839 M^{-1} cm^{-1}) are broad and less intense. The number of absorbance maxima is likely the product of the ligands existing in two oxidation states, absorbing at different wavelengths.

■ URANYL FUNCTIONALIZATION

Reactivity of 2-isq with B-Chlorocatecholborane. Boron is well-known for its Lewis acidic properties, making it an excellent candidate to examine reactivity with electron-rich **2-isq**. B-Chlorocatecholborane (Cl-BCat) features a B−Cl bond that can be heterolytically cleaved by the chlorophilic uranium. Treating **2-isq** with four equivalents of Cl-BCat causes the solution to change color from green to brown immediately. Resonances in the ^{1}H NMR spectrum of the reaction mixture (Figure S11) range from −20 to +20 ppm, suggesting that the uranyl was reduced to paramagnetic U(IV), f^2, a transformation that likely involves uranyl U−O_{uranyl} bond activation (eq 3). Further inspection of the data, coupled with ^{11}B NMR spectroscopic data (Figure S12), revealed that dicatecholatobisborylether ($BOBCat_2$) was produced during the reaction. In sealed-tube NMR experiments in benzene-d_6 and THF-d_8, free ligand is also observed but does not integrate to one full equivalent. On the basis of the stoichiometry of Cl-BCat and the number and integration values of resonances in the ^{1}H NMR spectrum, the resulting uranium product was hypothesized to be $UCl_4(^{dipp}iq^0)_n$ (n = 1, 2).

Identification of the U(IV) product from borylation of **2-isq** was achieved by an independent synthesis. Treating UCl_4 with an equivalent of ^{dipp}iq in THF produced a dark green solution (eq 4), and ^{1}H NMR data confirmed the product was the same

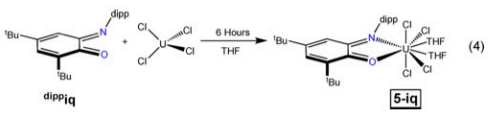

as that observed in the uranyl borylation reaction (Figure S14). The material from the independent synthesis was crystallized from THF, and subsequent X-ray analysis revealed the identity to be $UCl_4^{dipp}iq(THF)_2$ (**5-iq**) (Figure S23). The ligands are confirmed to be in the iminoquinone form with C−O and C−N distances of 1.234(3) and 1.298(3) Å, signifying double bonds and matching the distances observed in **1-iq** and **4-iq/isq**. Further evidence can be found in the U−O and U−N distances of 2.4878(16) and 2.8283(18) Å, which are longer than the contacts reported for iminosemiquinone-containing U(IV) complexes (^{tBu}isq)$_2$UI$_2$(THF) (U−O = 2.160(10) and 2.164(10), U−N = 2.514(12) and 2.567(14) Å).[21] These longer contacts highlight the dative nature of the ligand binding in **5-iq**.

To corroborate that the organic products observed were the result of U−O_{uranyl} bond cleavage and that the extracted oxygen atoms had originated from the U−O_{uranyl}, isotopic labeling studies were performed. ^{18}O-labeled uranyl dichloride ($[U^{18}O_2Cl_2(THF)_2]_2$) was synthesized through photolysis of uranyl chloride hydrate in ^{18}O-labeled water.[31] ^{18}O incorporation was confirmed by IR spectroscopy, with the expected OUO asymmetric stretching frequency reducing from 942.4 cm^{-1} ($[U^{16}O_2Cl_2(THF)_2]_2$) to 892.3 cm^{-1} ($[U^{18}O_2Cl_2(THF)_2]_2$) (Figure S20). Synthesis of (^{dipp}isq)$_2$U^{18}O$_2$THF (**2-isq^{18}**) was accomplished in an analogous manner to **2-isq**, using $[U^{18}O_2Cl_2(THF)_2]_2$ as the uranyl source. Successful incorporation was confirmed by IR spectroscopy (Figure S21).

Treating **2-isq^{18}** with Cl-BCat under the same conditions as previously described for the unlabeled isotopologue yielded analogous results as identified by ^{1}H and ^{11}B NMR spectroscopies. Analysis of the organic bisborylether, $B^{18}OBCat_2$, by EI-MS gave an increase in the $M^{\bullet+}$ peak appearing at m/z = 256, corresponding to the incorporation of one ^{18}O-labeled oxygen atom. $BOBCat_2$, obtained from the borylation of **2-isq**, shows an analogous peak at m/z = 254 (Figure 10). The shift from m/z of 254 to 256 is indicative of ^{18}O incorporation and supports that the source of the oxygen atom in $BOBCat_2$ is from the labeled uranyl U−O_{uranyl}.

Reactivity of 2-isq with Pivaloyl Chloride. Upon establishing that **2-isq** could mediate U−O_{uranyl} bond cleavage with Cl-BCat, we hypothesized that an analogous electrophilic carbon could be used to activate the uranyl ion. Pivaloyl chloride (Piv-Cl) was an attractive choice as the *tert*-butyl group provides steric pressure to aid product dissociation. Treating **2-isq** with four equivalents of pivaloyl chloride in benzene results in no observable reaction. Heating this solution to 50 °C for 4 h causes a color change from green to brown. Analysis of the reaction mixture by ^{1}H NMR spectroscopy revealed a singlet at 1.04 ppm and disappearance of the resonance at 0.89 ppm, suggesting conversion of pivaloyl chloride to pivalic anhydride. Additionally, resonances ranging from −80 to +60 ppm (Figure S13) show that a paramagnetic product is formed; however, these resonances do not match

DOI: 10.1021/jacs.8b11302
J. Am. Chem. Soc. 2019, 141, 1016−1026

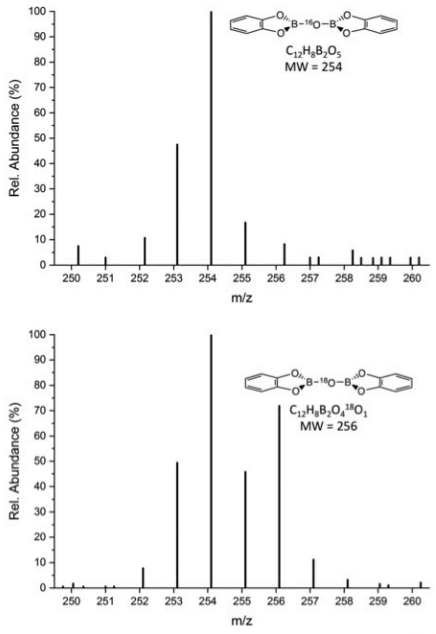

Figure 10. Electron ionization mass spectra (EI-MS) of $BOBCat_2$ from the reaction mixture of ClBCat and **2-isq** (top) and **2-isq**^{18} (bottom).

that of **5-iq**. We hypothesized that in the noncoordinating benzene solution, ligand displacement would not occur as in the borylation, which was performed in THF. To confirm this, UCl_4 was treated with two equivalents of iminoquinone in benzene and heated to 50 °C for 18 h, producing a ^{1}H NMR spectrum matching that of the acylation reaction, with no free ligand observed. In the absence of THF, a bis-ligand U(IV) complex, $UCl_4(^{dipp}iq^0)_2$ (**6-iq**), is formed (Figure S15). These spectroscopic results suggest that the two pivaloyl chloride molecules were able to exchange their chloride atoms for the oxygen atom of a uranyl ion, producing pivalic anhydride (eq 5), which is then displaced from the uranium ion.

Reactions of **2-isq** and **2-isq**^{18} were performed with pivaloyl chloride, and the organic anhydrides isolated and examined using CI-MS. The labile nature of the C−O bonds in pivalic anhydride causes dissociation in the mass spectrometer, thus, only the protonated carboxylic acid was detected (Figure S22). In the case of the unlabeled sample, a $[M + H]^+$ peak at m/z = 103 was observed. The data for the ^{18}O-labeled sample display an additional $[M + H]^+$ peak m/z = 105, assignable as the ^{18}O-labeled isotopologue. On the basis of the ratio of these peaks in the labeled sample, the percent incorporation of ^{18}O was calculated to be about 35%. These results, along with the spectroscopic data (*vide supra*), support that U−O_{uranyl} bonds are broken in the process of borylation and acylation, and the oxygen atoms in the organic byproducts originate from the U−O_{uranyl} bond.

■ CONCLUSION

In summary, a family of uranyl complexes bearing redox-active ligands has been isolated in three different oxidation states. Thorough characterization has provided insight into their electronic structures. Upon reduction, electrons are stored in the ligand π^* orbitals rather than in uranium-based orbitals, retaining the U(VI) oxidation state throughout the series. Notably, **2-isq** has two isolated, ligand-based radicals that can be harnessed for U−O_{uranyl} bond activation. U−O_{uranyl} bond functionalization and scission was carried out with B-chlorocatecholborane or pivaloyl chloride, furnishing either mono- or bis-iminoquinone U(IV) products and the corresponding organic ethers. The origin of the oxygen atom was established by isotopic labeling experiments. Formation of a C−O bond followed by complete U−O cleavage from a uranyl species is unprecedented, with previous examples limited to typical Lewis acidic atoms.

The expansion and understanding of ligand bonding and electronic structure in uranyl compounds is a crucial part of the processing and remediation of uranium in the environment. We have examined this bonding thoroughly with a variety of analytical techniques and exploited the activation of U−O_{uranyl} bonds to convert U(VI) to U(IV) with electrons stored in the iminosemiquinone ligand. The ability to convert U(VI) to U(IV) is an important requirement in manipulating uranium in the environment and would be a fundamental step in any catalytic cycle featuring high valent uranium. Future experiments will aim to generalize the coordination environment and expand the family of reagents capable of U−O_{uranyl} bond functionalization.

■ ASSOCIATED CONTENT

Supporting Information

The Supporting Information is available free of charge on the ACS Publications website at DOI: 10.1021/jacs.8b11302.

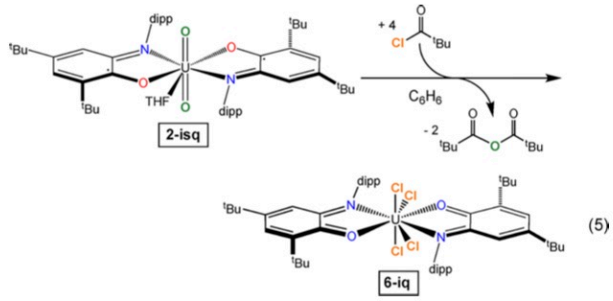

(5)

DOI: 10.1021/jacs.8b11302
J. Am. Chem. Soc. 2019, 141, 1016−1026

$UO_2^{dipp}IQ(OTf)_2THF$ (CIF)
$UO_2^{dipp}ISQ_2THF$ (CIF)
$UO_2^{dipp}AP_2(KEt_2O)_2$ (CIF)
$UO_2^{dipp}AP_2THF(K(18\text{-}C\text{-}6))_2$ (CIF)
$UO_2^{dipp}IQ^{dipp}ISQCl$ (CIF)
$UCl_4^{dipp}IQ(THF)_2$ (CIF)
Additional experimental procedures, spectroscopic data, and crystallographic details (PDF)

AUTHOR INFORMATION

Corresponding Author

*sbart@purdue.edu

ORCID

Yusen Qiao: 0000-0001-7654-8636
Matthias Zeller: 0000-0002-3305-852X
Eric J. Schelter: 0000-0002-8143-6206
Suzanne C. Bart: 0000-0002-8918-9051

Notes

The authors declare no competing financial interest.

ACKNOWLEDGMENTS

This material is based upon work supported by the U.S. Department of Energy, Office of Science, Office of Basic Energy Sciences under Award Number DE-SC0008479. E.J.S. acknowledges the U.S. Department of Energy, Office of Science, Office of Basic Energy Sciences, Separation Science program under Award Number DE-SC0017259 for financial support. The X-ray crystallographic data in this work was obtained on instruments funded by the National Science Foundation through the Major Research Instrumentation Program under Grant CHE 1625543. The authors acknowledge Professor Jay Kikkawa (Dept. of Physics, University of Pennsylvania) for assistance with the magnetic measurements.

REFERENCES

(1) Greenwood, N. N.; Earnshaw, A. *Chemistry of the Elements*, 2nd ed.; Butterworth Heinemann: Oxford, 1998.
(2) Briner, W. E. "The Evolution of Depleted Uranium as an Environmental Risk Factor: Lessons from Other Metals". *Int. J. Environ. Res. Public Health* **2006**, *3*, 129−135.
(3) Amme, M.; Wiss, T.; Thiele, H.; Boulet, P.; Lang, H. "Uranium Secondary Phase Formation During Anoxic Hydrothermal Leaching Processes of UO_2 Nuclear Fuel". *J. Nucl. Mater.* **2005**, *341*, 209−223.
(4) DeLemos, J. L.; Bostick, B. C.; Quicksall, A. N.; Landis, J. D.; George, C. C.; Slagowski, N. L.; Rock, T.; Brugge, D.; Lewis, J.; Durant, J. L. Rapid Dissolution of Soluble Uranyl Phases in Arid, Mine-Impacted Catchments near Church Rock, NM. *Environ. Sci. Technol.* **2008**, *42*, 3951−3957.
(5) Arnold, P. L.; Love, J. B.; Patel, D. "Pentavalent Uranyl Complexes". *Coord. Chem. Rev.* **2009**, *253*, 1973−1978.
(6) Kannan, S.; Moody, M. A.; Barnes, C. L.; Duval, P. B. "Fluoride Abstraction and Reversible Photochemical Reduction of Cationic Uranyl(VI) Phosphine Oxide Complexes". *Inorg. Chem.* **2006**, *45*, 9206−9212.
(7) Kiernicki, J. J.; Zeller, M.; Bart, S. C. "Facile Reductive Silylation of UO_2^{2+} to Uranium(IV) Chloride". *Angew. Chem., Int. Ed.* **2017**, *56*, 1097−1100.
(8) Arnold, P. L.; Jones, G. M.; Odoh, S. O.; Schreckenbach, G.; Magnani, N.; Love, J. B. "Strongly Coupled Binuclear Uranium-Oxo Complexes from Uranyl Oxo Rearrangement and Reductive Silylation". *Nat. Chem.* **2012**, *4*, 221−227.
(9) Arnold, P. L.; Pecharman, A.-F.; Lord, R. M.; Jones, G. M.; Hollis, E.; Nichol, G. S.; Maron, L.; Fang, J.; Davin, T.; Love, J. B. "Control of Oxo-Group Functionalization and Reduction of the Uranyl Ion". *Inorg. Chem.* **2015**, *54*, 3702−3710.
(10) Brown, J. L.; Mokhtarzadeh, C. C.; Lever, J. M.; Wu, G.; Hayton, T. W. "Facile Reduction of a Uranyl(VI) Beta-Ketoiminate Complex to U(IV) Upon Oxo Silylation". *Inorg. Chem.* **2011**, *50*, 5105−5112.
(11) Kiernicki, J. J.; Harwood, J. S.; Fanwick, P. E.; Bart, S. C. "Reductive Silylation of $Cp^*UO_2(^{Mes}PDI^{Me})$ Promoted by Lewis Bases". *Dalton Trans.* **2016**, *45*, 3111−3119.
(12) Pedrick, E. A.; Wu, G.; Hayton, T. W. "Reductive Silylation of the Uranyl Ion with Ph_3SiOTf". *Inorg. Chem.* **2014**, *53*, 12237−12239.
(13) Pedrick, E. A.; Wu, G.; Kaltsoyannis, N.; Hayton, T. W. "Reductive Silylation of a Uranyl Dibenzoylmethanate Complex: An Example of Controlled Uranyl Oxo Ligand Cleavage". *Chem. Sci.* **2014**, *5*, 3204−3213.
(14) Jones, G. M.; Arnold, P. L.; Love, J. B. "Oxo−Group-14-Element Bond Formation in Binuclear Uranium(V) Pacman Complexes". *Chem. - Eur. J.* **2013**, *19*, 10287−10294.
(15) Arnold, P. L.; Mansell, S. M.; Maron, L.; McKay, D. "Spontaneous Reduction and C-H Borylation of Arenes Mediated by Uranium(III) Disproportionation". *Nat. Chem.* **2012**, *4*, 668−674.
(16) Cowie, B. E.; Nichol, G. S.; Love, J. B.; Arnold, P. L. "Double Uranium Oxo Cations Derived from Uranyl by Borane or Silane Reduction". *Chem. Commun.* **2018**, *54*, 3839−3842.
(17) Kiernicki, J. J.; Cladis, D. P.; Fanwick, P. E.; Zeller, M.; Bart, S. C. "Synthesis, Characterization, and Stoichiometric U = O Bond Scission in Uranyl Species Supported by Pyridine(Diimine) Ligand Radicals". *J. Am. Chem. Soc.* **2015**, *137*, 11115−11125.
(18) Coughlin, E. J.; Zeller, M.; Bart, S. C. "Neodymium(III) Complexes Capable of Multi-Electron Redox Chemistry". *Angew. Chem.* **2017**, *129*, 12310−12313.
(19) Blackmore, K. J.; Ziller, J. W.; Heyduk, A. F. ""Oxidative Addition" to a Zirconium(IV) Redox-Active Ligand Complex". *Inorg. Chem.* **2005**, *44*, 5559−5561.
(20) Blackmore, K. J.; Sly, M. B.; Haneline, M. R.; Ziller, J. W.; Heyduk, A. F. "Group IV Imino-Semiquinone Complexes Obtained by Oxidative Addition of Halogens". *Inorg. Chem.* **2008**, *47*, 10522−10532.
(21) Matson, E. M.; Opperwall, S. R.; Fanwick, P. E.; Bart, S. C. ""Oxidative Addition" of Halogens to Uranium(IV) Bis-(Amidophenolate) Complexes". *Inorg. Chem.* **2013**, *52*, 7295−7304.
(22) Matson, E. M.; Franke, S. M.; Anderson, N. H.; Cook, T. D.; Fanwick, P. E.; Bart, S. C. "Radical Reductive Elimination from Tetrabenzyluranium Mediated by an Iminoquinone Ligand". *Organometallics* **2014**, *33*, 1964−1971.
(23) Abakumov, G. A.; Cherkasov, V. K.; Piskunov, A. V.; Meshcheryakova, I. N.; Maleeva, A. V.; Poddel'skii, A. I.; Fukin, G. K. "Zinc Molecular Complexes with Sterically Hindered O-Quinone and O-Iminoquinone". *Dokl. Chem.* **2009**, *427*, 168−171.
(24) Ranis, L. G.; Werellapatha, K.; Pietrini, N. J.; Bunker, B. A.; Brown, S. N. "Metal and Ligand Effects on Bonding in Group 6 Complexes of Redox-Active Amidodiphenoxides". *Inorg. Chem.* **2014**, *53*, 10203−10216.
(25) Pangborn, A. B.; Giardello, M. A.; Grubbs, R. H.; Rosen, R. K.; Timmers, F. J. "Safe and Convenient Procedure for Solvent Purification". *Organometallics* **1996**, *15*, 1518−1520.
(26) Chakraborty, S.; Chattopadhyay, J.; Guo, W.; Billups, W. E. *Angew. Chem., Int. Ed.* **2007**, *46*, 4486−4488.
(27) Wilkerson, M. P.; Burns, C. J.; Paine, R. T.; Blosch, L. L.; Andersen, R. A. Organometallic and Coordination Complexes. Di(μ-chloro)bis{chlorodioxobis(tetrahydrofuran)uranium(VI)}, $[UO_2Cl_2(THF)_2]_2$. *Inorg. Synth.* **2004**, *34*, 93−95.
(28) Berthet, J. C.; Lance, M.; Nierlich, M.; Ephritikhine, M. "Simple Preparations of the Anhydrous and Solvent-Free Uranyl and Cerium(IV) Triflates $UO_2(OTf)_2$ and $Ce(OTf)_4$ - Crystal Structures of $UO_2(OTf)_2(Py)_3$ and $[\{UO_2(Py)_4\}_2(\mu\text{-}O)][OTf]_2$". *Eur. J. Inorg. Chem.* **2000**, *2000*, 1969−1973.

DOI: 10.1021/jacs.8b11302
J. Am. Chem. Soc. 2019, 141, 1016−1026

(29) Kiplinger, J. L.; Morris, D. E.; Scott, B. L.; Burns, C. J. "Convenient Synthesis, Structure, and Reactivity of $(C_5Me_5)U(CH_2C_6H_5)_3$A Simple Strategy for the Preparation of Monopentamethylcyclopentadienyl Uranium(IV) Complexes". *Organometallics* **2002**, *21*, 5978−5982.
(30) Abergel, R. J.; de Jong, W. A.; Deblonde, G. J. P.; Dau, P. D.; Captain, I.; Eaton, T. M.; Jian, J.; van Stipdonk, M. J.; Martens, J.; Berden, G.; Oomens, J.; Gibson, J. K. "Cleaving Off Uranyl Oxygens through Chelation: A Mechanistic Study in the Gas Phase". *Inorg. Chem.* **2017**, *56*, 12930−12937.
(31) Fortier, S.; Hayton, T. W. "Oxo Ligand Functionalization in the Uranyl Ion (UO_2^{2+})". *Coord. Chem. Rev.* **2010**, *254*, 197−214.
(32) Herasymchuk, K.; Chiang, L.; Hayes, C. E.; Brown, M. L.; Ovens, J.; Patrick, B. O.; Leznoff, D. B.; Storr, T. "Synthesis and Electronic Structure Determination of Uranium(VI) Ligand Radical Complexes". *Dalton Trans.* **2016**, *45*, 12576−12586.
(33) Takao, K.; Tsushima, S.; Ogura, T.; Tsubomura, T.; Ikeda, Y. "Experimental and Theoretical Approaches to Redox Innocence of Ligands in Uranyl Complexes: What Is Formal Oxidation State of Uranium in Reductant of Uranyl(VI)?". *Inorg. Chem.* **2014**, *53*, 5772−5780.
(34) Budzelaar, P. H. M.; de Bruin, B.; Gal, A. W.; Wieghardt, K.; van Lenthe, J. H. "Metal-to-Ligand Electron Transfer in Diiminopyridine Complexes of Mn-Zn. A Theoretical Study". *Inorg. Chem.* **2001**, *40*, 4649−4655.
(35) Azam, M.; Al-Resayes, S. I.; Velmurugan, G.; Venuvanalingam, P.; Wagler, J.; Kroke, E. "Novel Uranyl(VI) Complexes Incorporating Propylene-Bridged Salen-Type N_2O_2-Ligands: A Structural and Computational Approach". *Dalton Trans.* **2015**, *44*, 568−577.
(36) Carter, S. M.; Sia, A.; Shaw, M. J.; Heyduk, A. F. "Isolation and Characterization of a Neutral Imino-Semiquinone Radical". *J. Am. Chem. Soc.* **2008**, *130*, 5838−5839.
(37) Kahn, O. *Molecular Magnetism*; Wiley-VCH: New York, NY, 1993; p 396.
(38) Bleaney, B.; Bowers, K. D. "Anomalous Paramagnetism of Copper Acetate". *Proc. R. Soc. London, Ser. A* **1952**, *214*, 451.
(39) Cobb, P. J.; Moulding, D. J.; Ortu, F.; Randall, S.; Wooles, A. J.; Natrajan, L. S.; Liddle, S. T. "Uranyl-Tri-Bis(Silyl)Amide Alkali Metal Contact and Separated Ion Pair Complexes". *Inorg. Chem.* **2018**, *57*, 6571−6583.
(40) Arnold, P. L.; Stevens, C. J.; Bell, N. L.; Lord, R. M.; Goldberg, J. M.; Nichol, G. S.; Love, J. B. "Multi-Electron Reduction of Sulfur and Carbon Disulfide Using Binuclear Uranium(III) Borohydride Complexes". *Chem. Sci.* **2017**, *8*, 3609−3617.
(41) Arnold, P. L.; Patel, D.; Wilson, C.; Love, J. B. "Reduction and Selective Oxo Group Silylation of the Uranyl Dication". *Nature* **2008**, *451*, 315−317.
(42) Seaman, L. A.; Pedrick, E. A.; Wu, G.; Hayton, T. W. "Promoting Oxo Functionalization in the Uranyl Ion by Ligation to Ketimides". *J. Organomet. Chem.* **2018**, *857*, 34−37.
(43) Anderson, N. H.; Odoh, S. O.; Yao, Y.; Williams, U. J.; Schaefer, B. A.; Kiernicki, J. J.; Lewis, A. J.; Goshert, M. D.; Fanwick, P. E.; Schelter, E. J.; Walensky, J. R.; Gagliardi, L.; Bart, S. C. "Harnessing Redox Activity for the Formation of Uranium Tris(Imido) Compounds". *Nat. Chem.* **2014**, *6*, 919−926.
(44) Anderson, N. H.; Xie, J.; Ray, D.; Zeller, M.; Gagliardi, L.; Bart, S. C. "Elucidating Bonding Preferences in Tetrakis(Imido)Uranate(VI) Dianions". *Nat. Chem.* **2017**, *9*, 850−855.

DOI: 10.1021/jacs.8b11302
J. Am. Chem. Soc. 2019, 141, 1016−1026